

HIGHWAY APPLICATIONS FOR RAMMED AGGREGATE PIERS IN IOWA SOILS

Iowa DOT Project TR-443
CTRE Project 00-60

Sponsored by
the Iowa Department of Transportation
and the Iowa Highway Research Board



**Iowa Department
of Transportation**



*Center for Transportation
Research and Education*

Department of Civil and Construction Engineering

IOWA STATE UNIVERSITY

Final Report • April 2003

The opinions, findings, and conclusions expressed in this publication are those of the authors and not necessarily those of the Iowa Department of Transportation, Federal Highway Administration, or Geopier Foundation Company. The sponsor(s) do not endorse products or manufacturers. Trade and manufacturers names appear in this report only because they are considered essential to the objective of this document.

CTRE's mission is to develop and implement innovative methods, materials, and technologies for improving transportation efficiency, safety, and reliability while improving the learning environment of students, faculty, and staff in transportation-related fields.

Technical Report Documentation Page

1. Report No. Iowa DOT Project TR-443	2. Government Accession No.	3. Recipient's Catalog No.	
4. Title and Subtitle Highway Applications for Rammed Aggregate Piers in Iowa Soils		5. Report Date April 2003	
		6. Performing Organization Code	
7. Author(s) John M. Pitt, David J. White, Aaron Gaul, and Kenneth Hoevelkamp		8. Performing Organization Report No. CTRE Project 00-60	
9. Performing Organization Name and Address Center for Transportation Research and Education Iowa State University 2901 South Loop Drive, Suite 3100 Ames, IA 50010-8632		10. Work Unit No. (TRAIS)	
		11. Contract or Grant No.	
12. Sponsoring Organization Name and Address Iowa Highway Research Board 800 Lincoln Way Ames, IA 50010		13. Type of Report and Period Covered Final Report	
		14. Sponsoring Agency Code	
15. Supplementary Notes			
16. Abstract <p>This report describes a study to evaluate Geopier® soil reinforcement technology in transportation construction. Three projects requiring settlement control were chosen for evaluation—an embankment foundation, a box culvert, and a bridge approach fill. For each project, construction observations, in situ soil testing, laboratory material characterization, and performance monitoring were carried out.</p> <p>For the embankment foundation project, Geopier elements were installed within and around an abutment footprint for the new I-35 overpass at the US Highway 5/Interstate 35 interchange in Des Moines, Iowa. Although the main focus of this investigation was to evaluate embankment foundation reinforcement using Geopier elements, a stone column reinforced soil provided an opportunity to compare systems. In situ testing included cone penetration tests (CPTs), pressuremeter tests (PMTs), Ko stepped blade tests, and borehole shear tests (BSTs), as well as laboratory material testing. Comparative stiffness and densities of Geopier elements and stone columns were evaluated based on full-scale modulus load tests and standard penetration tests. Vibrating wire settlement cells and total stress cells were installed to monitor settlement and stress concentration on the reinforcing elements and matrix soil. Settlement plates were also monitored by conventional optical survey methods. Results show that the Geopier system and the stone columns performed their intended functions.</p> <p>The second project involved settlement monitoring of a 4.2 m wide x 3.6 m high x 50 m long box culvert constructed beneath a bridge on Iowa Highway 191 south of Neola, Iowa. Geopier elements were installed to reduce total and differential settlement while ensuring the stability of the existing bridge pier foundations. Benefits of the box culvert and embankment fill included (1) ease of future roadway expansion and (2) continual service of the roadway throughout construction. Site investigations consisted of in situ testing including CPTs, PMTs, BSTs, and dilatometer tests. Consolidated drained triaxial compression tests, unconsolidated undrained triaxial compression test, oedometer tests, and Atterberg limit tests were conducted to define strength and consolidation parameters and soil index properties for classification. Vibrating wire settlement cells, total stress cells, and piezometers were installed for continuous monitoring during and after box culvert construction and fill placement. This project was successful at controlling settlement of the box culvert and preventing downdrag of the bridge foundations, but could have been enhanced by reducing the length of Geopier elements at the ends of the box culvert. This would have increased localized settlement while reducing overall differential settlement.</p> <p>The third project involved settlement monitoring of bridge approach fill sections reinforced with Geopier elements. Thirty Geopier elements, spaced 1.8 m apart in six rows of varying length, were installed on both sides of a new bridge on US Highway 18/218 near Charles City, Iowa. Based on the results of this project, it was determined that future applications of Geopier soil reinforcement should consider extending the elements deeper into the embankment foundation fill, not just the fill itself.</p>			
17. Key Words rammed aggregate piers, soil reinforcement technology		18. Distribution Statement No restrictions.	
19. Security Classification (of this report) Unclassified.	20. Security Classification (of this page) Unclassified.	21. No. of Pages 154	22. Price N/A

HIGHWAY APPLICATIONS FOR RAMMED AGGREGATE PIERS IN IOWA SOILS

Iowa DOT Project TR-443
CTRE Project 00-60

Principal Investigator

John M. Pitt

Associate Professor of Civil Engineering, Iowa State University

Co-Principal Investigator

David J. White

Assistant Professor of Civil Engineering, Iowa State University

Research Assistants

Aaron Gaul and Kenneth Hoevelkamp

Authors

David J. White, Aaron Gaul, and Kenneth Hoevelkamp

Preparation of this report was financed in part through funds provided by the Iowa Department of Transportation through its research management agreement with the Center for Transportation Research and Education.

Center for Transportation Research and Education

Iowa State University

2901 South Loop Drive, Suite 3100

Ames, IA 50010-8634

Phone: 515-294-8103

Fax: 515-294-0467

www.ctre.iastate.edu

Final Report • April 2003

TABLE OF CONTENTS

ACKNOWLEDGMENTS	IX
EXECUTIVE SUMMARY	XI
INTRODUCTION	1
Project No. 1: Embankment Foundation Reinforcement at US Hwy 5/I-35 (Des Moines, IA) 1	
Project No. 2: Box Culvert Foundation Reinforcement at IA Hwy 191 (Neola, IA)	1
Project No. 3: Bridge Approach Embankment Reinforcement at US Hwy 18/218 (Charles City, IA)	2
BACKGROUND	4
Research and Development	4
Engineering Properties	5
Stiffness	5
Angle of Internal Friction	5
Drainage	5
Comparison with Stone Columns	8
Design of Geopier Foundation Systems	8
RESULTS AND DISCUSSION	11
Project No. 1: Embankment Foundation Reinforcement at US Hwy 5/I-35 (Des Moines, IA) 11	
Stone Column Site	15
Geopier Site	21
Comparison of Site Characteristics	21
Geotechnical Measurements	28
Borehole Shear Test Results	28
Standard Penetration Test Results	29
Ko Stepped Blade Results	30
Pressuremeter Test Results	32
Load Test Results	34
Settlement Measurements	37
Instrumentation Monitoring	39
Settlement Cell Measurements	40
Total Stress Cell Measurements	42
Summary Observations	44
Project No. 2: Box Culvert Foundation Reinforcement at IA Hwy 191 (Neola, IA)	47
Site Conditions	49
Cone Penetrometer Test Results	49
Flat Dilatometer Test Results	54
Pressuremeter Test Results	55
Borehole Shear Test Results	57
Laboratory Testing Program	58
CD Triaxial Compression Test Results	58
UU Triaxial Compression Test Results	60
Confined Compression (Oedometer) Consolidation Test Results	60

Soil Index Test Results	62
Full-Scale Modulus Load Test Results	63
Individual Load Test Results	63
Group Load Test Results	71
Performance Monitoring	77
Instrumentation Results	77
Comparison to Design Predictions	84
Summary and Conclusions	90
Project No. 3: Bridge Approach Embankment Reinforcement at US Hwy 18/218 (Charles City, IA)	91
Design	91
Performance Monitoring	92
SUMMARY AND CONCLUSIONS	97
Project No. 1: Embankment Foundation Reinforcement at US Hwy 5/I-35 (Des Moines, IA)	97
Project No. 2: Box Culvert Foundation Reinforcement at IA Hwy 191 (Neola, IA)	97
Project No. 3: Bridge Approach Embankment Reinforcement at US Hwy 18/218 (Charles City, IA)	98
REFERENCES	99
APPENDIX A: PROJECT NO. 1 CPT RESULTS	103
APPENDIX B: PROJECT NO. 1 BST RESULTS	119
APPENDIX C: PROJECT NO. 1 PMT RESULTS	123
APPENDIX D: PROJECT NO. 2 CPT RESULTS	129
APPENDIX E: PROJECT NO. 2 DMT RESULTS	134
APPENDIX F: PROJECT NO. 2 PMT RESULTS	139
APPENDIX G: PROJECT NO. 2 BST RESULTS	148
APPENDIX H: PROJECT NO. 2 DESIGN CALCULATIONS	150

LIST OF FIGURES

Figure 1. Embankment Foundation Reinforcement at US Hwy 5/I-35 (Des Moines, IA)	3
Figure 2. Box Culvert Foundation Reinforcement at Iowa Hwy 161 (Neola, IA)	3
Figure 3. Bridge Approach Embankment Reinforcement at US Hwy 18/218 (Charles City, IA).....	3
Figure 4. Geopier Construction Process: (1) Drill Cavity; (2) Place Stone; (3) Ram Stone to Form Bottom Bulb; and (4) Place and Ram Lifts to Form Undulated-Sided Shaft.....	4
Figure 5. Stress Concentration Factors Measured for Instrumented Footing (Lawton and Merry 2000).....	6
Figure 6. Results of Shear Strength Tests (Fox and Cowell 1998; White et al. 2002).....	6
Figure 7. IA Hwy 5/I-35 Research Site	12
Figure 8. Ramp C Embankment Cross Section	12
Figure 9. Ramp C Test and Instrumentation Locations for Geopier Installation.....	13
Figure 10. Ramp B Test and Instrumentation Locations for Stone Column Installations	13
Figure 11. Ramp C Geopier Supported Embankment	14
Figure 12. Ramp B Stone Column Supported Embankment.....	14
Figure 13. Cone Penetration Test Results for Ramp B (CPTU-5)—Stone Column Site.....	16
Figure 14. Stone Column and Geopier Element Spacings.....	18
Figure 15. Relationship Between Amperage Pulled by Vibroflot Motor and CPT Skin Friction at Stone Column Site	19
Figure 16. Grain-Size Distribution of Aggregate Used in Construction of Stone Columns and Geopier Elements (Same Aggregate for Both Sites)	19
Figure 17. Stone Column Construction Operations.....	20
Figure 18. Cone Penetration Test Results for Ramp C (CPTU-2)—Geopier Site.....	22
Figure 19. Consolidated Drained Triaxial Compression Test Results for Soil at Depth of 2.59 m at Geopier Site....	24
Figure 20. e-log-p Curve for the Normally Consolidated, Compressible Clay at Depth of 2.7 m at Geopier Site	25
Figure 21. Unconfined Compressive Strength Results at Geopier Site	26
Figure 22. Soil Index Test Results for Geopier Site.....	26
Figure 23. Geopier Construction Operations.....	27
Figure 24. Comparative SPT N-values through Production Stone Columns and Geopier Elements	30
Figure 25. K_o Stepped Blade Measurements Conducted 70 cm from Stone Column and 85 cm from Geopier Element (All Tests Oriented to Measure Radial Stress).....	31
Figure 26. K_o Stepped Blade Test Equipment	31
Figure 27. Pressuremeter Test Results after 0, 7, and 73 Days at Geopier Site	33
Figure 28. Comparative Stress-Deformation Plot for Stone Column and Geopier Elements.....	35
Figure 29. Stiffness Versus Applied Stress for Stone Column and Geopier Elements—Trend Lines are Best-Fit Hyperbolic Decay Functions.....	35
Figure 30. Geopier Field Modulus Load Test	36
Figure 31. Settlement Plates 0.9 m x 0.9 m	37
Figure 32. Settlement Versus Fill Height from 0.9 x 0.9 m Settlement Plates Installed Immediately after Pier Installations—Monitored for One Year	38
Figure 33. Settlement Cells and Total Stress Cells at Geopier Site.....	39
Figure 34. Ramp C (Stage 1) Settlement Cell Readings as a Function of Time (Locations 1 and 2).....	41
Figure 35. Ramp C (Stage 1) Settlement Cell Readings as a Function of Time (Location 3).....	41
Figure 36. Total Stress Cell Locations 1 and 2 at Geopier Site.....	42
Figure 37. Geopier Stress Concentration Ratios - Ramp C	43
Figure 38. Ramp C Total Stress Cell Location No. 3	43
Figure 39. Ramp B Total Stress Cell Locations 1, 2, and 3.....	45
Figure 40. Stone Column Stress Concentration Ratios (Ramp B).....	45
Figure 41. Project Site and Grading Operations for Box Culvert.....	48
Figure 42. Plan View of Project Site showing DMT and CPT Test Locations	50
Figure 43. Cone Penetration Testing at CPT3	51
Figure 44. CPT1 Results.....	52
Figure 45. Undrained Shear Strength (S_u) Estimated from CPT Results ($N_{kT} = 15$)	54
Figure 46. Dilatometer Parameters and Correlation to Undrained Shear Strength.....	56
Figure 47. Calculated Pressuremeter Modulus at PMT1 and PMT2	57
Figure 48. Borehole Shear Test Results at Load Test Area.....	58
Figure 49. CD Triaxial Stress-Strain and Volume-Change Behavior of Alluvial Clay.....	59
Figure 50. UU Triaxial Stress-Strain Behavior of Alluvial Clay	60

Figure 51. e-log(p) Curves including Void Ratio Measurements from Several Field Samples	61
Figure 52. (a) Soil Index Properties and (b) Void Ratio Versus Depth for Alluvial Clay	62
Figure 53. Plan of Individual Pier No. 1 with Instrumentation Locations (Dimensions Shown are in Meters).....	64
Figure 54. Test Pier No. 1	64
Figure 55. Load-Settlement Results for Pier No. 1	65
Figure 56. Stiffness Results for Pier No. 1	65
Figure 57. Vertical Stress Distribution from Total Stress Cell Readings in Pier No. 1 (Legend Indicates Applied Stress at Top of Pier).....	66
Figure 58. Inclinomater Casing Profiles after Pier No. 1 Installation	67
Figure 59. Inclinomater Casing No. 1 Profiles during Pier No. 1 Loading.....	67
Figure 60. Inclinomater Casing No. 2 Profiles during Pier No. 1 Loading.....	68
Figure 61. Load-Settlement Results for Pier No. 2	69
Figure 62. Stiffness Results for Pier No. 2.....	69
Figure 63. Load-Settlement Results for Pier No. 3	70
Figure 64. Stiffness Results for Pier No. 3	70
Figure 65. Group Load Test No. 1 Profile View Showing Instrumentation Locations (Dimensions Shown in Meters Unless Indicated).....	72
Figure 66. Group Load T No. 1 Instrumentation Plan (Dimensions Shown in Meters Unless Indicated).....	73
Figure 67. Group Load Test No. 1 Construction and Load Frame.....	73
Figure 68. Settlement vs. Applied Load at Top of Footing of Group No. 1 and 2.....	74
Figure 69. Comparison of Group and Individual Pier Behavior	74
Figure 70. Group Efficiency Compared to Individual Load Tests	75
Figure 71. Total Stress Cell Readings for Group No. 1	75
Figure 72. Stress Concentration Ratio for Group Load Test No. 1	76
Figure 73. Inclinomater Profile for Group Load Test No. 1 during Loading.....	76
Figure 74. Locations of Instrumentation and Geopier Installation Zones	78
Figure 75. Piezometer Layout	79
Figure 76. Wet Conditions during Piezometer Borehole Installation and Geopier Construction.....	80
Figure 77. Piezometer Readings for First Half of Dynamic Pore Pressure Test	81
Figure 77. Piezometer Readings for Second Half of Dynamic Pore Pressure Test (<i>continued</i>).....	81
Figure 78. Piezometer Readings Before, During, and After Embankment Construction.....	82
Figure 79. Stress Cell Readings Before and After Embankment Construction	83
Figure 80. Settlement Cell Readings Before and After Embankment Construction	84
Figure 81. Settlement of Box Culvert along Survey Pins (pin 1 west to pin 11 east)	86
Figure 82. Completed Box Culvert.....	87
Figure 83. Settlement of Pin 5 as a Function of Fill Height	88
Figure 84. Settlement of Pin 5 as a Function of Time	88
Figure 85. Crack Opening at Construction Joints in Box Culvert.....	89
Figure 86. Design Details for Geopier Installation.....	93
Figure 87. Approach Slab Settlement for Geopier Reinforced Section.....	94
Figure 88. Approach Slab Settlement for Non-Reinforced Section	95
Figure 89. Comparison between Geopier Reinforced Section and the Non-Reinforced Section.....	96

LIST OF TABLES

Table 1. Geopier Stress Concentration Factors	6
Table 2. Selected Geopier Transportation Projects to Date.....	7
Table 3. Comparison of Stone Columns and Geopier Rammed Aggregate Piers	9
Table 4. Summary Consolidation Parameters from Iowa DOT and ISU Tests at Geopier Site	25
Table 5. Comparison of Site Characteristics	28
Table 6. BST Shear Strength Parameter Values at Geopier Site	29
Table 7. Results of Lateral Stress Measurements.....	32
Table 8. Comparison of Stiffness Values Derived from Load Test Results	36
Table 9. Results of Settlement Survey Measurements.....	38
Table 10. Ramp C Geopier Instrumentation.....	40
Table 11. Ramp B Stone Columns Instrumentation	40
Table 12. Summary of Consolidation Parameter Values for Alluvial Clay.....	61
Table 13. Design Settlement Calculations.....	86
Table 14. Settlement of each Surveying Pin One-Week Prior to and Five Weeks after Embankment Construction..	87
Table 15. Geopier Design Drill Lengths	91

ACKNOWLEDGMENTS

The Highway Division of the Iowa Department of Transportation and the Iowa Highway Research Board sponsored this study under contract TR-443. The authors would like to thank Geopier® Foundation Company for participating in this study and the Federal Highway Administration for sponsoring instrumentation. The support of these agencies is greatly appreciated. The authors are indebted to Peterson Contractors, Inc., for their assistance during testing. In addition, assistance from the Iowa Department of Transportation Office of Soils Design and Office of Construction, especially Mr. Barnes, is greatly appreciated. Geotechnical Services, Inc., provided cone penetration testing at two sites. Assistance from the Iowa Department of Transportation offices in Council Bluffs and New Haven is greatly appreciated.

EXECUTIVE SUMMARY

This report describes a study to evaluate Geopier® soil reinforcement technology in transportation construction. Three projects requiring settlement control were chosen for evaluation—an embankment foundation, a box culvert, and a bridge approach fill. For each project, construction observations, in situ soil testing, laboratory material characterization, and performance monitoring were carried out.

For the embankment foundation project, Geopier elements were installed within and around an abutment footprint for the new I-35 overpass at the US Highway 5/Interstate 35 interchange in Des Moines, Iowa. The Geopier elements were installed to reduce total settlement and increase the rate of settlement of a 5 m to 6 m alluvial clay layer beneath the proposed 8 m fill. The goal was to reduce construction delay between embankment and abutment construction from 120 days to less than 30 days. At an adjacent embankment foundation site, stone columns were installed in the foundation soils to increase the factor of safety against global slope instability at the interface between a silty alluvium layer and weathered shale bedrock. Although the main focus of this investigation was to evaluate embankment foundation reinforcement using Geopier elements, the stone column reinforced soil provided an opportunity to compare systems.

In situ testing included cone penetration tests (CPTs), pressuremeter tests (PMTs), Ko stepped blade tests, and borehole shear tests (BSTs), as well as laboratory material testing. Comparative stiffness and densities of Geopier elements and stone columns were evaluated based on full-scale modulus load tests and standard penetration tests. Vibrating wire settlement cells and total stress cells were installed to monitor settlement and stress concentration on the reinforcing elements and matrix soil. Settlement plates were also monitored by conventional optical survey methods. Results show that the Geopier system and the stone columns performed their intended functions.

The second project involved settlement monitoring of a 4.2 m wide x 3.6 m high x 50 m long box culvert constructed beneath a bridge on Iowa Highway 191 south of Neola, Iowa. Geopier elements were installed to reduce total and differential settlement while ensuring the stability of the existing bridge pier foundations. Challenges to construction included a groundwater table at the working surface, very soft soil conditions, and low clearance for machinery beneath the bridge. Benefits of the box culvert and embankment fill included (1) ease of future roadway expansion and (2) continual service of the roadway throughout construction.

Site investigations consisted of in situ testing including CPTs, PMTs, BSTs, and dilatometer tests. Results were used to characterize the subsurface soil engineering properties and to define the depth of a compressible alluvial clay layer. Consolidated drained triaxial compression tests, unconsolidated undrained triaxial compression test, oedometer tests, and Atterberg limit tests were conducted to define strength and consolidation parameters and soil index properties for classification.

Vibrating wire settlement cells, total stress cells, and piezometers were installed for continuous monitoring during and after box culvert construction and fill placement. In addition, several settlement pins was positioned in the culvert and monitored by conventional survey techniques.

Data gathered from subsurface investigations were used to estimate total settlement and rate of settlement within the alluvial clay layer. Estimates were contrasted with values obtained from field performance monitoring. Full-scale modulus load tests of individual and groups of piers were carried out for purposes of investigating Geopier group interaction behavior. This project was successful at controlling settlement of the box culvert and preventing downdrag of the bridge foundations, but could have been enhanced by reducing the length of Geopier elements at the ends of the box culvert. This would have increased localized settlement while reducing overall differential settlement.

The third project involved settlement monitoring of bridge approach fill sections reinforced with Geopier elements. Thirty Geopier elements, spaced 1.8 m apart in six rows of varying length, were installed on both sides of a new bridge on US Highway 18/218 near Charles City, Iowa. Performance was monitored for a period of two years after installation and indicates similar results to a non-reinforced bridge section. Based on the results of this project, it was determined that future applications of Geopier soil reinforcement should consider extending the elements deeper into the embankment foundation fill, not just the fill itself.

INTRODUCTION

This report describes three demonstration projects where Geopier® soil reinforcement technology was used in construction of transportation systems—an embankment foundation, a box culvert, and a bridge approach fill. For each project, construction observations, in situ soil testing, laboratory material characterization, and performance monitoring were carried out. Results show that Geopier soil reinforcement provides an effective ground improvement alternative to control settlement and improve the factors of safety against bearing capacity and slope instability. Projects evaluated in the study include the following:

- Embankment foundation reinforcement at US Highway 5/Interstate 35 in Des Moines, Iowa
- Box culvert foundation reinforcement at Iowa Highway 191 in Neola, Iowa
- Bridge approach embankment reinforcement at US Highway 18/218 in Charles City, Iowa

The primary application for each of the three demonstration projects was to control the magnitude and time rate of settlement.

In addition to documenting the performance at each project, this report provides brief details of Geopier construction methods, engineering properties, recent applications of Geopier technology in transportation construction, and comparisons to stone columns. Finally, conclusions and recommendations/limitations are provided for future application of this technology in Iowa soil conditions.

Project No. 1: Embankment Foundation Reinforcement at US Hwy 5/I-35 (Des Moines, IA)

The primary objective of this project was to investigate settlement control using Geopier soil reinforcement in an embankment foundation for the US Highway/I-35 overpass project located southwest of Des Moines, Iowa. Because stone columns were installed in an adjacent embankment foundation, this project provided the opportunity to compare engineering behavior and performance with a different ground improvement system. In situ testing at the project site included cone penetration tests (CPTs), pressuremeter tests (PMTs), and borehole shear tests (BSTs), as well as laboratory index tests. Performance monitoring was achieved from load-displacement relationships from full-scale modulus load tests, aggregate density from standard penetration tests (SPTs), and settlement from settlement plates on both the Geopier reinforced embankment and the stone column reinforced embankment. Changes in matrix soil lateral stress between Geopier foundations and stone columns were made from in situ K_0 stepped blade tests. Vibrating wire instrumentation including settlement cells and total stress cells were monitored. Figure 1 presents the application of this project.

Project No. 2: Box Culvert Foundation Reinforcement at IA Hwy 191 (Neola, IA)

In lieu of replacing a deteriorating, three-span bridge built in 1927 on IA Hwy 191 south of Neola, Iowa, a 4.2 m wide x 3.6 m high x 50 m long box culvert and embankment was constructed beneath the bridge. Ultimately, the guardrails were removed and a shoulder was

constructed leaving no visual evidence that the pavement is supported by a bridge structure. Because soils at this site are highly compressible (moisture contents over 40 percent), it was estimated that the box culvert could settle up to 50 cm, thus risking differential settlement and deleterious cracking of the box culvert and potential downdrag on the existing bridge foundations—a combination of steel H-pile and timber pile of unknown length. Figure 2 shows the exposed abutment foundations during construction of the box culvert. To reduce total and differential settlement while ensuring the stability of the existing bridge piers, Geopier soil reinforcement was selected for installation beneath the box culvert. Challenges to construction included a groundwater table approximately 1 m above the working surface, very soft soil conditions, and low clearance for machinery beneath the bridge. Despite these construction challenges it was determined that the benefits of the box culvert and embankment (i.e., ease of future roadway expansion and continual service of the highway throughout construction) outweighed the cost of replacing of the bridge structure.

Site investigations consisted of CPTs, PMTs, dilatometer tests (DMTs), and BSTs. Laboratory testing consisted of consolidated drained (CD) triaxial, unconsolidated undrained (UU) triaxial, oedometer, and Atterberg limit tests.

Vibrating wire instrumentation including settlement cells, total stress cells, and piezometers were installed for continuous monitoring during and after box culvert construction and fill placement. In addition, settlement pins were installed in the culvert and monitored by optical survey techniques. Data gathered from subsurface investigations were used to estimate total settlement and rate of settlement within a compressible alluvial clay layer. Estimates were then contrasted with values obtained from field performance monitoring. Load testing of individual and groups of piers was carried out for purposes of investigating group interaction behavior.

Project No. 3: Bridge Approach Embankment Reinforcement at US Hwy 18/218 (Charles City, IA)

The purpose of this project was to evaluate Geopier soil reinforcement for control or prevention of the “bump at the end of the bridge.” Many state department of transportation (DOTs), including the Iowa DOT, consider bridge approach settlement a problem of significant cost that requires regular maintenance. Settlement of the natural foundation soils and compression of the embankment fill material are the two most significant factors contributing to the formation of the bump (Briaud et al. 1997). To support the reinforced concrete bridge approach sections, 30 Geopier elements of varying length were installed on each side of the new bridge (see Figure 3). Long-term (five-year) settlement data of the bridge approach slabs are being collected and contrasted with a companion bridge with no reinforcement.

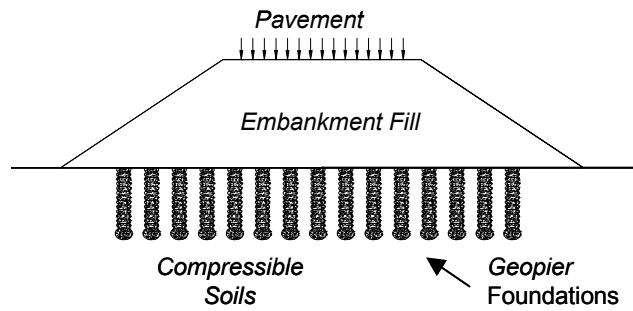


Figure 1. Embankment Foundation Reinforcement at US Hwy 5/I-35 (Des Moines, IA)

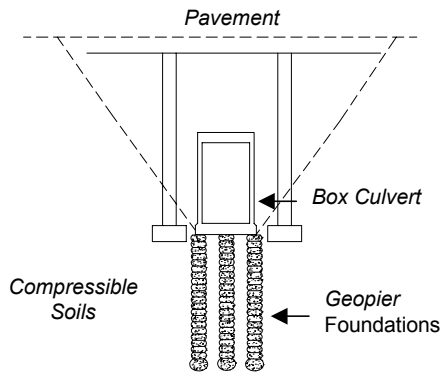


Figure 2. Box Culvert Foundation Reinforcement at Iowa Hwy 161 (Neola, IA)

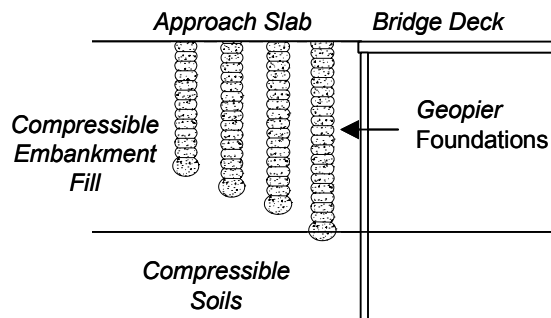


Figure 3. Bridge Approach Embankment Reinforcement at US Hwy 18/218 (Charles City, IA)

BACKGROUND

Research and Development

Geopier soil reinforcement was invented in the mid-1980s by Dr. Nathaniel Fox to provide a technology that could be used to reduce settlement below shallow spread footings. The system was introduced to commercial building construction in 1989 and received U.S. and foreign patents for the system in the mid-1990s. Since then, research efforts and the use of Geopier foundations in transportation applications have grown.

In 1998, the Federal Highway Administration (FHWA) and the Utah DOT funded a research project that incorporated Geopier elements into a large research effort involving the dynamic response of a full-scale elevated bridge bent subjected to simulated seismic loading (see Lawton and Merry 2000). That same year, Maryland State Highway Administration evaluated specially outfitted Geopier elements for controlling uplift forces at the heel of a concrete cantilever retaining wall. More recently, the elements have been installed to support railroad embankments, support MSE walls, stabilize failing slopes, and reduce potential soil liquefaction. Research projects in these areas have been performed at the University of Utah, University of Massachusetts-Amherst, Virginia Tech, and Iowa State University (ISU).

Construction

Geopier construction, shown in Figure 4, is initiated by drilling 600 mm to 900 mm diameter holes into the ground to depths typically ranging between 2 m to 7 m below the ground surface (1). A stable bottom bulb is then formed by placing a layer of clean, crushed stone into the hole (2) and ramming the stone using a patented specially designed, high-energy beveled tamper (3) (see Handy et al. 1999). Thin 300 mm lifts of well-graded aggregate are then introduced into the hole and rammed with the tamper to form the remainder of the shaft (4). The result is a highly densified stiff element that exhibits a high angle of internal friction and high lateral stress development in the matrix soils (Handy et al. 2003). When constructed with open graded stone, the elements may also exhibit sufficient permeability to serve as drainage pathways for the dissipation of excess pore water.

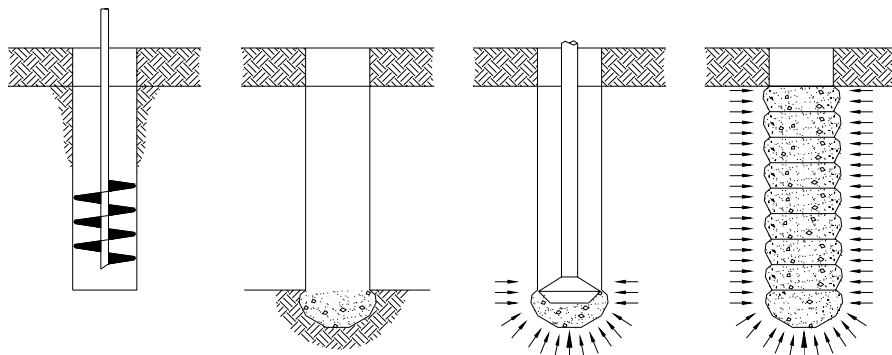


Figure 4. Geopier Construction Process: (1) Drill Cavity; (2) Place Stone; (3) Ram Stone to Form Bottom Bulb; and (4) Place and Ram Lifts to Form Undulated-Sided Shaft

Engineering Properties

Stiffness

The construction of Geopier elements results in a stiff vertical inclusion within the matrix soil. The relative stiffness between the aggregate pier elements and the matrix soil is called the stiffness ratio. Table 1 lists a range of measured stiffness ratios. Figure 5 shows stiffness ratios plotted against applied footing pressures for instrumented footings (Lawton and Merry 2000). The stiffness ratio values were determined from pressure plate readings installed at the bottom of the instrumented footing. For most projects, the stiffness of the Geopier element is established from an on-site modulus load test, which is performed to establish the relationship between downward stress applied to the top of the pier and pier deflection. To date more than 400 load tests have been performed in North America, Europe, and Asia. The high stiffness ratios for Geopier elements are related to the lateral prestressing of the matrix soil that occurs during construction and the high friction angle of the aggregate after ramming (see Handy 2001).

Angle of Internal Friction

Post-construction angles of internal friction have been measured for installed piers using a full-scale direct shear apparatus (Fox and Cowell 1998) and for reconstituted samples of aggregate compacted to relative densities approximating that of installed piers (see White et al. 2002). Figure 6 presents results of the field and lab test measurements, which indicate angles of internal friction of approximately 49 degrees for densified open-graded crushed stone and 51 and 52 degrees for densified well-graded crushed stone aggregate. Friction angle is particularly significant for slope stability and bearing capacity improvement applications. Recycled aggregates including reclaimed concrete and steel slag have been used in Geopier construction.

Drainage

When open-graded stone is used to construct the shafts of the elements, the elements are more permeable than the matrix fine-grained soils. For saturated soils, the elements will act as drains similar to prefabricated vertical drains and aid in dissipation of excess pore water pressures generated from vertical loads. Open-graded aggregates are typically used below the water table. Well-graded aggregates are typically used above the water table and can exhibit permeability values similar to fine-grained soils.

Transportation Applications

Table 2 lists a range of recent transportation projects using Geopier foundation systems in the United States. Of the 15 projects listed, nine were constructed in Iowa, two each in Texas and Maryland, and one each in Virginia and North Carolina. Six of the projects support mechanically stabilized earth (MSE) walls and concrete retaining walls, four provide slope reinforcement, and one each provide bridge approach settlement control (this study), tunnel repair, box culvert settlement control (this study), embankment support (this study), and railroad track support.

Table 1. Geopier Stress Concentration Factors

Applied Load	Stiffness Ratio	Reference
Footing	5 to 40	Lawton and Fox (1994)
Footing	30 to 45	Lawton and Merry (2000)
Embankment Fill	2 to 5	This study

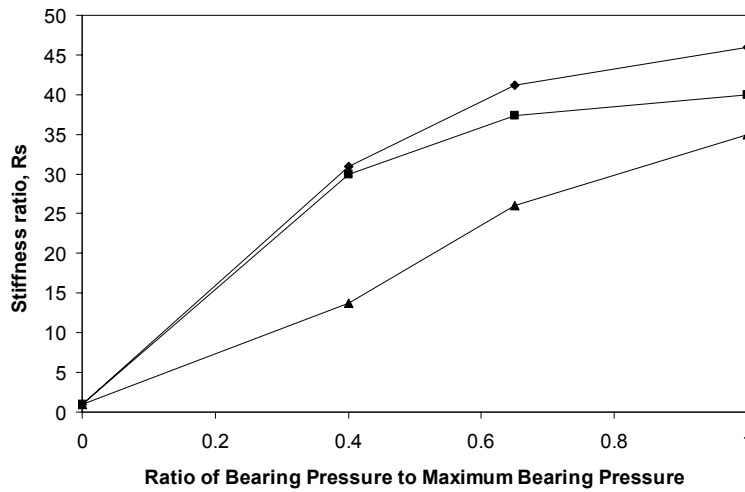


Figure 5. Stress Concentration Factors Measured for Instrumented Footing (Lawton and Merry 2000)

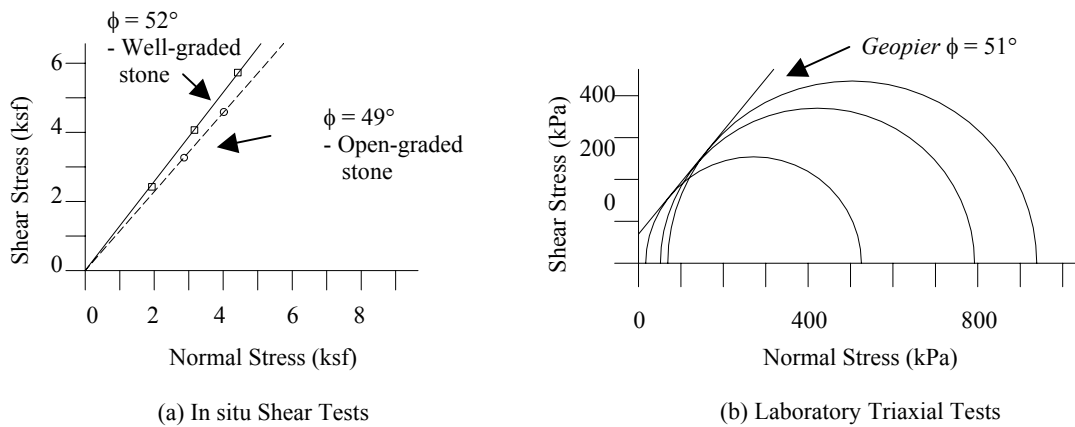


Figure 6. Results of Shear Strength Tests (Fox and Cowell 1998; White et al. 2002)

Table 2. Selected Geopier Transportation Projects to Date

Project	Location	Transportation Application
Maryland Rte 5 Widening	Prince George County, MD	Geopier support of concrete retaining wall including uplift anchors installed at heel of wall
Baltimore-Washington Parkway Slope Stability	Laurel, MD	Stabilization of failing embankment slopes along sections of B-W Parkway
Park Center	Alexandria, VA	Support of MSE retaining wall for grade separation near Morven Lane
Target Store	Raleigh, NC	Support of MSE retaining wall used to stop an active landslide near Lynn Road
Railroad Tunnel Reinforcement	Madrid, IA	Reduction of lateral stresses adjacent to RR tunnel culvert
Floyd County Bridge Approach – US Hwy 18/218	Floyd Co., IA	Reinforcement of a new embankment to reduce “bump at the end of a bridge”
Railroad Spur	Eddyville, IA	Global stability below a new RR embankment
50th Street Bridge	West Des Moines, IA	Global stability and settlement control below MSE wall for highway approach ramps
I35/Hwy 5 Embankment Foundations	Des Moines, IA	Settlement magnitude and time reduction for highway embankment
Road P48 Landslide Repair	Dallas County, IA	Stabilization of an active landslide adjacent to Road P48
Box Culvert Support – Hwy 191	Neola, IA	Support of new box culvert below highway bridge
U.S. Hwy 30 Embankment Stability	Le Grand, IA	Reinforcement of foundation soils beneath new highway embankment for global stability improvement
Union Pacific Railroad Bridge	Cedar Rapids, IA	Reinforcement of weak foundation soils and track support for railroad line.
Sienna Parkway MSE Wall Support	Missouri City, TX	Reinforcement beneath 35-ft tall MSE walls to improve global stability, increase bearing capacity, and control settlement
Westpark Tollway MSE Wall Support	Harris County, TX	Bearing capacity increase and settlement control of MSE walls

Comparison with Stone Columns

Geopier foundation systems are both like and unlike traditional stone columns. For both systems, construction results in an inclusion of aggregate within the matrix soil. Because of this similarity, design methods implemented to analyze each system are similar. However, the construction processes and end product are different. The results shown by this research, and the results of other evaluations, along with cited references, are presented in Table 3. A comparison of selected field test results is described later in this report.

Design of Geopier Foundation Systems

Fox and Cowell (1998) describe design procedures for Geopier foundation systems including settlement, slope stability, bearing capacity, and uplift resistance. Development of alternative design procedures for Iowa transportation applications is not warranted. Consistent with their patent protection, the Geopier® Foundation Company reserves the right to license construction operations and review designs.

Table 3. Comparison of Stone Columns and Geopier Rammed Aggregate Piers

Characteristic	Stone Columns	Geopier Rammed Aggregate Piers
<i>Construction</i>		
Formation of cavity	Vibroflot	Drilling
Backfill	Crushed stone	Crushed stone
Backfill lift thickness	2 to 4 ft. (Barksdale and Bachus 1983, p. 20)	1 ft. (Fox and Cowell 1998)
Depth of installation possible	Up to ~ 100 ft.	Up to ~ 30 ft.
Column diameter	2 to 5 ft. (Barksdale and Bachus 1983, p. 13)	2 to 3 ft. (Fox and Cowell 1998)
Backfill densification	Vibroflot	Impact ramming with beveled tamper
Site condition after construction	Jetting, if used, causes water ponding at ground surface (Barksdale and Bachus 1983); ground heave (no reference)	Spoils from drilling must be removed (no reference)
Densification of clean sand to large radial distances	Effective	Not effective
<i>Measured Design Parameter Values</i>		
Aggregate friction angle	40 to 45 degrees (Barksdale and Bachus 1983, p. 158)	48 to 52 degrees (Fox and Cowell 1998; White 2002)
Response of matrix soil to construction	Complete remolding of soil during installation – formation of smear zone (Barksdale and Bachus 1983, p. 19); lateral earth pressure approximately represented by K_o conditions (Gaul 2001; White et al. 2002a)	Increase in lateral earth pressure to approximate K_p conditions (Lawton and Merry 2000; White et al. 2000; Gaul 2001; White et al. 2002; Handy et al. 2002)
Average SPT N-value in column	11 (Gaul 2001; White et al. 2002)	17 (Gaul 2001; White et al. 2002)
Stress concentration ratio	2 to 5 (Barksdale and Bachus 1983, p. 143)	4 to 45 (Lawton and Fox 1994; Lawton and Merry 2000; Hoevelkamp 2002)
Modulus of elasticity	600 ksf to 1,200 ksf	3,000 to 4,000 ksf (Wissmann et al. 2001)
Typical unit cell loading	40 to 100 kips (Barksdale and Bachus 1983, p. 3)	30 to 150 kips for foundation support (Fox and Cowell 1998); as high as 200 kips for floor slab applications (Minks et al. 2001); as high as 800 kips for stability applications (Hall et al. 2002)
Ratio of applied stress required to initiate bulging (Geopier: stone column)	~ 4:1 (Gaul 2001)	
Ratio of Geopier rammed aggregate pier stiffness to stone column stiffness	~ 2 to 15 (Gaul 2001; White et al. 2002)	

Table 3. Comparison of Stone Columns and Geopier Rammed Aggregate Piers (continued)

Generalized Behavior		
Design stress during load test	100% to 150% top of stone column design stress (Barksdale and Bachus 1983, p. 23)	150% top of pier design stress (Fox and Cowell 1998)
Typical load transfer mechanism	End-bearing (Barksdale and Bachus 1983, p. 27)	Floating (Lawton and Fox 1994; Lawton et al. 1994; Fox and Cowell 1998; Lawton and Merry 2000; Wissmann et al. 2000; Wissmann et al. 2002)
Typical mode of deformation	Bulging (Barksdale and Bachus 1983, p. 27)	Bulging or tip stress (Wissmann et al. 2001c)
Effect of adjacent elements on propensity for bulging	More elements provides less propensity for bulging (Barksdale and Bachus 1983, p. 29)	More elements provides less propensity for bulging (Hoevelkamp 2002)
Effect of group on punching bearing capacity	—	Bearing capacity of group \geq sum of bearing capacities of individual piers (Hoevelkamp 2002)
Design Approaches		
Method of calculation of bulging stress	Cavity expansion theory (Hughes and Withers 1974; Mitchell 1981; Barksdale and Bachus 1983)	Cavity expansion theory considering rammed aggregate pier construction process (Hughes and Withers 1974; Mitchell 1981; Wissmann 2000)
Method of computing time rate of settlement using radial drainage	Combined vertical and radial flow using principle of stress concentration; account for smearing (Barksdale and Bachus 1983, pp. 69-74; Han and Ye 2001)	Combined vertical and radial flow using principal of stress concentration; no smearing (Han and Ye 2001; Wissmann et al. 2002; FitzPatrick and Wissmann 2002)
Method of computing settlement magnitude	Chart solution based on unit cell equilibrium method (Barksdale and Bachus 1983, pp. 42-46)	Upper zone/lower zone model – upper zone model incorporates unit cell equilibrium method (Lawton and Fox 1994; Lawton et al. 1994; Fox and Cowell 1998; Wissmann et al. 2000; Hoevelkamp 2002; Wissmann et al. 2002)
Method of computing bearing capacity of a group of elements	Terzaghi linear “lower bound” triangular block method (Barksdale and Bachus 1983)	Terzaghi linear “lower bound” triangular block method with shape correction factor (Barksdale and Bachus 1983; Wissmann et al. 2002)
Method of calculating increase in global stability	Weighted average of shear strength values including concept of stress concentration (Mitchell 1981, pp. 37-38; Barksdale and Bachus 1983, pp. 76-83)	Weighted average of shear strength values including concept of stress concentration (Mitchell 1981, pp. 37-38; Barksdale and Bachus 1983; FitzPatrick and Wissmann 2002)

RESULTS AND DISCUSSION

Project No. 1: Embankment Foundation Reinforcement at US Hwy 5/I-35 (Des Moines, IA)

This section of the report presents the results of geotechnical measurements obtained at two adjacent embankment sites where the foundation soils were improved with stone columns and Geopier soil reinforcing elements. Figure 7 shows the location of the research site. Although the purposes of the installations are different, the installation of granular columnar elements at adjacent sites with similar foundation soil characteristics provided the opportunity to compare the behavior and engineering properties of both systems.

At the test site, stone columns were installed to depths ranging from 3 to 14 m to reduce settlement and increase the factor of safety against global slope instability prior to construction of a 9 m high bridge approach embankment. On the adjacent test site, Geopier elements were installed around the abutment footprint to depths ranging from 4.5 to 6.5 m prior to construction of the 8 m fill embankment. The purpose of the Geopier elements was simply to reduce the magnitude and increase the time rate (≤ 30 days) of settlement to facilitate rapid abutment construction. The initial four to five meters of fill was placed in July 2000 and the final four to five meters of fill was placed during summer 2001. Figure 8 is a simplified cross-section of the Ramp C embankment. Figures 9 through 12 show the installation plans and embankment construction at both sites.

Prior to placement of embankment fill, SPTs, BSTs, PMTs, and K_0 stepped blade tests were conducted. SPTs through production piers provide a measure of density of the compacted aggregate. BST friction angle measurements provide for the estimation of the in situ coefficient of lateral earth pressure prior to placement of the aggregate piers. Lateral stress was measured in the matrix soils surrounding both types of elements with the K_0 stepped blade. Until recently, effects of lateral prestressing, induced by a variety of foundation systems, have been conservatively neglected largely due to lack of field data showing a contribution to the performance of the system. Handy (2001) describes a lateral stress theorem suggesting that lateral stress induced from foundation systems such as displacement piles, tapered piles, Geopier elements, and others can theoretically reduce settlement by creating a near-linear-elastic, stress-reinforced zone within the matrix soils.

Lastly, full-scale load tests on isolated elements were conducted and settlement plates and stress cell instrumentation were installed and monitored for a period of one year. The settlement plates were installed to monitor and compare settlements on individual pier elements and on the surrounding matrix soils. This research represents the first reported comparison of stone columns and Geopier soil reinforcing elements used below bridge approach embankments.

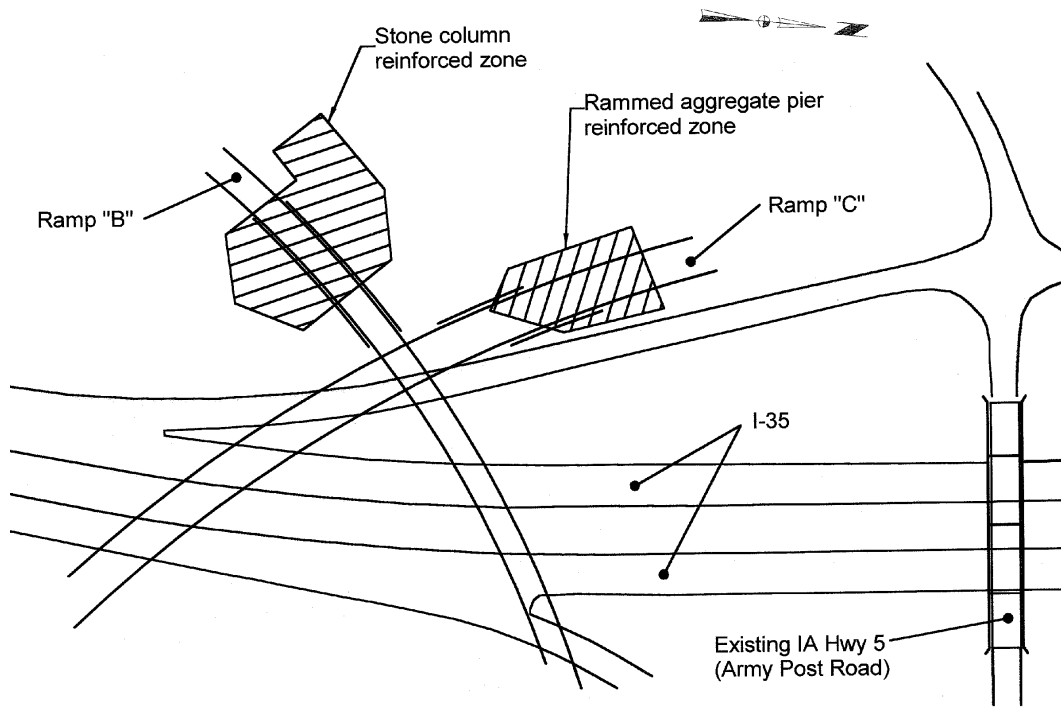


Figure 7. IA Hwy 5/I-35 Research Site

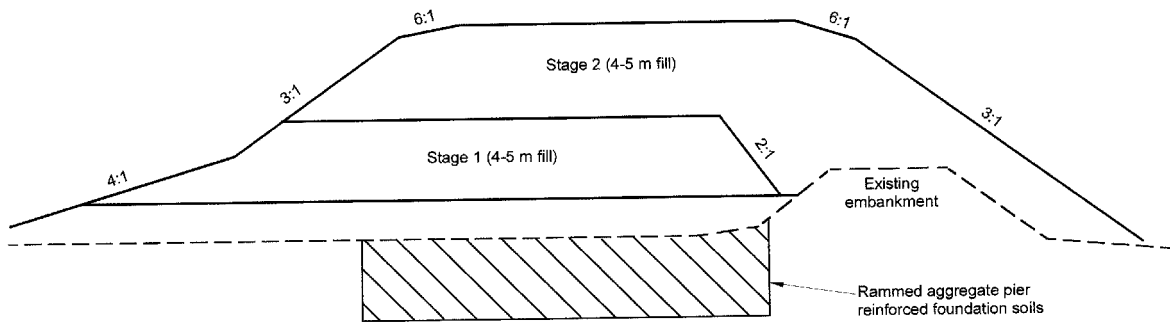


Figure 8. Ramp C Embankment Cross Section

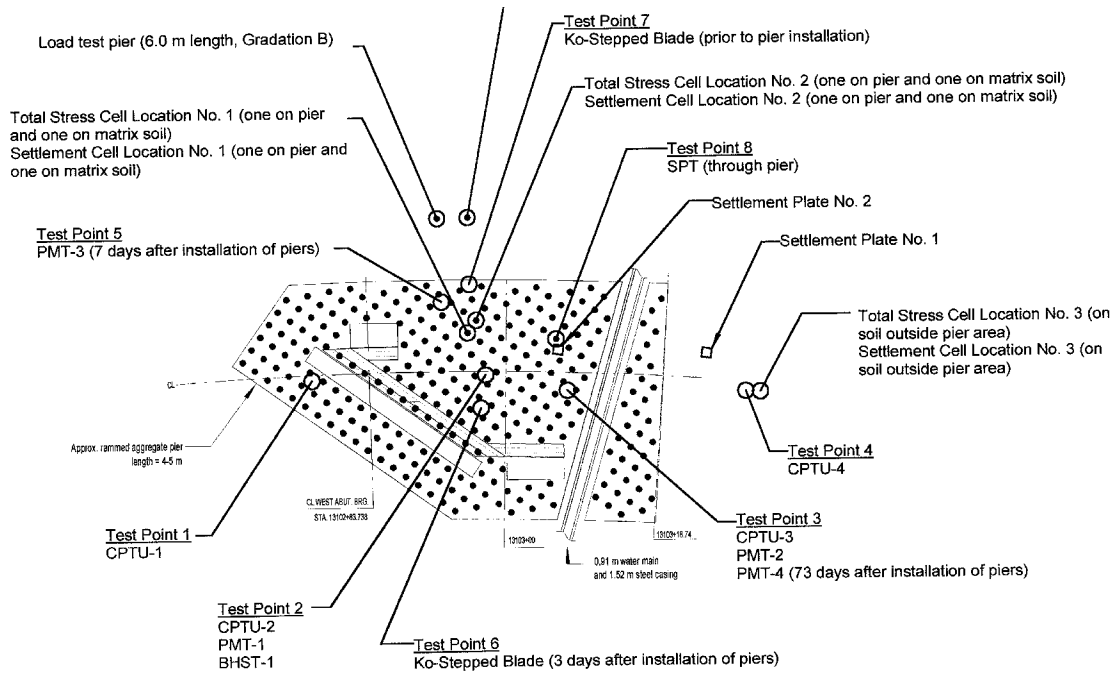


Figure 9. Ramp C Test and Instrumentation Locations for Geopier Installation

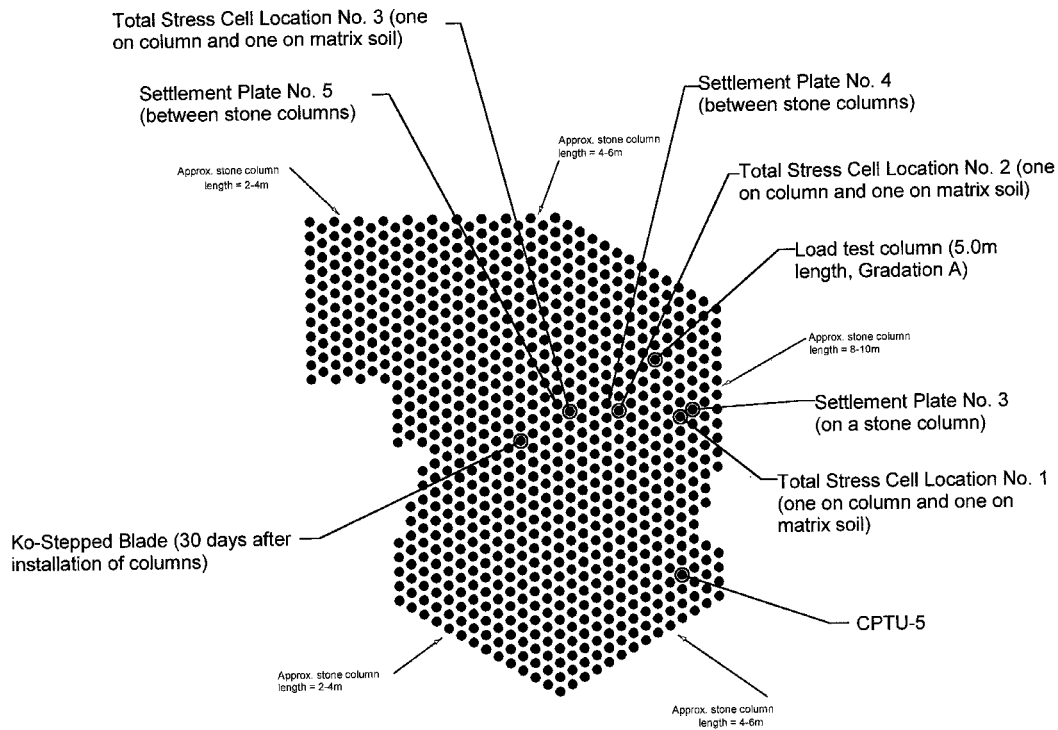


Figure 10. Ramp B Test and Instrumentation Locations for Stone Column Installations



Figure 11. Ramp C Geopier Supported Embankment



Figure 12. Ramp B Stone Column Supported Embankment

Stone Column Site

This site is underlain by 2 to 13 m of compressible clay and silt overlying highly weathered shale, dipping approximately 11 degrees. CPT results, shown in Figure 13, indicate that corrected tip resistances (q_T) in the clay and silt generally range between about 650 to 1000 kPa and CPT friction ratio (R_f) values range between about 2 to 3. Slope stability calculations performed prior to construction revealed inadequate factors of safety against global instability along the sloping weathered shale interface. Stability concerns led to the specification of stone columns for shear reinforcement. A friction angle equal to 38 degrees was assumed in design stability calculations.

Stone columns were installed in an equilateral triangular pattern 1.8 m on-center (see Figure 14) to depths of 3 to 14 m below grade using the dry bottom feed technique (vibro-displacement). Stone column installations were facilitated with a horizontal oscillating vibroflot well described in the literature (e.g. Jebe and Bartels 1983; Munfakh et al. 1987; Elias et al. 2000). The crane-mounted, vibroflot probe penetrated the ground under static weight with the assistance of vibration and air. After reaching the design elevation, the vibroflot was withdrawn while aggregate was deposited out through the probe. As a possible quality-control tool during construction, the amperage pulled by the oscillating vibroflot motor was recorded and compared to CPT skin friction values (f_s). A comparison is presented in Figure 15. With more evaluation and study, future stone column projects could use this relationship to determine required vibroflot penetration depth to a suitable bearing layer.

Aggregate was placed in approximately 1.5 m lifts and compacted by raising and lowering the probe. Aggregate gradation characteristics are provided in Figure 16. The installation of stone columns at this site was advantageous because large diameter and long elements were needed. Figure 17 shows the equipment and construction operations.

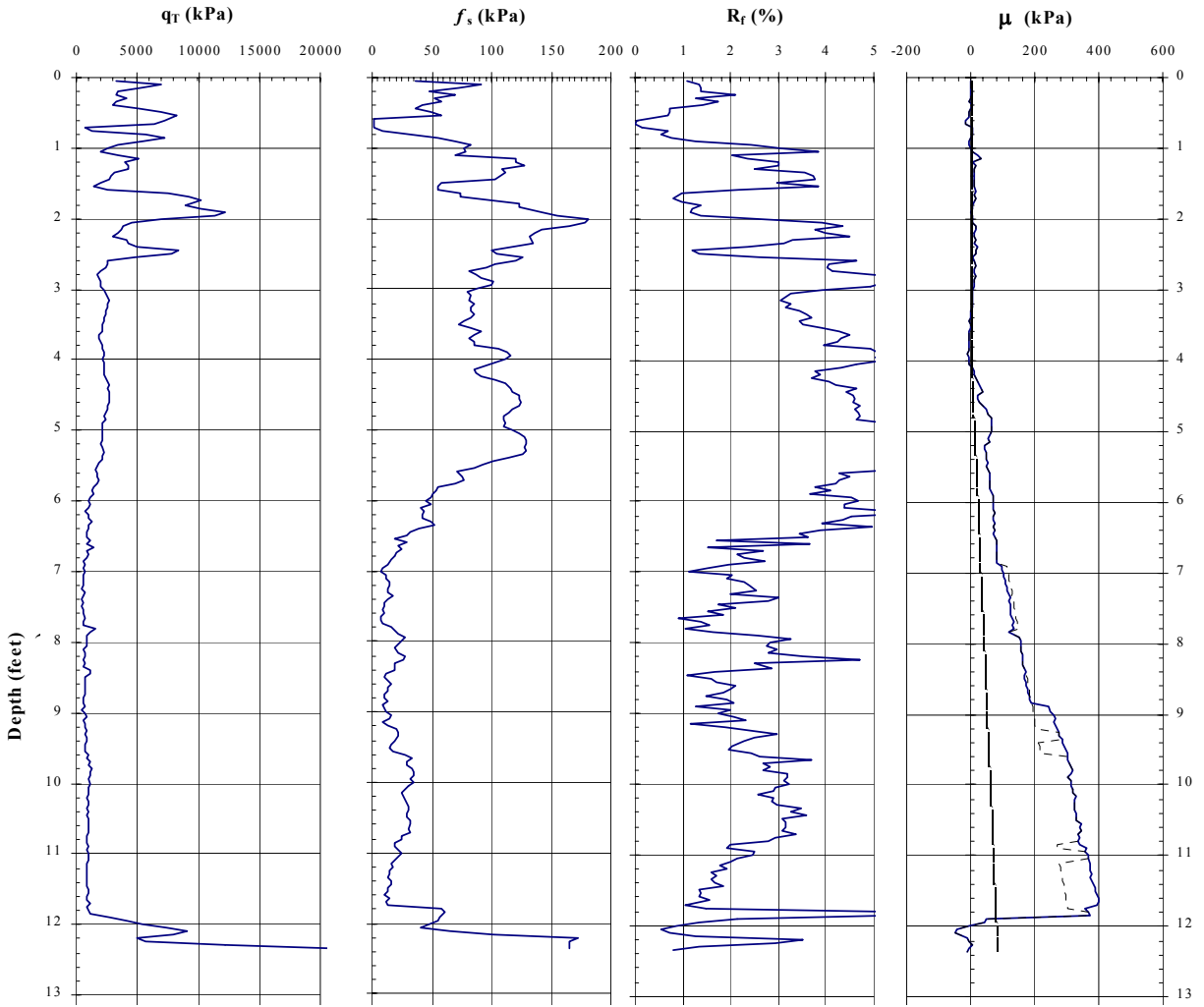
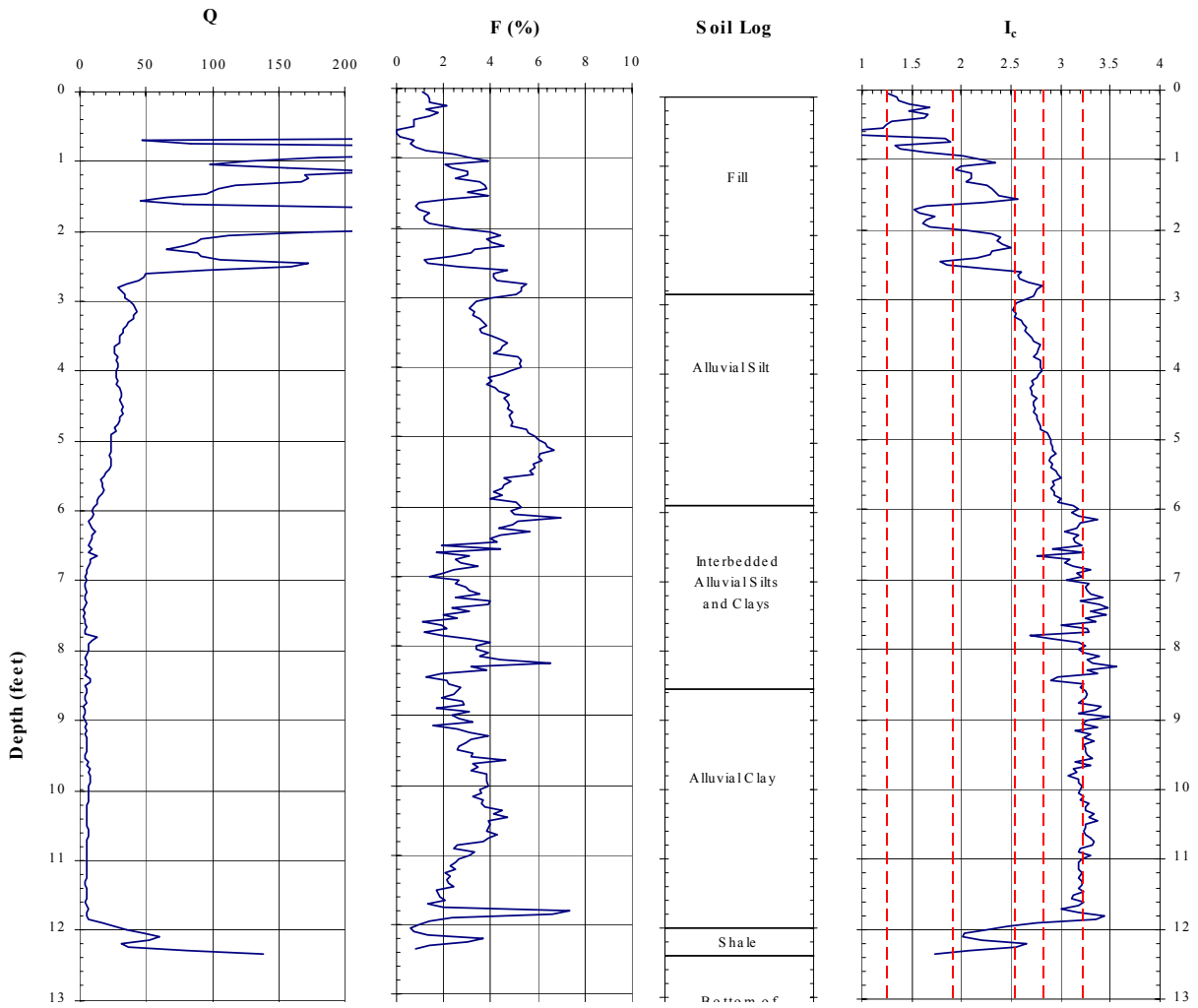


Figure 13. Cone Penetration Test Results for Ramp B (CPTU-5)—Stone Column Site



**Figure 13. Cone Penetration Test Results for Ramp B (CPTU-5) – Stone Column Site
(continued)**

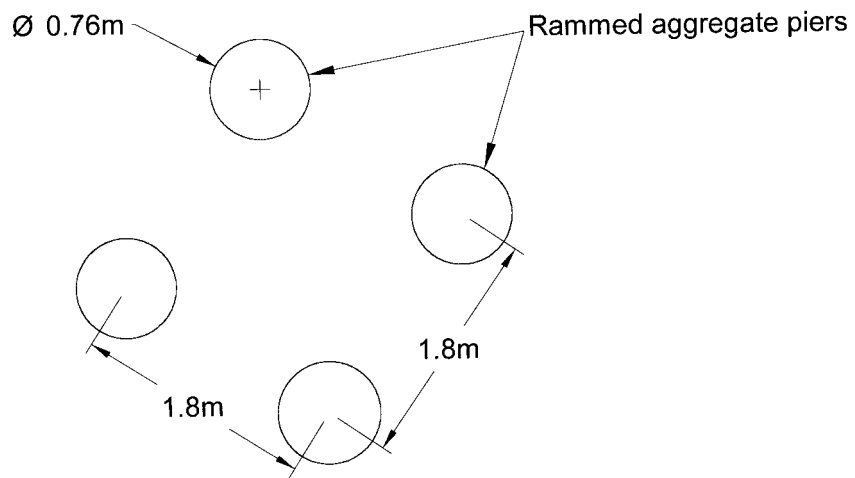
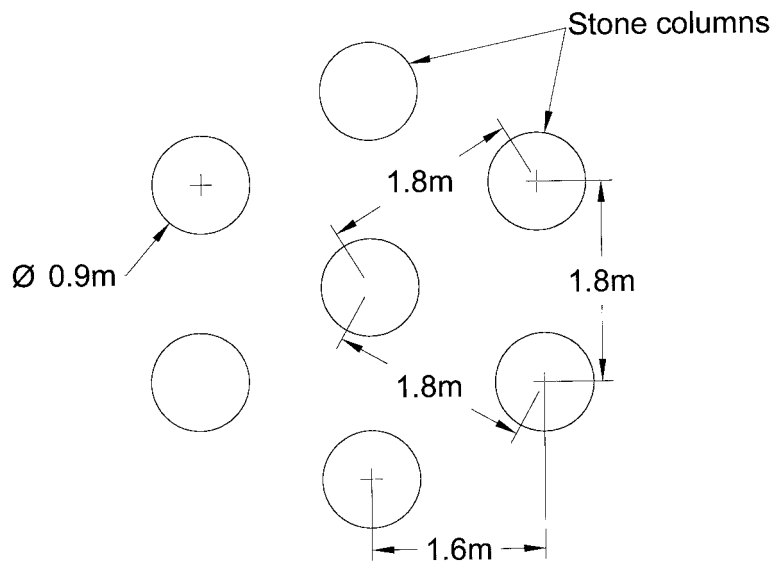


Figure 14. Stone Column and Geopier Element Spacings

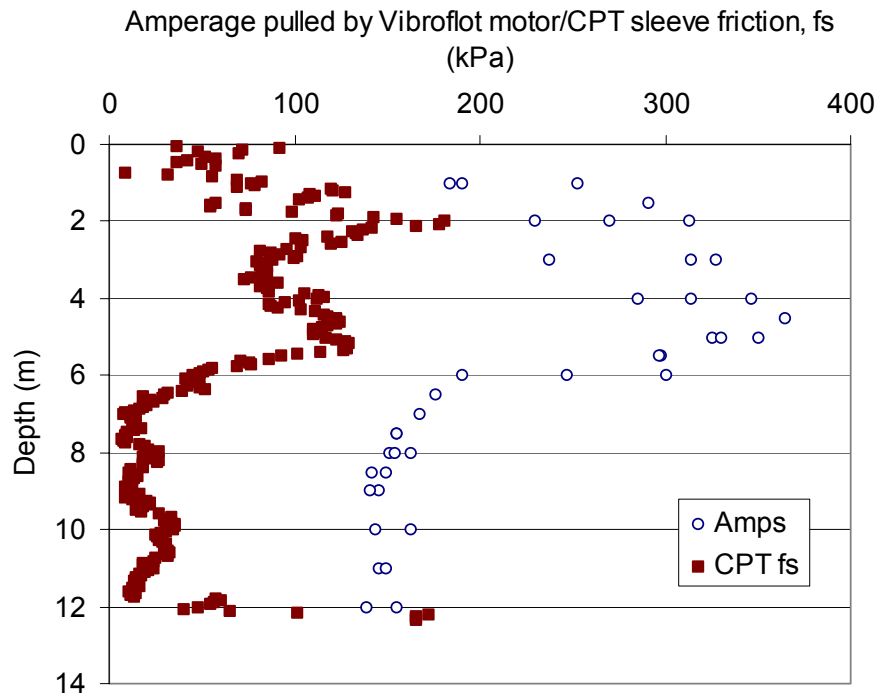


Figure 15. Relationship Between Amperage Pulled by Vibroflot Motor and CPT Skin Friction at Stone Column Site

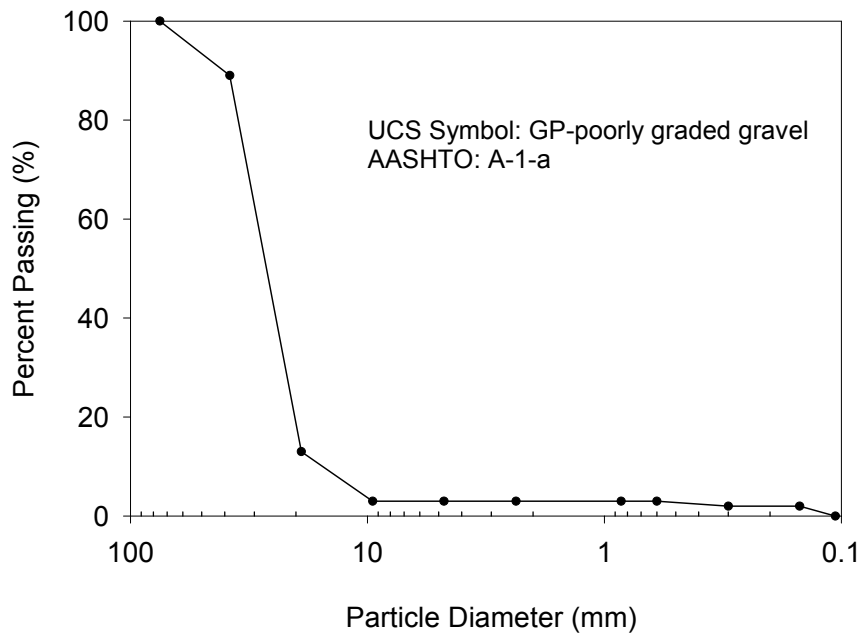


Figure 16. Grain-Size Distribution of Aggregate Used in Construction of Stone Columns and Geopier Elements (Same Aggregate for Both Sites)



Figure 17. Stone Column Construction Operations

Geopier Site

This site is underlain by 5 to 6 m of compressible clay overlying alluvial sand and highly weathered shale. CPT results, shown in Figure 18, indicate that the corrected tip resistances (q_T) in the clay layer ranges from about 400 to 950 kPa. CPT friction ratio (R_f) values range from about 4 to 7 within the clay layer. The complete CPT results are provided in Appendix A.

Settlement calculations, based on laboratory odometer testing performed prior to construction, predicted excessive settlement magnitudes (about 34 cm) and inadequate time rates as a result of fill placement. Figure 20 and Table 4 present the consolidation parameters used in the settlement predictions. Geopier elements were specified to reduce the total settlement magnitude (<8 cm) and time of consolidation (≤ 30 days). Since the open-graded granular Geopier elements have a higher permeability than the matrix soil, increased rate of consolidation was expected. Aggregate gradation characteristics are the same as used for stone columns, shown in Figure 16.

Laboratory consolidated drained triaxial compression, unconfined compressive strength, and soil index test results are presented in Figures 19, 21 and 22, respectively.

The Geopier elements were constructed in a square pattern 1.8 m on-center. Depths ranged from 4.5 to 6.5 m, which correspond to an underlying sand layer identified from CPT results (Figure 18). Each element, 0.76 m in diameter, was constructed by building successive layers (0.3 m thick) of densely compacted aggregate. Construction operations are shown in Figure 23. It is estimated that each aggregate lift is subjected to about 0.8 MNm of high-energy impact ramming action (Handy et al. 1999), which reportedly generates about 2500 kPa of lateral stress in the surrounding matrix soils (White et al. 2000). On a per meter basis, Geopier soil reinforcement and stone column installations were comparable in cost at this project.

Comparison of Site Characteristics

Although the test sites are very close together, some differences in site conditions were observed. Table 5 presents a comparison of characteristics for the stone column and Geopier sites. The ratio of the CPT tip resistances for the stone column site to the Geopier site is approximately 1.2. This ratio suggests that the clay and silt material at the stone column site is slightly stiffer than the materials at the Geopier site. During stone column construction some holes had to be pre-drilled due to vibroflot refusal. CPT friction ratio values at the stone column site are lower than those at the Geopier site. Lower friction ratio values are generally interpreted to suggest a less cohesive response for the tested soils (Douglas and Olsen 1981).

Element spacings for both sites are similar; however, the end bearing materials are different. The stone columns were designed to extend much deeper and to a minimum of 0.6 m into the underlying highly weathered shale; whereas, the Geopier elements only extend to the underlying sand layer. The Geopier elements were designed to penetrate the underlying sand layer to complete the drainage pathway out of the clay layer, thus facilitating consolidation. The smaller diameter of the Geopier elements results in a smaller replacement ratio (ratio of the cross-sectional area of an element to the area of each unit “cell” reinforced by the element) than the area replacement ratio for the stone column site.

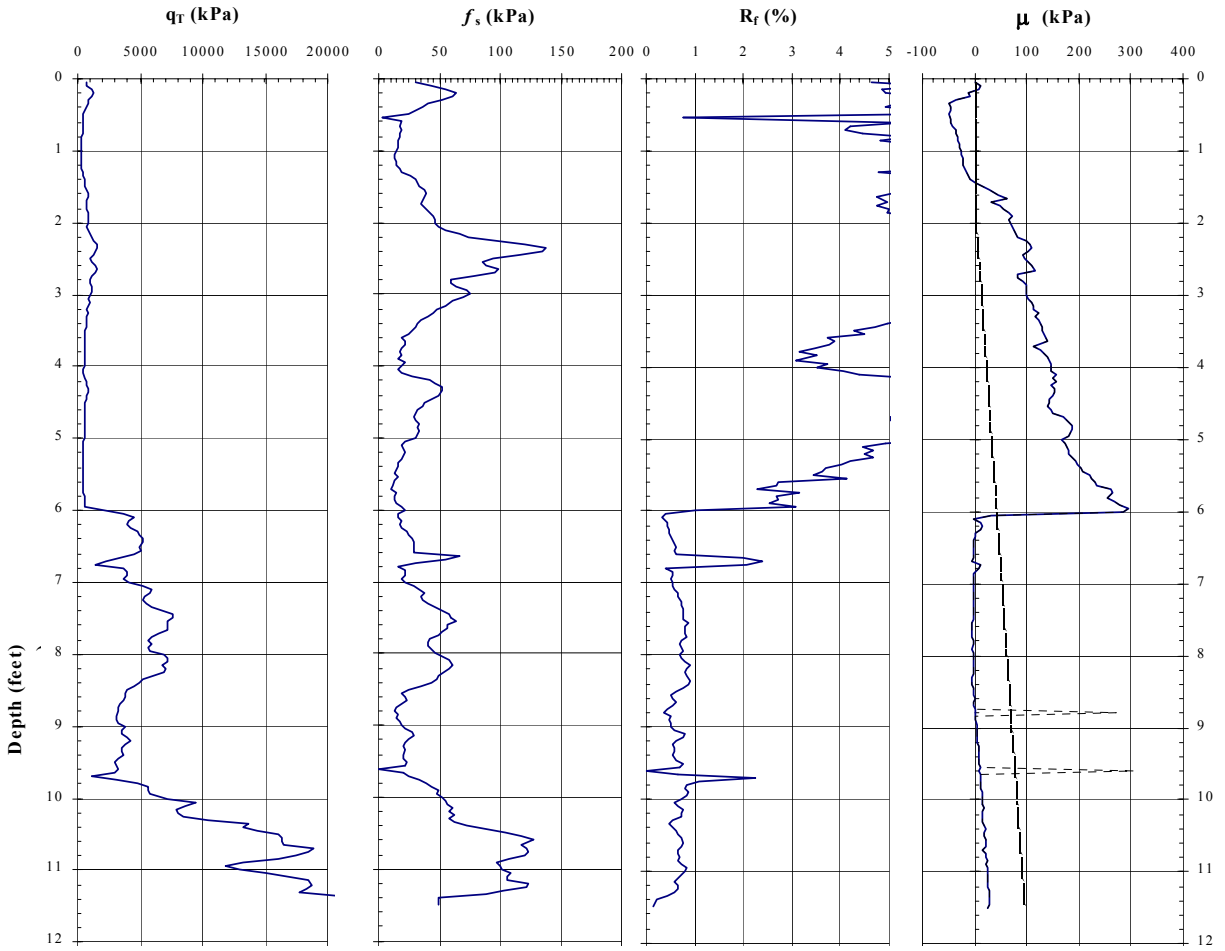


Figure 18. Cone Penetration Test Results for Ramp C (CPTU-2)—Geopier Site

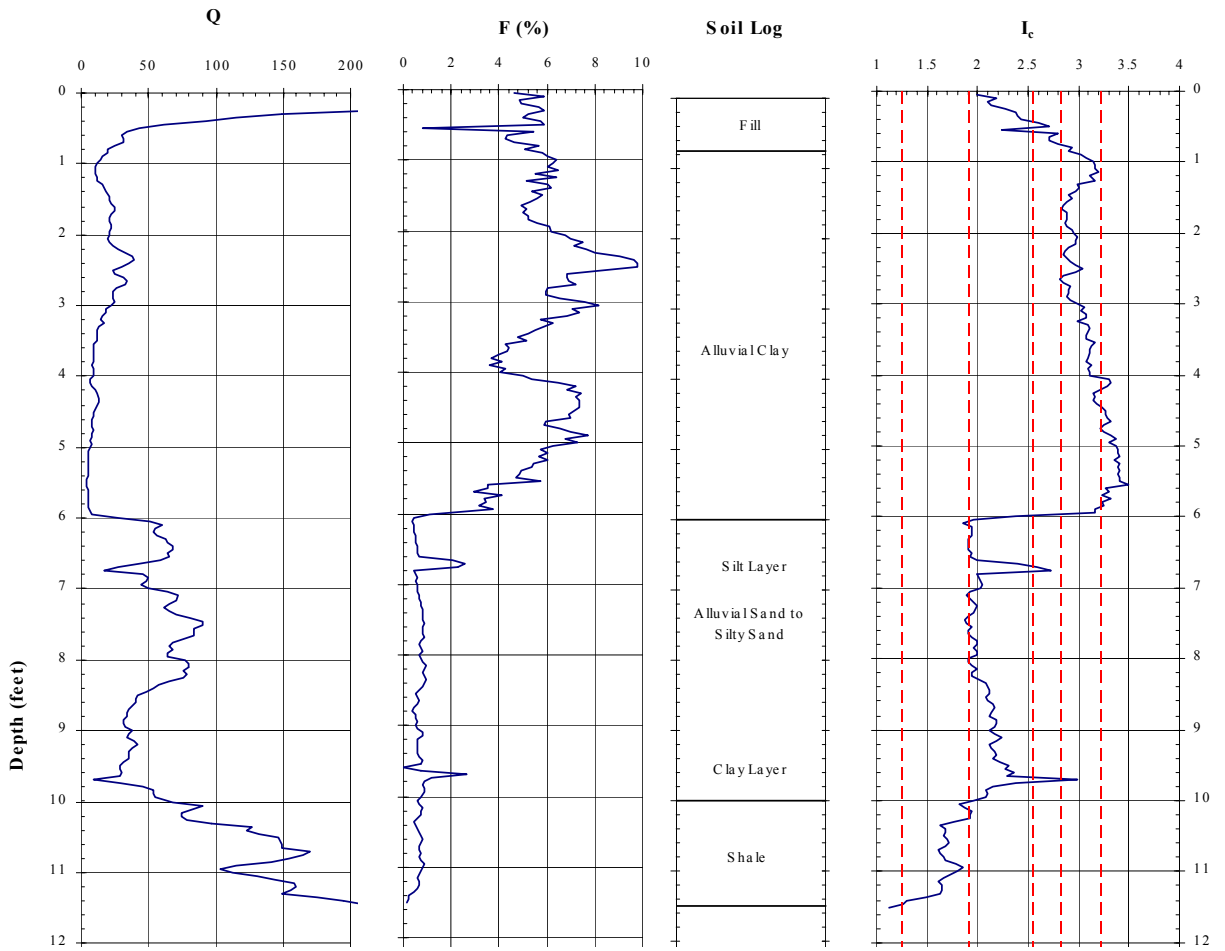


Figure 18. Cone Penetration Test Results for Ramp C (CPTU-2) – Geopier Site (continued)

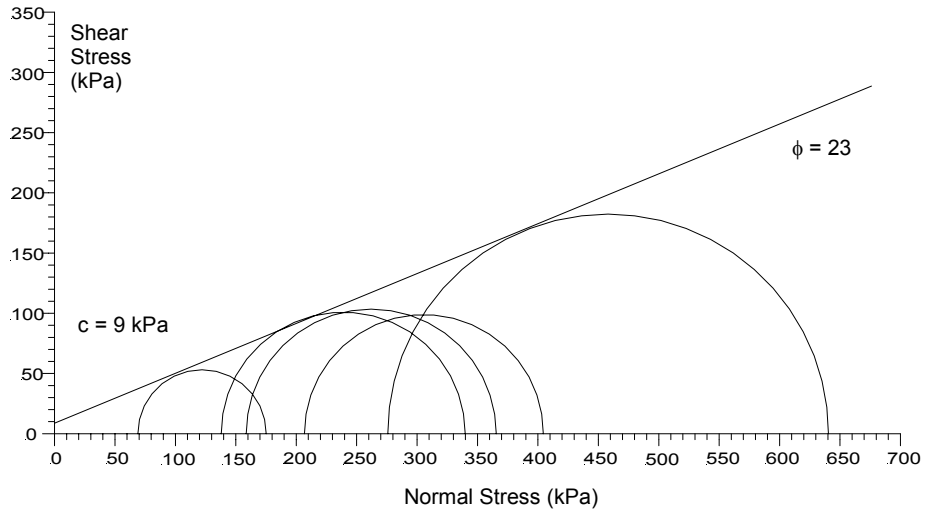
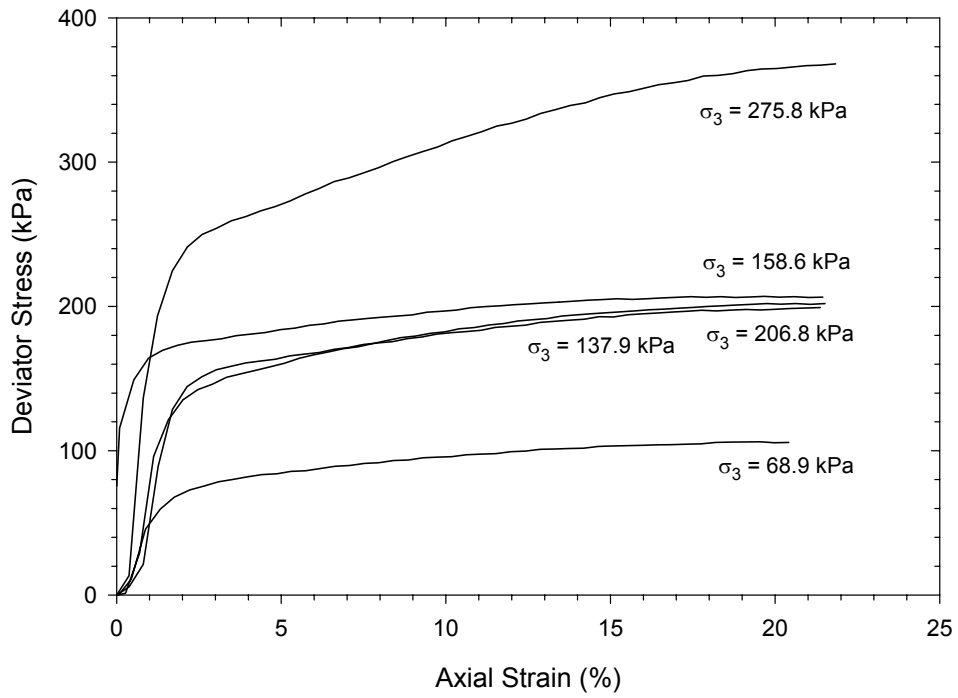


Figure 19. Consolidated Drained Triaxial Compression Test Results for Soil at Depth of 2.59 m at Geopier Site

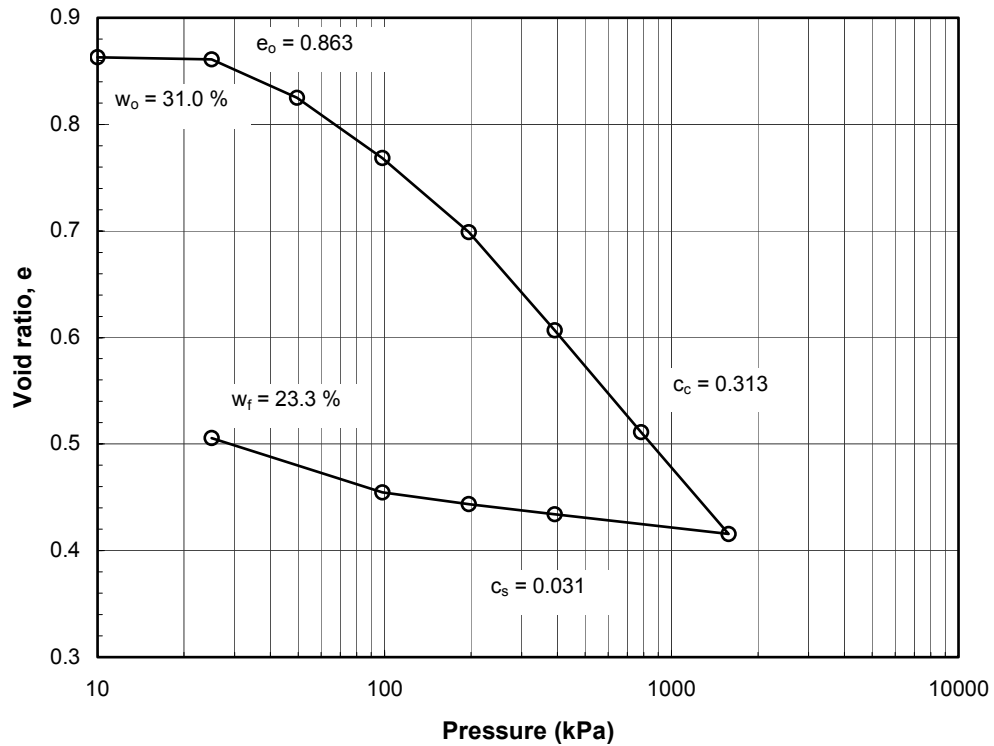


Figure 20. e-log-p Curve for the Normally Consolidated, Compressible Clay at Depth of 2.7 m at Geopier Site

Table 4. Summary Consolidation Parameters from Iowa DOT and ISU Tests at Geopier Site

Test No.	c_v (m^2/day)	AASHTO Classification	Depth (m)	Moisture Content (%)	Source
1	0.232	A-6 (19)	1.0	32	Iowa DOT
2	0.074	A-6	2.7	31	ISU
3	0.130	A-6 (15)	4.0	29	Iowa DOT

Note: Average $c_v = 0.145 m^2/day$ used for time-settlement calculations.

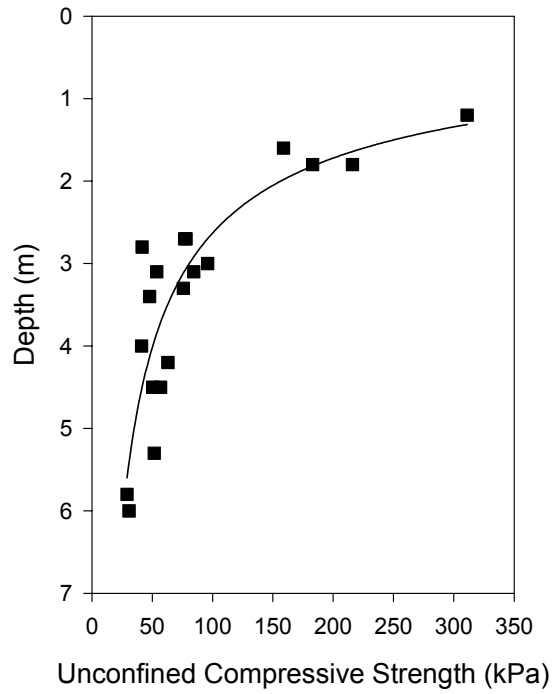


Figure 21. Unconfined Compressive Strength Results at Geopier Site

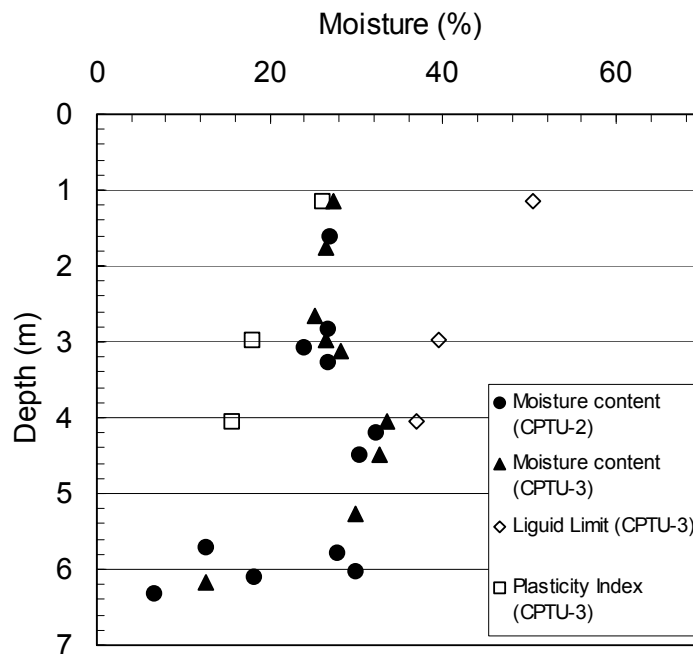


Figure 22. Soil Index Test Results for Geopier Site



Figure 23. Geopier Construction Operations

Table 5. Comparison of Site Characteristics

Characteristic	Stone Column Site	Geopier Site
Depth to bearing layer (m)	3 to 13	4 to 6
CPT tip resistance (kPa)	650 to 1000	400 to 950
CPT friction ratio (%)	1.7 to 2.9	3.8 to 6.7
Element installation depth (m)	3.0 to 14.0	4.5 to 6.5
Element diameter (m)	0.91	0.76
Element spacing (m)	1.8 (equilateral triangle)	1.8 (square)
Area replacement ratio (%)	23	14
Embankment fill height (m)	9	8
Number of elements	871	234

Geotechnical Measurements

To characterize engineering properties of the stone column and Geopier elements the following in situ tests were performed:

- BSTs within the matrix foundation soils
- SPTs within production stone column and Geopier elements
- Ko stepped blade tests within the matrix soils surrounding production stone column and Geopier elements
- PMTs within matrix soils surrounding production Geopier elements
- Full-scale load tests on individual stone column and Geopier elements

Borehole Shear Test Results

BSTs were performed prior to installation of Geopier elements as a rapid and direct means to measure soil cohesion (c') and friction angle (ϕ') on a drained or effective stress basis. Handy and Fox (1967) described the test procedure in detail. The test consists of expanding diametrically opposed contact plates into a borehole under constant normal stress, then allowing the soil to consolidate, and finally by pulling and measuring the shear stress. Points are generated on the Mohr-Coulomb shear envelope by measuring the maximum shear resistance at successively higher increments of applied normal stress.

The results of the BST measurements, shown in Table 6, indicate that the effective stress friction angle of the clay soils at the Geopier site vary between 11 and 32 degrees; the effective stress cohesion intercept varies between 3 kPa and 36 kPa. The variability in the measured shear strength parameter values is likely related to the alluvial nature of the soil. Complete BST data are provided in Appendix B.

Table 6. BST Shear Strength Parameter Values at Geopier Site

Depth (m)	Cohesion, c' (kPa)	Friction Angle, ϕ' (degrees)
1.20	38	13
1.80	36	19
2.59*	9*	23*
2.70	22	25
2.80	9	23
3.40	16	24
4.11	20	18
4.60	15	30
5.20	16	11
6.00	3	32

* Note: Consolidated drained triaxial test (see Figure 19).

Standard Penetration Test Results

The results of 42 SPT N-values taken within stone columns and 6 SPT N-values taken within Geopier elements are shown in Figure 24. An average N-value of approximately 11 was achieved for the stone columns; an average N-value of approximately 17 was achieved for the Geopier elements. The ratio of the average N-value for the Geopier elements to the stone columns is about 1.5. Reportedly, N-value is proportional to friction angle (Shioi and Fukui 1982). In the literature stone column friction angle varies from 35 to 45 degrees (Greenwood 1970; Rathgeb and Kutzner 1975; Goughnour and Barksdale 1984), whereas, Geopier friction angle measurements are reported at 49 to 52 degrees (Fox and Cowell 1998).

The ratio of shear strength of the Geopier elements to the stone columns can be calculated by assuming equal normal stress and taking the ratio of the average coefficient of friction angle of the Geopier elements ($\tan 50^\circ$) to the average coefficient of friction angle of the stone columns ($\tan 40^\circ$). The ratio of the tangents of the friction angle values for Geopier elements and stone columns is about 1.4, a value similar to the ratio of the tested N-values for the elements. The difference in friction angle is attributed to increased compaction.

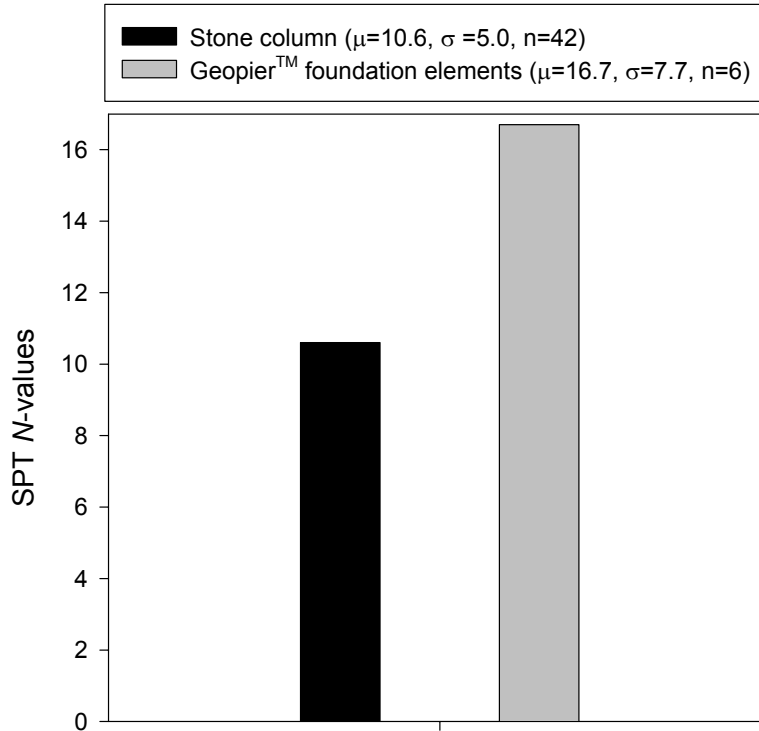


Figure 24. Comparative SPT N-values through Production Stone Columns and Geopier Elements

Ko Stepped Blade Results

The results of Ko stepped blade test measurements are presented in Figure 25. The Ko stepped blade (see Figure 26) is a device developed at ISU and uses lateral stress measurements taken at pressure cells embedded in the blade with variable thickness to determine in situ (zero blade width) lateral stress (Handy et al. 1982). Measurements adjacent to the stone columns were made in a tangential orientation (perpendicular to lines extending outward from the center of the element) at a radial distance of 70 cm from the edge of the stone column. Measurements adjacent to the Geopier elements were also made in a tangential orientation at a slightly larger distance of 85 cm from the edge of the pier. As shown in Figure 25, test measurements are normalized by the estimated in situ vertical effective stress at the test depth, and thus may be interpreted to be the effective horizontal earth pressure coefficient (k) after pier installation. Also shown in Figure 25 is the estimated in situ coefficient of lateral earth pressure at rest, using the well-know expression for normally consolidated soils ($1 - \sin\phi$). Estimated values are made using the BST test results summarized in Table 6.

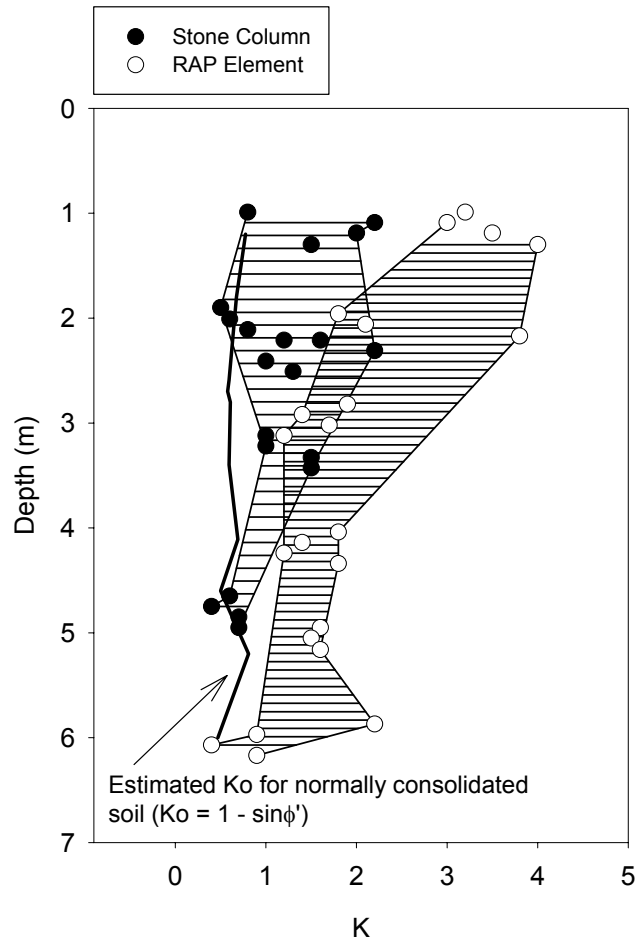


Figure 25. K_o Stepped Blade Measurements Conducted 70 cm from Stone Column and 85 cm from Geopier Element (All Tests Oriented to Measure Radial Stress)



Figure 26. K_o Stepped Blade Test Equipment

Results of the measurements shown in Figure 25 indicate that the post-installation values for coefficient of lateral earth pressure at the stone column site range between 0.4 and 2.2 with an average of 1.2. At the Geopier site, the coefficient of lateral earth pressure ranges between 0.4 and 4.0 with an average of 2.1, which is very close to the calculated Rankine coefficient of passive earth pressure, 2.3. Test results are summarized in Table 7. Lateral stress measurements at other Geopier sites have also shown passive stress development in the foundation soils (Handy et al. 2002; White et al. 2000).

Table 7. Results of Lateral Stress Measurements

Lateral Earth Pressure Coefficient Condition	Stone Column Site (70 cm radial distance)	Geopier Site (85 cm radial distance)
Range of data	0.4 to 2.2	0.4 to 4.0
Average of data	1.2	2.1
Ratio of average of data to K_0 average	1.8	3.3
Ratio of average of data to Rankine K_p average	0.5	0.9

Test results indicate that greater post-installation lateral earth pressures are measured in the soil surrounding the Geopier elements than in the soil surrounding the stone columns, despite the measurements for the stone column being 15 cm closer to the edge of the element than are the measurements for the Geopier test element. During stone column installation, ground heave (0.8 to 1.0 m) and radial cracking were observed at the surface, whereas no ground heave and minimal radial cracking were observed at the Geopier site. Furthermore, field diameter measurements indicate that cavity expansion during stone column construction averaged about 30 percent; whereas, the Geopier element installations resulted in about 10 percent cavity expansion. An explanation of why higher lateral stress was measured at the Geopier site is that soil fabric at the stone column site was highly disturbed due to excessive cavity expansion, subsequent ground heave, and radial cracking. Thus, the shear strength may have been reduced to residual values and therefore did not have that capacity (i.e. strength) to retain high lateral stresses.

Pressuremeter Test Results

To further study changes in matrix soil properties at the Geopier site, PMTs were performed before installation and 7 and 73 days after construction. The purpose of repeating the tests after construction was to provide an assessment of changes in soil stiffness and strength. PMTs were conducted at the locations shown in Figure 9. All tests were conducted within the alluvial clay layer with the exception of the 5.9 and 6.1 m tests where sand may have been encountered. Further, all tests were conducted within a 7 m radius of each other, for this reason it is assumed that tests at like depths within this region encountered similar material.

Figure 27 shows the results of pressuremeter tests prior to and following installation of Geopier elements. No significant changes in pressuremeter modulus (E_p) or limit pressure (p_L) were evident from these tests. Future PMT testing should be conducted to evaluate the long-term (>6 months) effects of Geopier foundation installation on matrix soil stiffness and strength. Complete PMT pressure-volume results are provided in Appendix C.

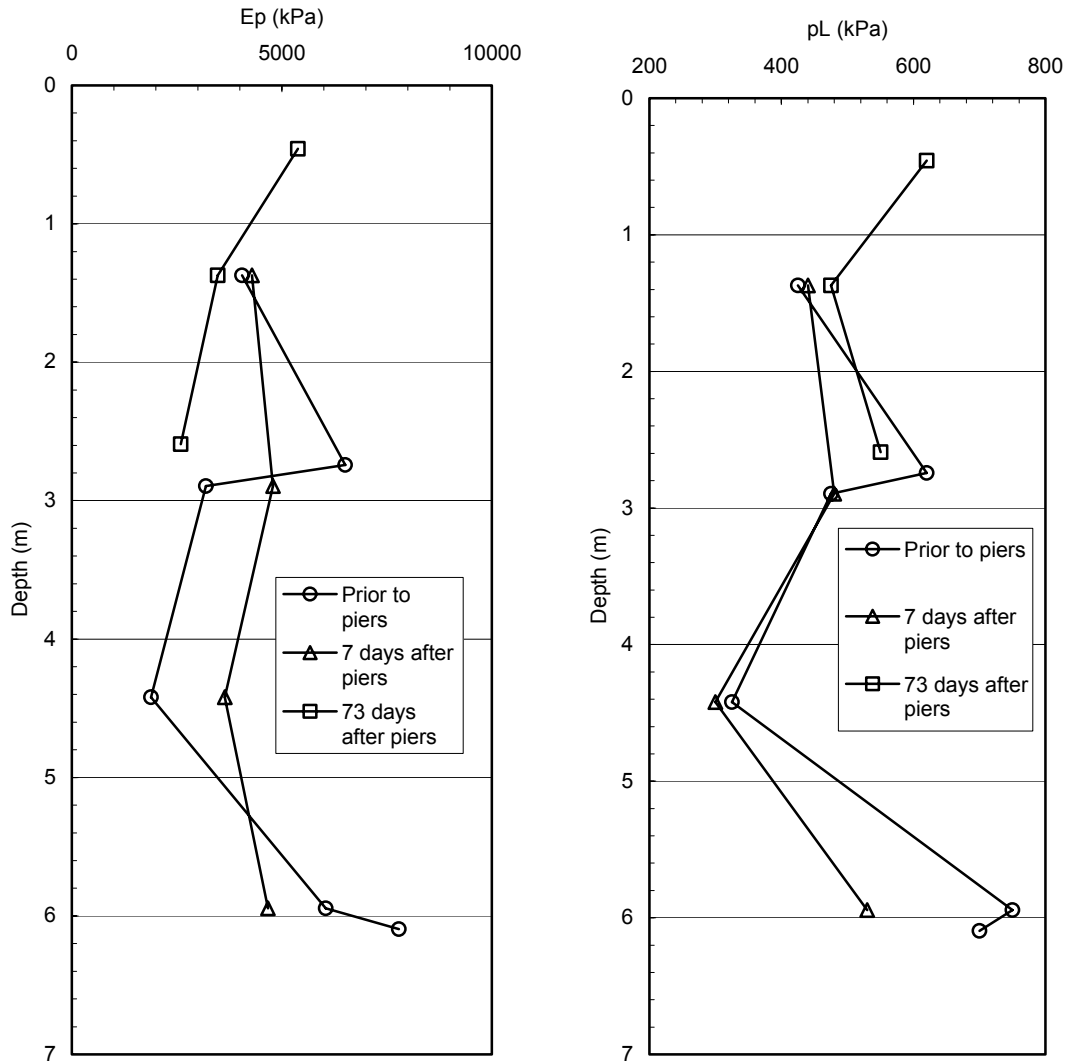


Figure 27. Pressuremeter Test Results after 0, 7, and 73 Days at Geopier Site

Load Test Results

Figure 28 shows load test results performed on a production stone column (7 days after installation) and a Geopier element (3 days after installation). The tested stone column was 91 cm in diameter and installed to a depth of 5.0 m. The tested Geopier element was 76 cm in diameter and installed to a depth of 5.4 m. To measure deflection near the bottom of the Geopier element a telltale was installed at a depth of 4.9 m. To compensate for the effects of the greater diameter of the stone column element the load test results are presented as applied stress versus settlement.

Test results for the stone column suggest bi-linear stress-deformation behavior as increasing stress is applied. A steeper stress-deformation response is noted at applied stresses greater than about 70 kPa. Test results for the Geopier element also suggests a bi-linear response with a steeper stress-deformation response noted at applied stresses greater than about 300 kPa. The Geopier telltale installed at the base of the pier indicates essentially no movement for the full range of applied stresses. The authors interpret this response as initiation of pier bulging at stresses greater than about 300 kPa.

The ratio of stresses, at which a steepened stress-deformation response is noted, for the Geopier and stone column elements is about 4. This ratio could be interpreted to represent the ratio of the elastic compressive behavior of the two elements prior to plastic deformation (bulging). Initiation of bulging type deflection for granular columnar elements is a function of the friction angle of the aggregate and the soil limiting radial stress (Hughes and Withers 1974). Pier bulging is not necessarily undesirable, as it should increase load transfer to the matrix soils.

Figure 29 presents the relationship between stiffness and applied stress for both the stone column and Geopier elements. Stiffness is defined as the slope of the stress deformation curve shown in Figure 28. Stiffness values of the stone column decrease from about 80 MN/m^3 at low levels of applied stress to less than 10 MN/m^3 at stresses of about 200 kPa. Stiffness values of the Geopier element decrease from about 190 MN/m^3 at low levels of applied stress to about 80 MN/m^3 at an applied stress of 600 kPa. Table 8 presents ratios of stiffness values for the stone column and Geopier elements. The ratio of Geopier to stone column stiffness values increase from approximately 2 to 9 with increasing applied stress.

Figure 30 shows the load test setup at the Geopier site. Four helical anchors drilled to about 9 m provided uplift reaction. Load was applied with a 100-ton hydraulic jack with a 15 cm stroke.

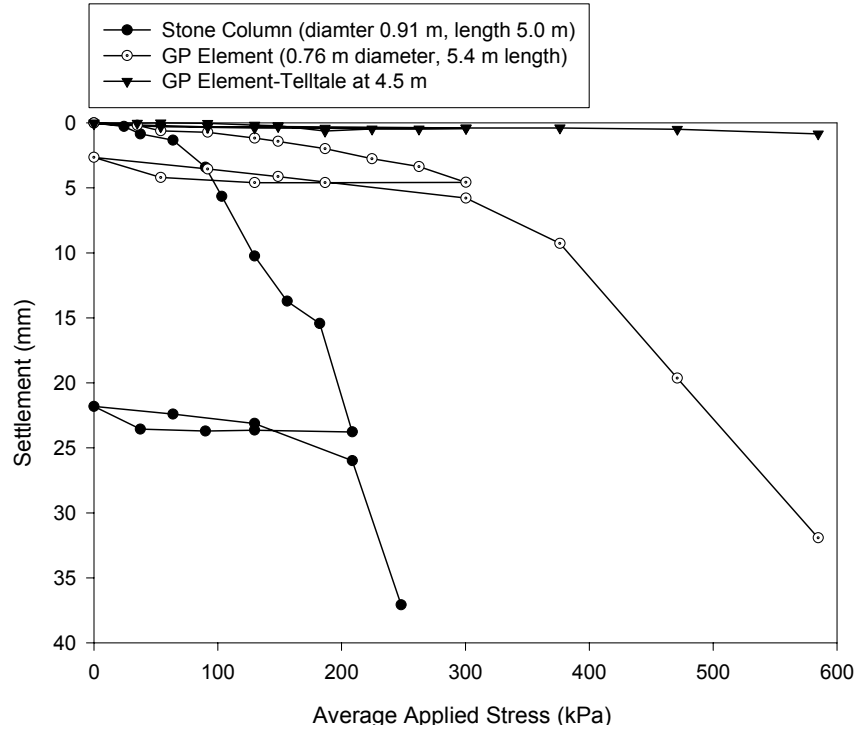


Figure 28. Comparative Stress-Deformation Plot for Stone Column and Geopier Elements

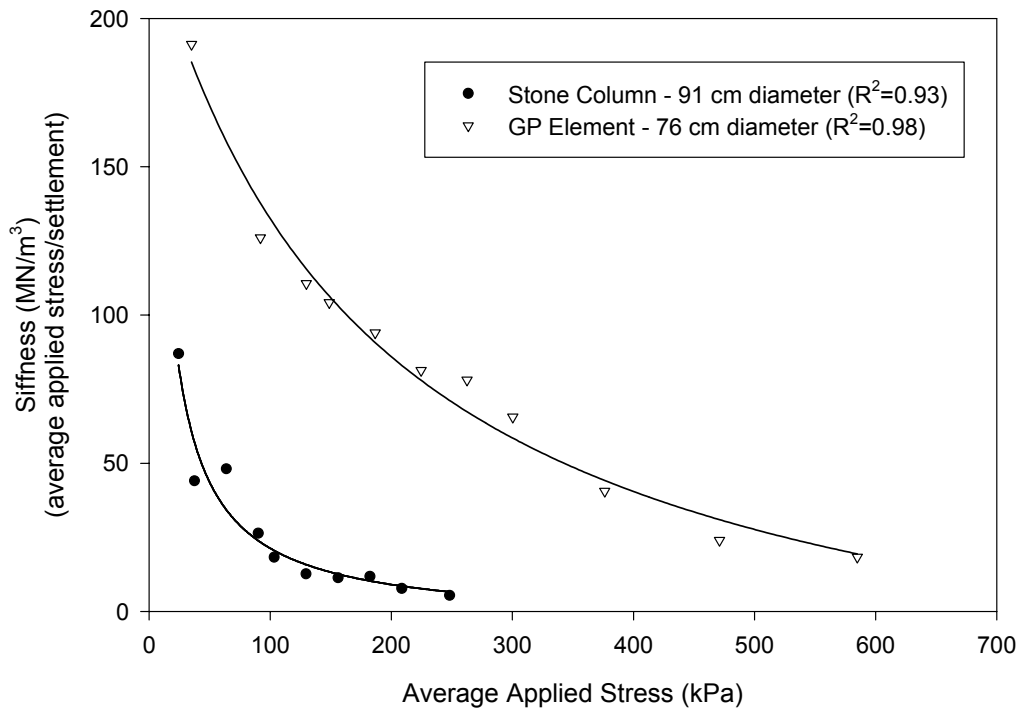


Figure 29. Stiffness Versus Applied Stress for Stone Column and Geopier Elements—Trend Lines are Best-Fit Hyperbolic Decay Functions



Figure 30. Geopier Field Modulus Load Test

Table 8. Comparison of Stiffness Values Derived from Load Test Results

Applied Stress (kPa)	SC Stiffness (MPa)	GP Stiffness (MPa)	GP to SC Stiffness Ratio
25	81	196	2.4
50	44	171	3.9
100	21	132	6.3
200	9	86	9.6
400	—*	40	—
600	—	18	—

* Note: Data not available.

Settlement Measurements

During the placement of fill soils, settlement surveys were made at the stone column and Geopier sites. Measurements at both sites were made using 0.9 m square settlement plates (see Figure 31) placed on individual aggregate elements and on the matrix soils between the elements. The results of the settlement measurements are presented in Figure 32 and summarized in Table 9. The settlement measurements indicate the following:

- After the placement of 6 m of fill, the stone column matrix soils settled about 19.5 cm. The Geopier matrix soils settled about 5.4 cm under this same fill pressure.
- The ratio of the settlement of the stone columns (4.8 cm) to the settlement of Geopier elements (1.5 cm) is approximately 3.2 at a fill height of 6 m.
- The differential settlement between the stone columns and adjacent soil is significantly larger than the differential settlement between the Geopier elements and the adjacent matrix soil.
- The ratio of the settlement of the stone column matrix soils to the settlement of the Geopier matrix soils is about 3.6 at a fill height of 6 m.

One explanation for the stone columns settling more than the Geopier elements is that the remolded stone column matrix soils did not restrain the columns and the columns expanded (see Mckenn et al. 1975). This theory is supported by the K_0 stepped blade lateral stress measurements, which indicate lower lateral stress development at the stone column site compared to the Geopier site. The magnitude of lateral stress surrounding aggregate piers and other foundation systems is a phenomenon of considerable significance and should be studied more extensively.



Figure 31. Settlement Plates 0.9 m x 0.9 m

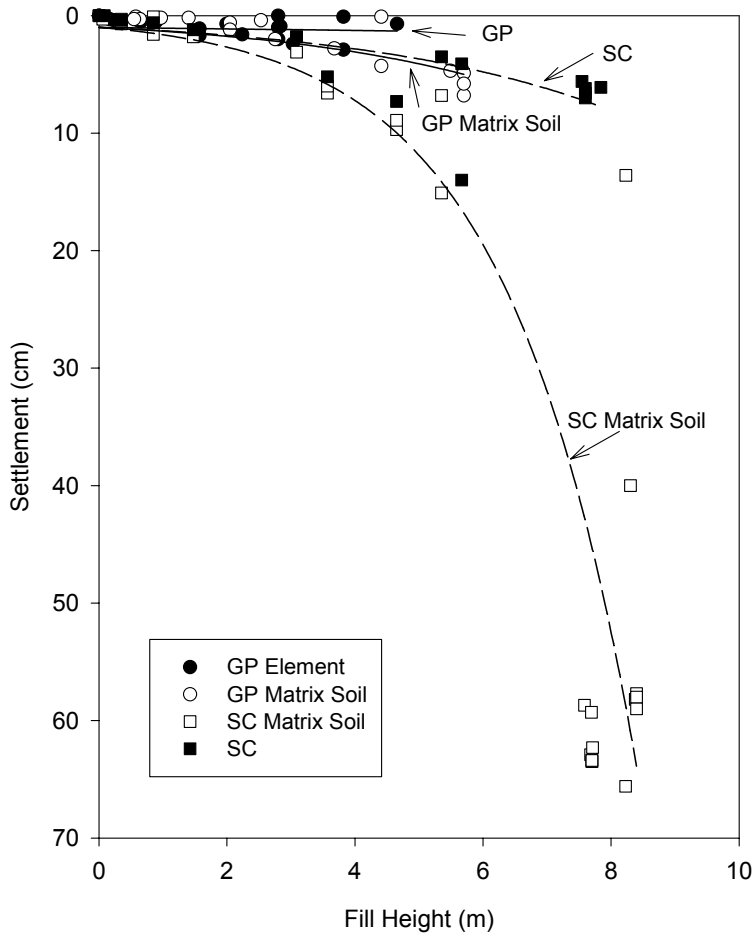


Figure 32. Settlement Versus Fill Height from 0.9 x 0.9 m Settlement Plates Installed Immediately after Pier Installations—Monitored for One Year

Table 9. Results of Settlement Survey Measurements

Settlement (cm)	Embankment Fill Height (m)			
	2	4	6	8
Stone column element	1.7	2.8	4.8	8.1
Stone column matrix soil	2.7	7.2	19.5	52.4
Ratio of stone column matrix soil to stone column element	1.6	2.6	4.1	6.5
Geopier element	1.1	1.3	1.5	—*
Geopier matrix soil	1.8	3.1	5.4	—
Ratio of Geopier matrix soil to Geopier element	1.6	2.4	3.6	—

* Note: Fill height at test location did not exceed 6 m.

Instrumentation Monitoring

Vibrating wire settlement cells and total stress cells were installed for monitoring during stage 1 of the embankment construction at the Geopier site. At the stone column site total stress cells were monitored throughout the duration of embankment fill construction. The stress cells provided an opportunity to measure stress concentrations on Geopier elements and stone columns. The settlement cells provide time-settlement relationships for the Geopier site.

Figure 33 shows a group of settlement cells and total stress cells at the Geopier site. As shown, both stress and settlement cells were placed on the pier elements and on the matrix soils. Sand was used as a leveling base for the instrumentation. Tables 10 and 11 list the instrumentation placement locations.

Three groups of vibrating wire settlement cells were installed at Ramp C prior to embankment construction. Settlement cell locations 1 and 2 each include a cell positioned on a Geopier element and a cell positioned on the adjacent matrix soil. For comparison, settlement cell location number 3 was located outside the Geopier reinforced foundation area.

Five vibrating wire total stress cells were installed at Ramp C prior to embankment construction. Stress cell locations 1 and 2 each include a cell positioned on top of a Geopier element and a cell positioned on the adjacent matrix soil. Stress cell location number 3 is located outside the Geopier reinforced area and includes a single stress cell positioned on the foundation soil.

Six vibrating wire total stress cells were installed at Ramp B. Each stress cell location includes a cell positioned on top of a stone column and a cell positioned on the adjacent matrix soil.



Figure 33. Settlement Cells and Total Stress Cells at Geopier Site

Table 10. Ramp C Geopier Instrumentation

Instrument Description	Fill Height (m)	Notes
Settlement Cell Location No. 1	2.4	One cell on and one adjacent to pier No. 105
Settlement Cell Location No. 2	2.4	One cell on and one adjacent to pier No. 106
Settlement Cell Location No. 3	5.7	Located outside Geopier area
Total Stress Cell Location No. 1	2.4	One cell on and one adjacent to pier No. 105
Total Stress Cell Location No. 2	2.4	One cell on and one adjacent to pier No. 106
Total Stress Cell Location No. 3	5.7	Located outside Geopier area

Table 11. Ramp B Stone Columns Instrumentation

Instrument Description	Fill Height (m)	Notes
Total Stress Cell Location No. 1	6.4	One cell on and one adjacent to a stone column
Total Stress Cell Location No. 2	8.6	One cell on and one adjacent to a stone column
Total Stress Cell Location No. 3	9.0	One cell on and one adjacent to a stone column

Settlement Cell Measurements

Stage 1 of embankment construction was completed by August 2000. Figure 34 shows the results of vibrating wire settlement cell locations 1 and 2 as a function of time. Results indicate movements of about 20 cm in the Geopier reinforced area. Compared to the results of the settlement plate measurements, the settlements cells indicate about 17 cm more settlement. If the movements of cell locations 1 and 2 are compared to the movement of cell location 3 (13 cm) shown in Figure 35, a question of the accuracy of these measurements is raised. It is unlikely that the reinforced matrix soils settled nearly twice as much as the unreinforced soils. The nature of the error at settlement cell locations 1 and 2 is believed to be a result of the data logging system, which consistently sampled the instruments prior to establishing a constant reading.

Although there may be uncertainty in the actual magnitude of the settlement at settlement cell locations 1 and 2, it appears that the Geopier elements and matrix soils settled nearly identical amounts. This would support the previous hypothesis that lateral confinement of the matrix soil between piers reduces vertical settlement.

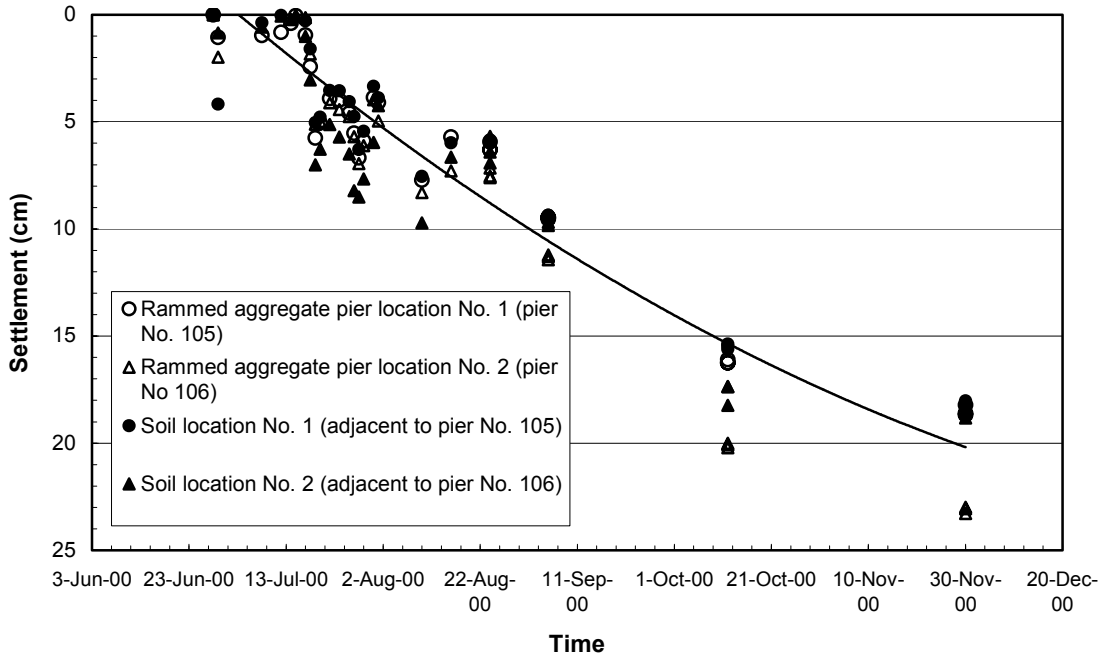


Figure 34. Ramp C (Stage 1) Settlement Cell Readings as a Function of Time (Locations 1 and 2)

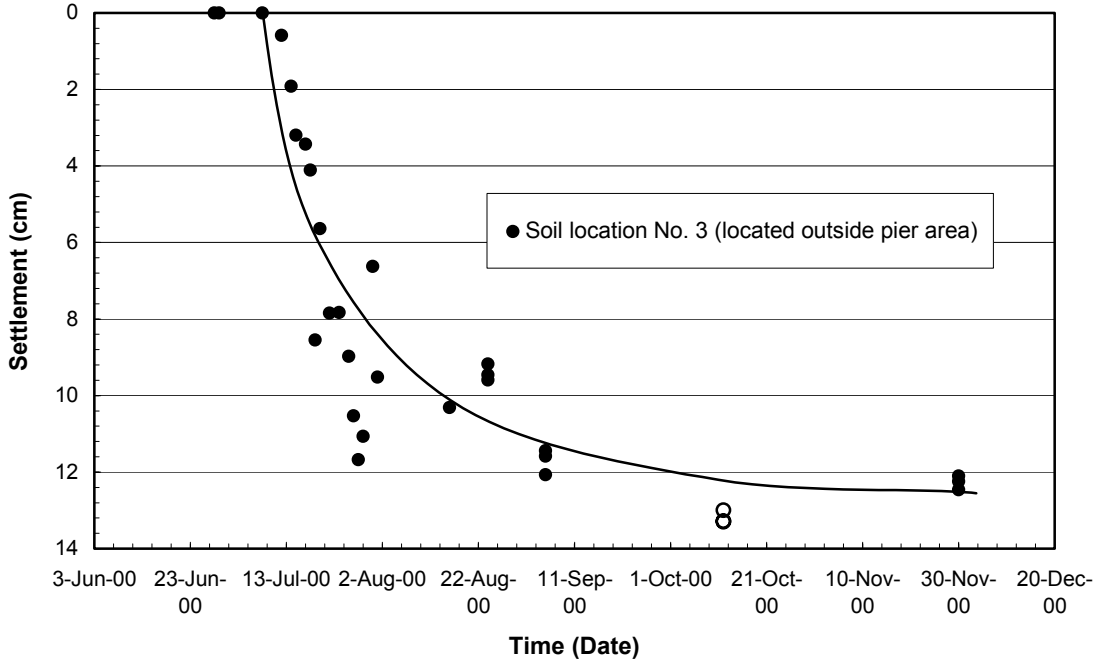


Figure 35. Ramp C (Stage 1) Settlement Cell Readings as a Function of Time (Location 3)

Total Stress Cell Measurements

Five vibrating wire total stress cells were installed at the Geopier site prior to embankment construction. Stress cell locations 1 and 2 as shown in Figure 9, included a cell positioned on top of a Geopier element and a cell positioned on the adjacent matrix soil, each covered by approximately 2.4 m of fill. Again, stress cell location number 3 is located outside the Geopier reinforced area and includes a single stress cell positioned on the unreinforced foundation soil. Figure 36 shows total stress cell measurements at locations 1 and 2 as a function of embankment fill height. For reference the theoretical vertical stress (fill thickness x total soil unit weight) is shown. Stress cells at locations 1 and 2 show increasing stress with time, with greater stress increases on the Geopier elements compared to the matrix soil. Stress increase with time is presumed to be a result of soil creep and stress concentration on the stiffer total stress cells.

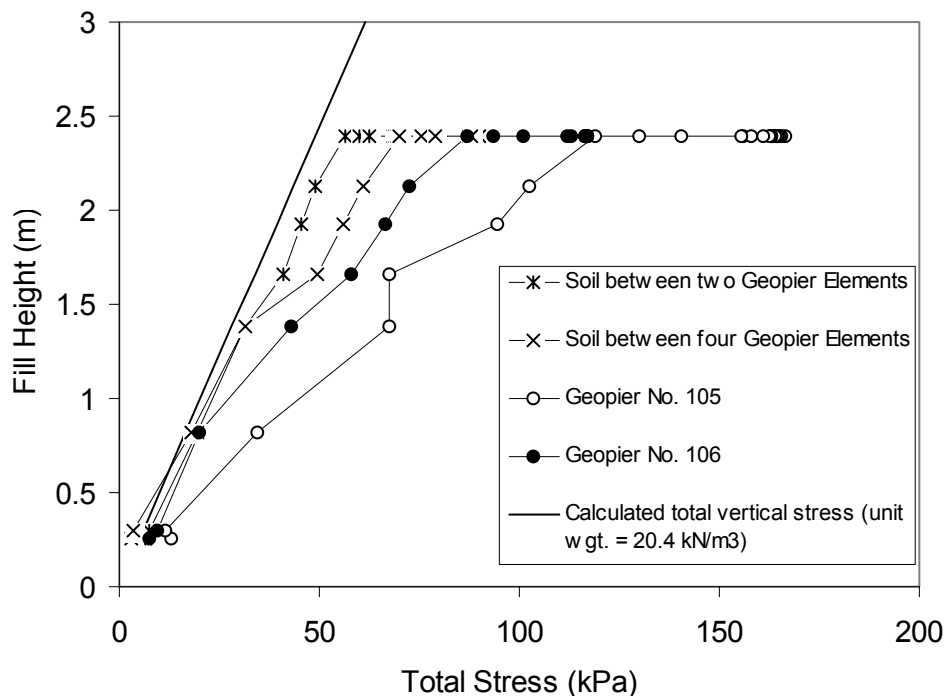


Figure 36. Total Stress Cell Locations 1 and 2 at Geopier Site

Figure 37 shows the stress concentration ratio (load carried by the Geopier elements to the load carried by the matrix soil). Stress concentration ratios greater than unity indicate that the stiffer Geopier pier elements are carrying more load than the surrounding matrix soils. As expected, as consolidation takes place, stress concentration ratio increases (see Fox and Lawton, 1994). The average stress concentration ratio for about 2.5 m of fill was about 1.7. It is expected that stress concentration values would increase as fill height increases. Figure 38 presents stress cell measurements at location number 3 as a function of fill height. Again the theoretical vertical stress is shown for reference. Similar to stress cell locations 1 and 2, the soil is showing a slightly larger vertical stress than that calculated. Unlike stress cell locations 1 and 2, the total stress at cell location 3 is decreasing with time.

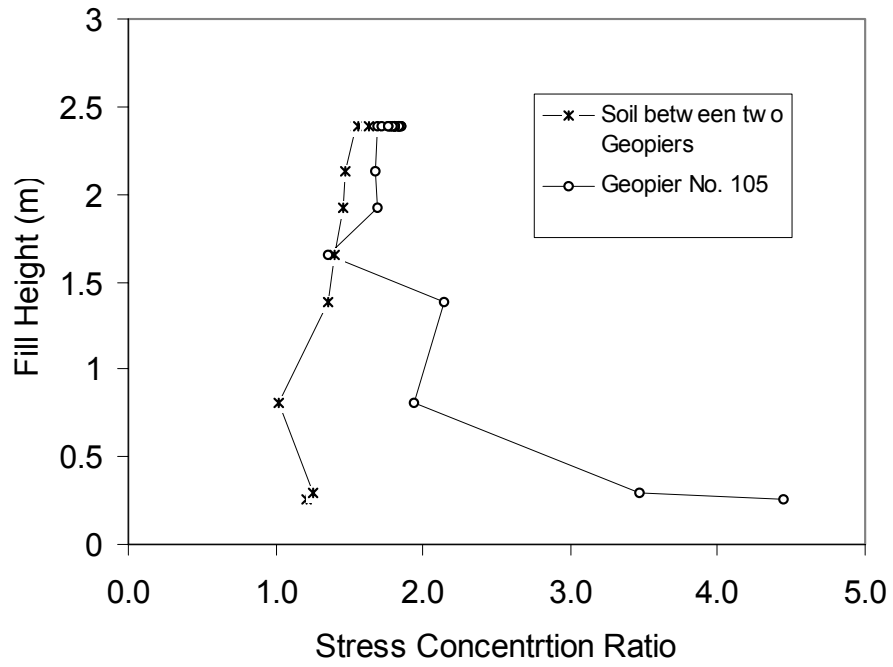


Figure 37. Geopier Stress Concentration Ratios - Ramp C

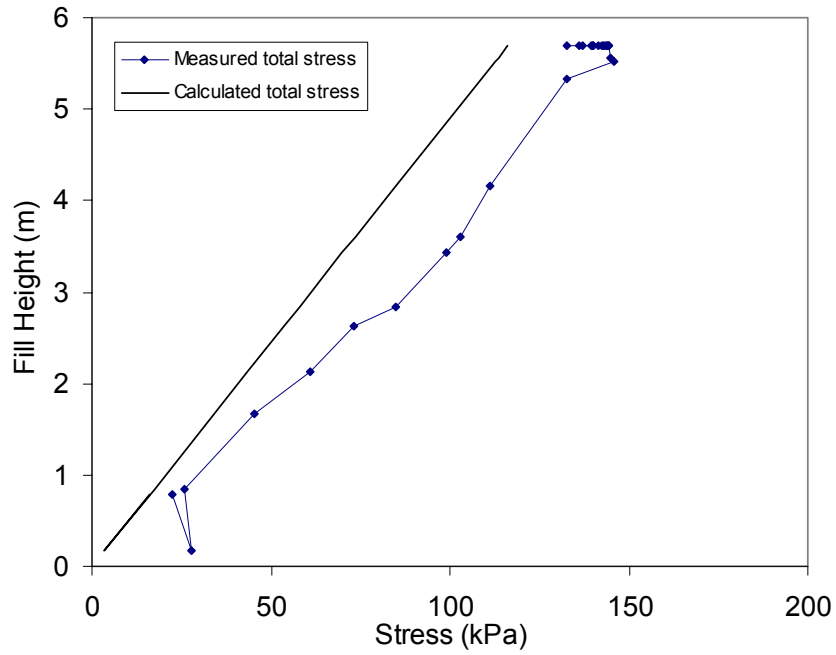


Figure 38. Ramp C Total Stress Cell Location No. 3

Six vibrating wire total stress cells were installed at the stone column site prior to embankment construction. Figure 10 shows the locations of the total stress cells at Ramp B. Each stress cell location includes a cell positioned on top of a stone column and a cell positioned on the soil matrix. 6.4, 8.6 and 9.0 m of fill cover stress cell locations 1, 2 and 3, respectively. Figure 39 shows the total stress cell readings as a function of fill height. Similar to the Geopier site the stress readings on the stone columns increase with time. Unlike the surrounding soil matrix of the Geopier site, however, the load carried by the stone column soil matrix did not increase with time. Figure 40 shows the stress concentration ratios for cell locations 1, 2 and 3 at Ramp B and indicates that the stone columns are carrying more load than the adjacent soil matrix. As settlement progresses, a greater portion of the overburden load is transferred to the stone columns and the stress concentration ratio increases. The average stress concentration ratio for the stone columns at Ramp B was about 4.

Summary Observations

Geotechnical measurements were taken at two adjacent embankment foundation sites improved with stone columns and Geopier elements. A summary of the measurements is as follows:

- The subsurface conditions at the stone column site were slightly stiffer and less cohesive than the subsurface conditions at the Geopier site, based on interpretation of CPT data.
- Element spacings at both sites were 1.8 m on-center. The greater diameters of the stone column elements and application of a triangular spacing pattern result in a greater area replacement ratio.
- SPT results for tests performed within the elements indicate an average N-value of 11 for the stone columns and an average N-value of 17 for the Geopier elements.
- PMT tests before Geopier construction and 7 and 73 days after construction do not show significant changes in pressuremeter modulus or limit pressure.
- The ratio of post-installation matrix soil lateral stress for the Geopier elements to the post-installation matrix soil lateral stress for the stone columns is about 2.
- Load test results indicate that the ratio of pre-bulging compressive strength for the Geopier element to the pre-bulging compressive strength for the stone column is about 4.
- Load test results indicate that the ratio of Geopier stiffness to stone column stiffness ranges from about 2 to 9 as a function of applied stress.
- Settlement of matrix soils surrounding the stone columns was about 3 times as large as the settlement of matrix soil surrounding the Geopier elements.
- Settlement cell instrumentation yielded uncertain results in terms of magnitude, but supports the observation that the Geopier matrix soils are settling similarly to the Geopier elements.
- Total stress cell instrumentation at these sites shows that stress concentrations for Geopier elements and stone columns are in the range of 2 to 7.

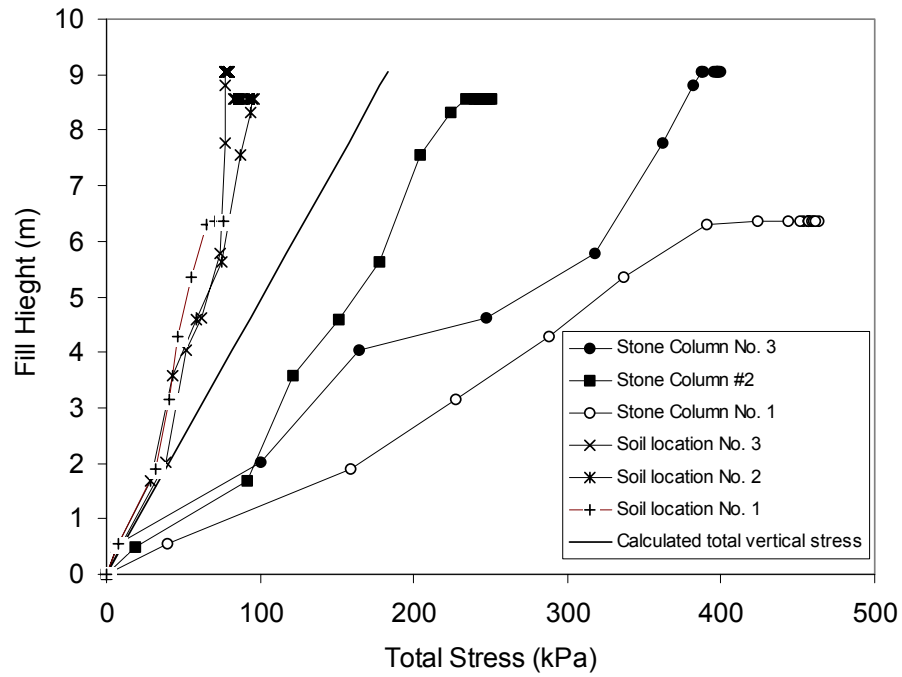


Figure 39. Ramp B Total Stress Cell Locations 1, 2, and 3

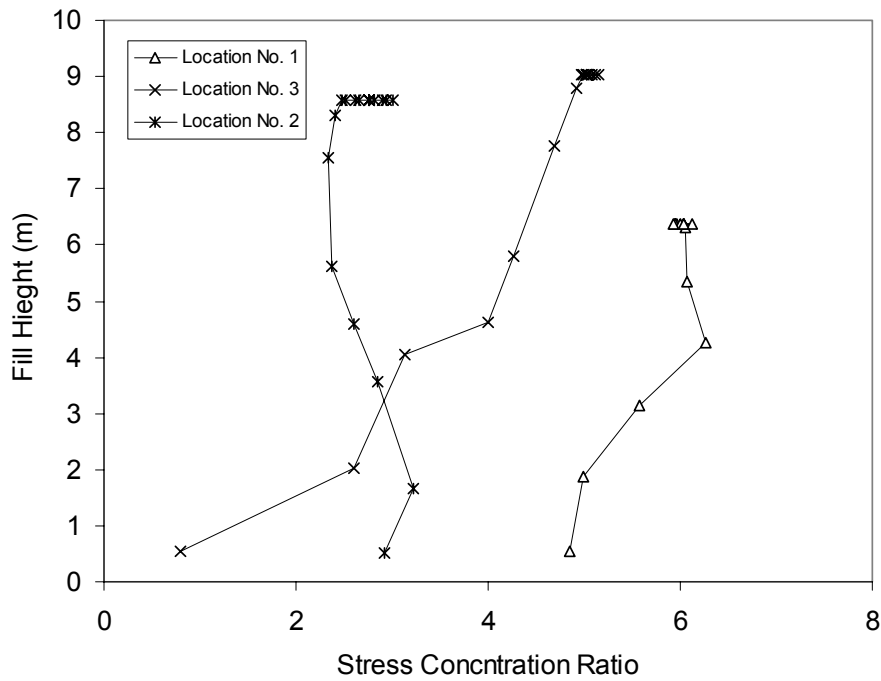


Figure 40. Stone Column Stress Concentration Ratios (Ramp B)

Lastly, the stone column site has performed its intended function for global slope reinforcement. This is evidenced by the fact that the embankment has not failed. The Geopier installations also have performed as intended by reducing settlement and the construction delay between embankment completion and abutment construction from the original 120 days to less than 30 days. In short, advantages of the stone columns at this site include larger diameter and shaft length, whereas the Geopier elements were smaller but stiffer. Future comparative investigations are highly encouraged with emphasis on documenting the influence of lateral stress on the load-settlement behavior.

Project No. 2: Box Culvert Foundation Reinforcement at IA Hwy 191 (Neola, IA)

This section of the report describes the application of Geopier soil reinforcement to control settlement of a 4.2 m wide x 3.6 m high x 50 m long box culvert constructed under a three-span bridge on Iowa Highway 191 south of Neola, Iowa. The purpose of the box culvert construction was to eliminate replacement of a previously widened, deteriorating bridge built in 1927. Geopier elements were installed not only to reduce total and differential settlement of the culvert, but also to prevent downdrag on the existing bridge pier foundations. Soil conditions at the site consisted of highly compressible alluvial clay overlying glacial till and weathered shale bedrock. Construction began in July 2001 and was finished in December 2001. Backfilling operations began in November 2001 and were finished in about 3 weeks. Embankment fill height reached a maximum depth of 7.5 m beneath the bridge.

A wide range of in situ and laboratory testing was conducted prior to construction to characterize soil conditions. Further, full-scale modulus load tests were performed to better characterize individual versus group Geopier behavior. Vibrating wire instrumentation was installed within the embankment to monitor soil conditions during and after filling operations. Near continuous instrumentation monitoring was maintained to verify total and differential settlement of the box culvert. Settlement of the bridge piers was conducted to monitor downdrag.

The results of this project are presented by describing the site conditions, the load testing program, and performance monitoring. Figure 41 shows the project site during initial grading operations.



Figure 41. Project Site and Grading Operations for Box Culvert

Site Conditions

To assess conditions at this site, several in situ and laboratory tests were conducted. In situ testing included CPTs, DMTs, BSTs, and PMTs. Laboratory soil tests included particle size distribution, moisture content, Atterberg limits, drained and undrained triaxial, and one-dimensional consolidation tests. Figure 42 shows a scaled drawing of the sampling and in situ testing locations.

Cone Penetrometer Test Results

CPT data were obtained at the three locations indicated in Figure 42. Test points were selected to provide a representative cross section of the site. All tests were performed prior to construction. As shown in Figure 43, it was not possible to access the area directly beneath the bridge. Hydraulically pushing the cone and sampling data at 5 cm intervals facilitated the CPTs. An average 25 cm depth interval was used to report data. Geotechnical Services, Inc. (GSI) of Omaha, Nebraska, was subcontracted to conduct and analyze the CPT data. Complete CPT measurements are provided in Appendix D.

Results for CPT1 are presented in Figure 44. The parameters displayed are defined as q_T for corrected tip resistance, f_s for sleeve friction, R_f for friction ratio ($f_s/q_c \times 100\%$), μ the pore water pressure, Q the normalized net tip resistance, F the normalized friction ratio, and I_c the soil behavior and classification index. Also provided, is a soil log identifying soil behavior type. The alluvial clay layer is underlain by a thin layer of glacial till outwash overlying weathered shale bedrock.

CPT2 and CPT3 also indicate a thick alluvial clay layer underlain by glacial till and weathered shale bedrock. Overall, the profiles indicate a layer of fill averaging 1.2 m thick underlain by 12.5 m of alluvial clay underlain by 2 m of glacial till outwash overlying weathered shale bedrock.

The alluvial clay was of primary interest for this project, as it is highly compressible. A correlation from CPT data gives an average drained friction angle of about 20° to 25° in the alluvial clay. Undrained shear strength (s_u) was estimated using a relationship proposed by Robertson and Campanella (1986) and is shown in Figure 45. S_u averages 17 ± 5 kPa (+/- denotes one standard deviation herein) for the alluvial clay layer, which classifies as very soft clay according to Terzaghi and Peck (1967). Based on these site conditions, bearing capacity and settlement were both controlling factors in the design of the Geopier reinforcement.

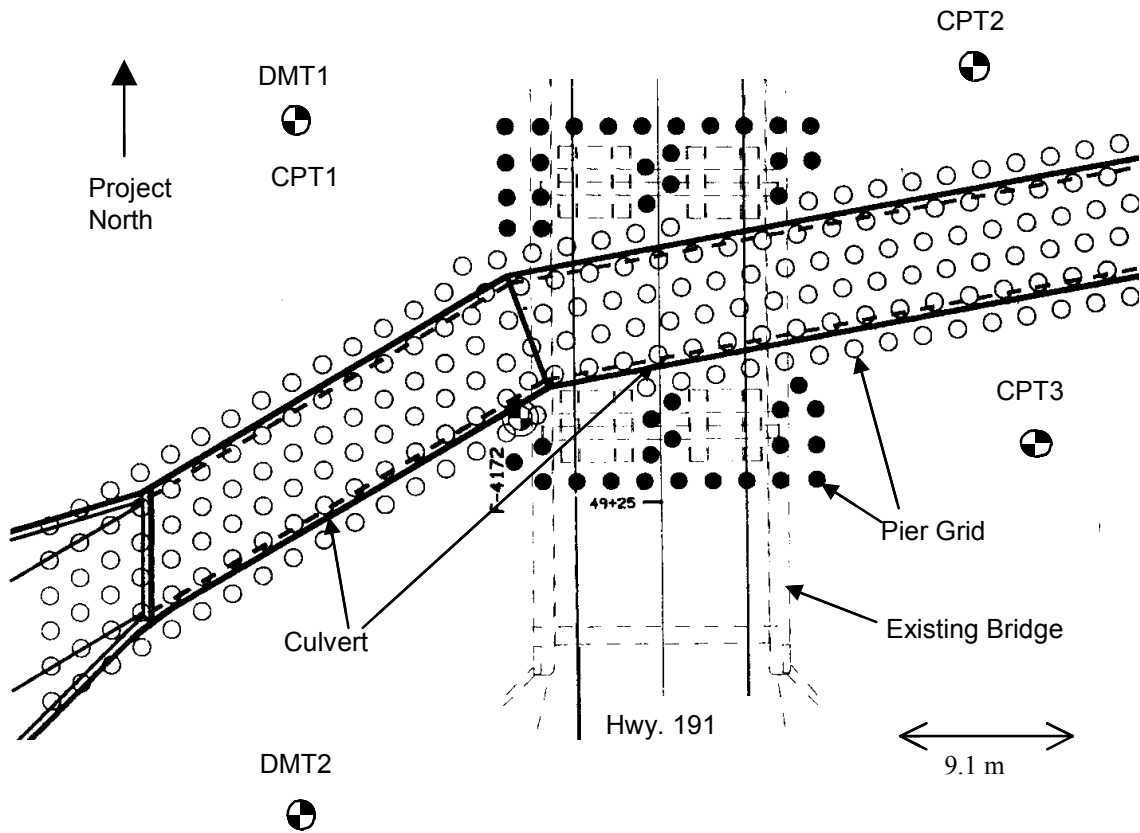


Figure 42. Plan View of Project Site showing DMT and CPT Test Locations



Figure 43. Cone Penetration Testing at CPT3

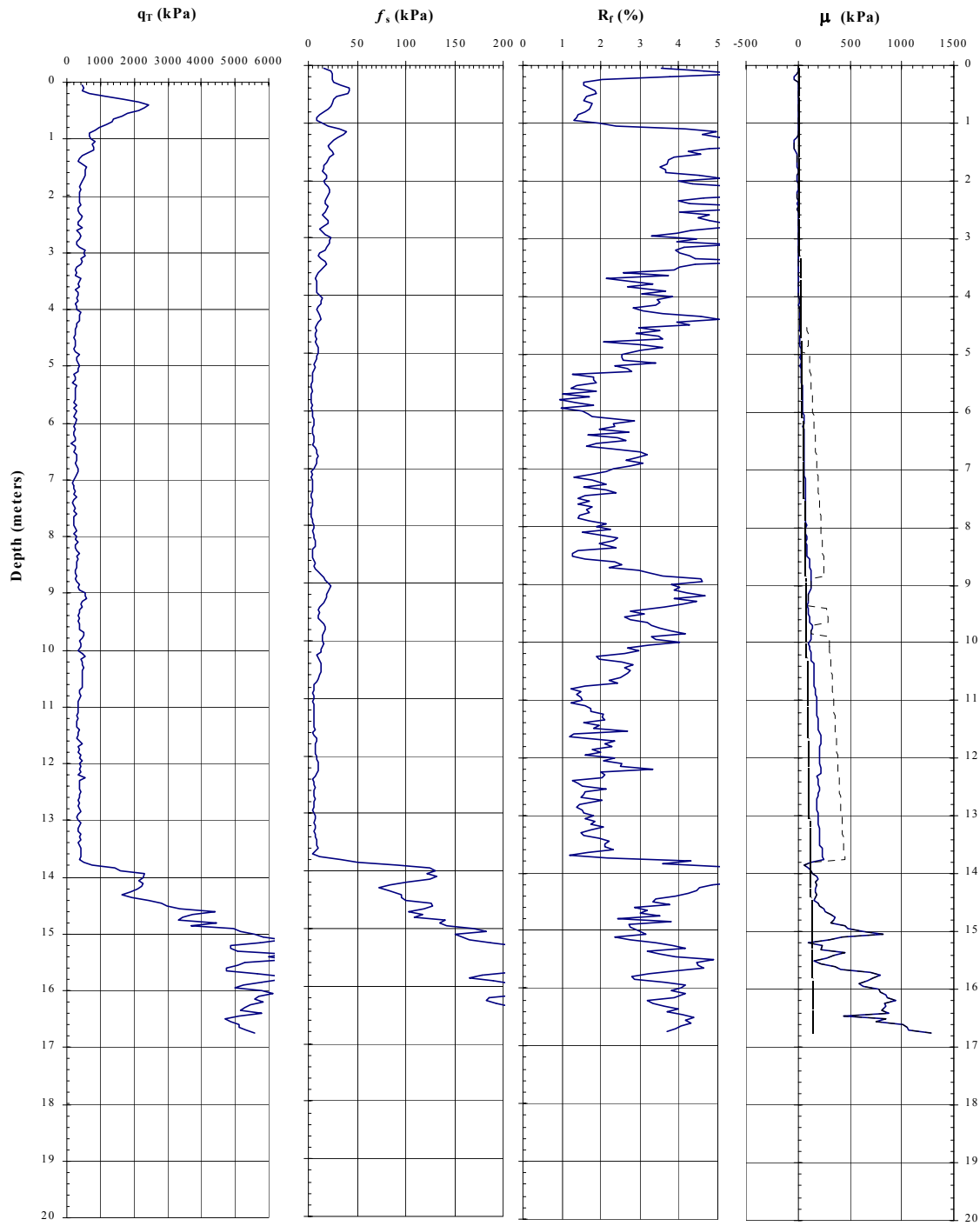


Figure 44. CPT1 Results

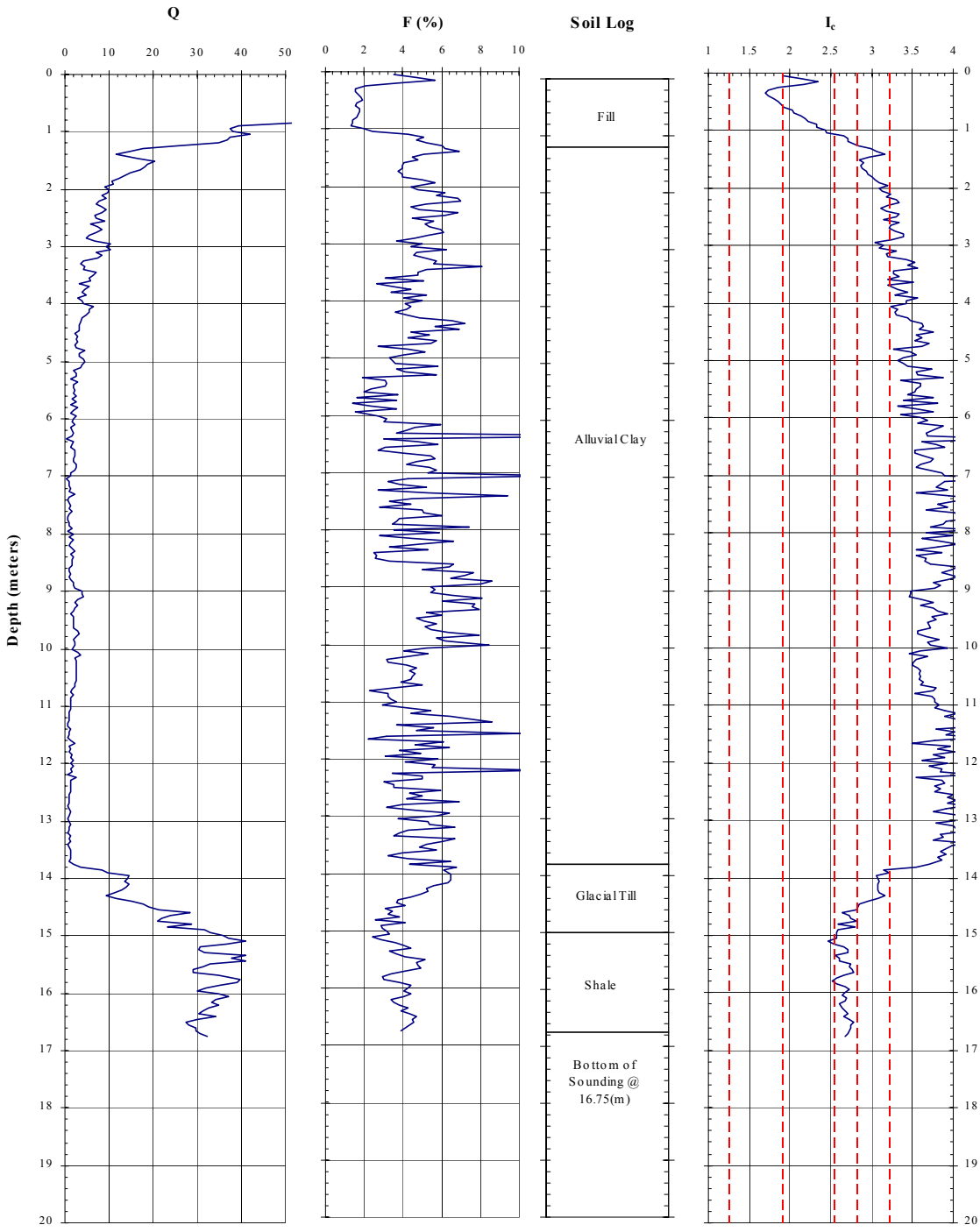


Figure 44. CPT1 Results (continued)

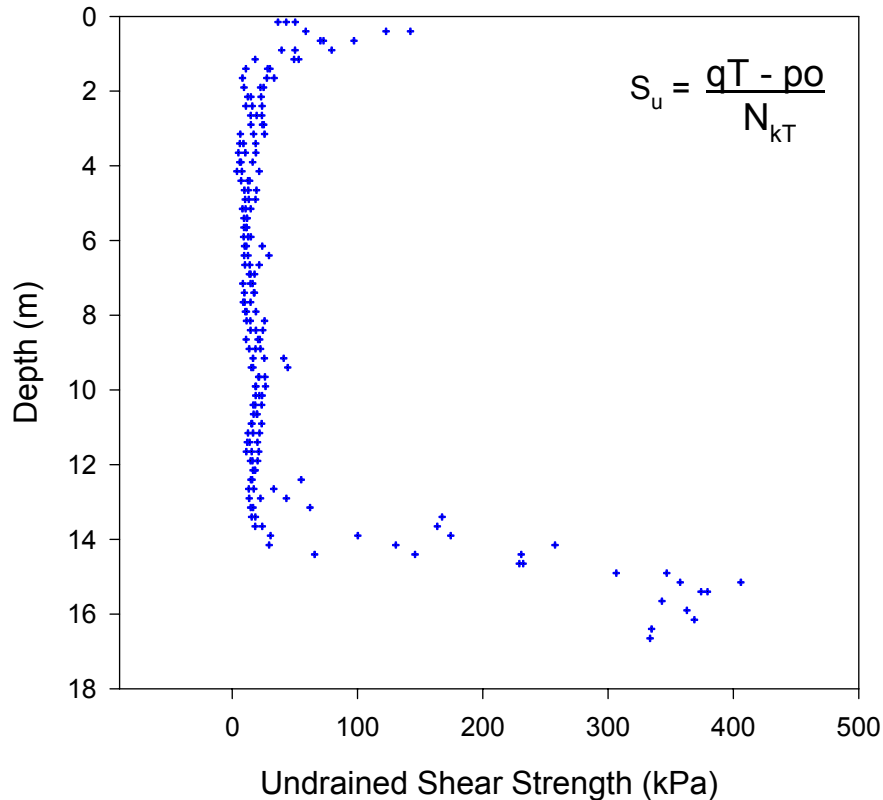


Figure 45. Undrained Shear Strength (S_u) Estimated from CPT Results ($N_{kT} = 15$)

Flat Dilatometer Test Results

The DMT was pushed hydraulically using the ISU Mobile B-40, truck mounted drill rig. Two borings were performed. The first, DMT1, was performed at the CPT1 location, and the second, DMT2, was performed in the center of the load test area. Procedures described by Marchetti (1980) were used to carry out the tests and reduce the data. Readings were taken at 0.3 m intervals.

The first step in data reduction was to produce the three primary dilatometer variables at each data point: Material Index (I_d), Horizontal Stress Index (K_d), and Dilatometer Modulus (E_d). Subsequent correlations are based on the soil behavior type obtained from the material index and dilatometer modulus. Results classify the soil behavior as soft silty clay to very nearly mud (Marchetti, 1980). For $I_d < 1.2$, Marchetti (1980) indicates that it is reasonable to correlate the undrained shear strength (s_u) and horizontal earth pressure (K_o) to DMT measurements. Figure 46 shows the profile for the undrained shear strength (s_u) at DMT1 and 2— s_u averages about 10 kPa. Previously, CPT data correlated to an average s_u of about 17 kPa. K_o estimates were averaged to be 0.4 for DMT1 and 2. With plasticity index of 16 percent for a normally consolidated soil, Lambe and Whitman (1969) list a typical value of 0.5 for K_o , which is in reasonable agreement with the DMT correlation. All DMT data and correlations are presented in Appendix E.

Comparisons of CPT with DMT data reveal similar profiles. The dilatometer soundings indicate a moderately stiff zone for the first meter, which confirms the fill layer indicated by the CPT profile. Further, DMT results show fill underlain by a soft layer to a depth of 13.5 m. The soil begins to stiffen at 13.5 m as indicated by the dilatometer modulus profile. This is in agreement with the top of the glacial till layer indicated in the CPT1 profile. Push refusal was reached at a depth of 14 m.

Pressuremeter Test Results

PMTs were conducted to estimate modulus of the clay layer. Previous research has shown that soft clay conditions yield reliable data from the pressuremeter (Briaud, 1989). PMT testing was performed at the CPT1 and CPT2 locations. For simplicity, data profiles are referred to as PMT1 and PMT2. PMTs were performed in a pre-bored hole after sampling with a standard 7.9 cm diameter Shelby tube. The procedures used to carry out testing and data reduction were in general accordance with recommendations from Briaud (1989).

PMT1 was performed at 1.52 m intervals beginning at a depth of 4.5 m. Tests continued to a depth of 12.5 m. At a depth of 13.5 m hollow-stem augers could not be advanced. PMTs were conducted on a constant pressure increment basis while observing volume change. Figure 47 presents the calculated pressuremeter modulus (E_{pmt}) for each depth at PMT1. The average for the alluvial clay layer is about 1320 ± 460 kPa, which classifies as very soft clay (Briaud, 1989). The data collected in PMT2 gives similar E_{pmt} values. Complete PMT results are provided in Appendix F.

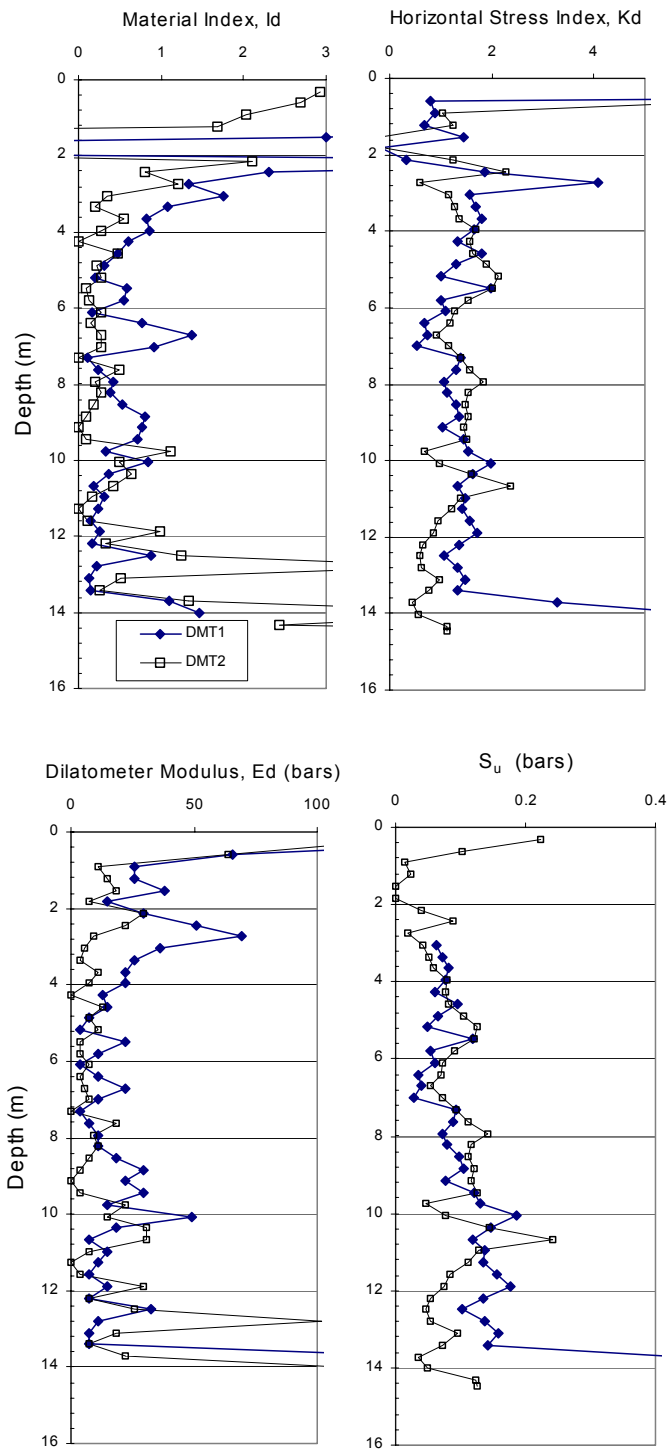


Figure 46. Dilatometer Parameters and Correlation to Undrained Shear Strength

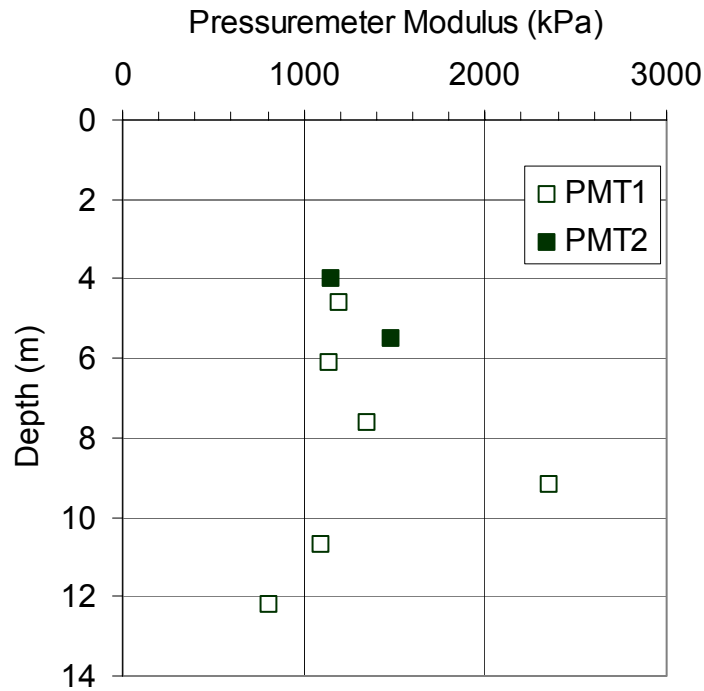


Figure 47. Calculated Pressuremeter Modulus at PMT1 and PMT2

Borehole Shear Test Results

Two BSTs were performed in the load test area to measure effective stress friction angle and cohesion values in the alluvial clay layer. Again, the BST consists of lowering an expandable shear head into a borehole (created by a standard 7.9 cm Shelby tube), expanding the shear head against the walls under a constant normal stress, allowing the soil to consolidate, and pulling vertically on the shear head measuring shear resistance. Several studies have compared the BST to CD and CU triaxial tests (e.g. Wineland 1976, Schmertmann 1976) and have supported a previous assessment that the BST is usually a drained test (see Handy 1976). Points are produced on the Mohr-Coulomb shear envelope by measuring the maximum shear resistance at successive increments of applied normal stress. Friction angle (ϕ') and cohesion intercept (c') are given by a regression of the data.

Figure 48 presents the BST results. At a depth of 3.8 m, $\phi' = 22^\circ$ and $c' \cong 0$ kPa for the clay. A strong correlation for the test is indicated by an R^2 value of 0.99. The value of friction angle agrees closely with the data indicated by the CPT results. The second BST was conducted at a depth of 2.3 m and indicates $\phi' = 25^\circ$ and $c' = 9$ kPa. BST data are presented in Appendix G.

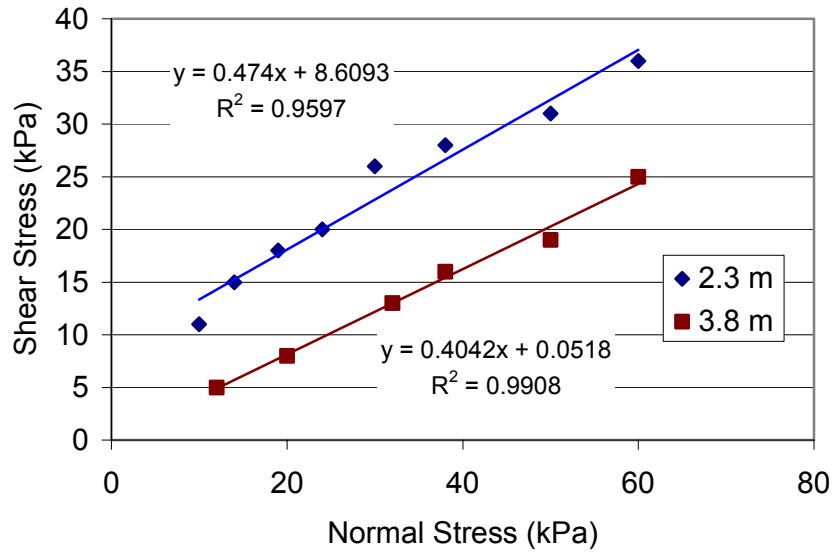


Figure 48. Borehole Shear Test Results at Load Test Area

Laboratory Testing Program

Consolidated drained (CD) triaxial compression tests, unconsolidated undrained (UU) triaxial compression tests, confined compression (oedometer) tests, particle size distribution, and Atterberg limit tests were performed on representative portions of relatively undisturbed samples obtained from Shelby tubes. Following is a description of the testing and results.

CD Triaxial Compression Test Results

A series of CD triaxial compression tests were conducted to measure shear strength parameter values of the soil in terms of effective stresses. Three CD tests were performed on alluvial clay extracted from a depth of 4.2 m at CPT2. Each triaxial sample was prepared with a height to diameter ratio of 2.0. Tests were conducted at confining pressures (σ_3) of 21, 41, and 62 kPa. The stress-strain behavior for the series of CD triaxial tests is shown in Figure 49. Results reveal a typical increase in peak strength with higher consolidation stress. Volume decreased (contraction) during loading, indicative of normally consolidated soils (Lambe and Whitman 1969). A linear regression of the peak p' and q values produces $\phi' = 24^\circ$ and $c' = 12$ kPa.

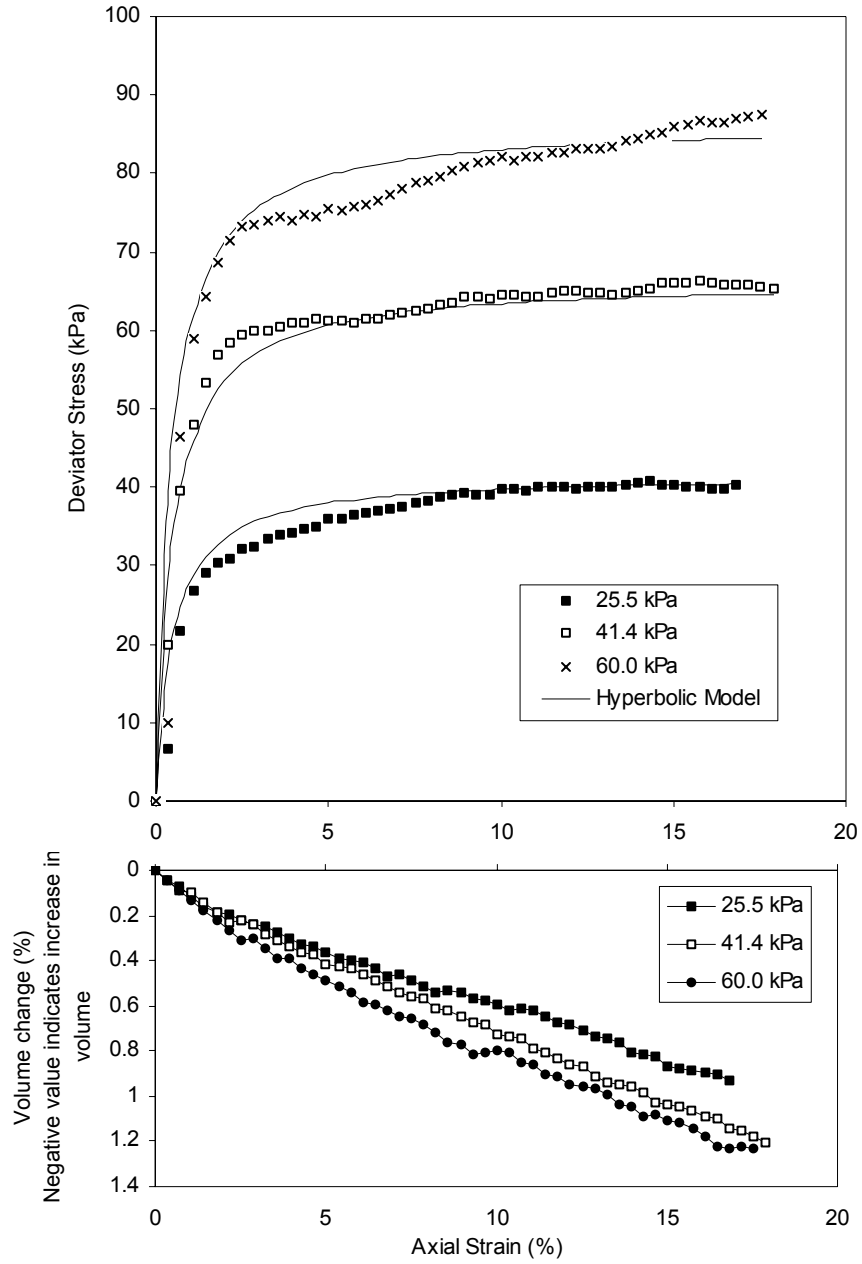


Figure 49. CD Triaxial Stress-Strain and Volume-Change Behavior of Alluvial Clay

UU Triaxial Compression Test Results

UU triaxial compression tests were performed to determine shear strength of the soil in terms of total stress. Three UU tests were conducted on the alluvial clay extracted from a depth of 5.8 m at CPT2. Each sample was prepared with a height to diameter ratio of 2.0. Tests were conducted at confining pressures (σ_3) of 62, 83, and 103 kPa. The stress-strain behaviors are shown in Figure 50. Results indicate average undrained shear strength of about 30 kPa.

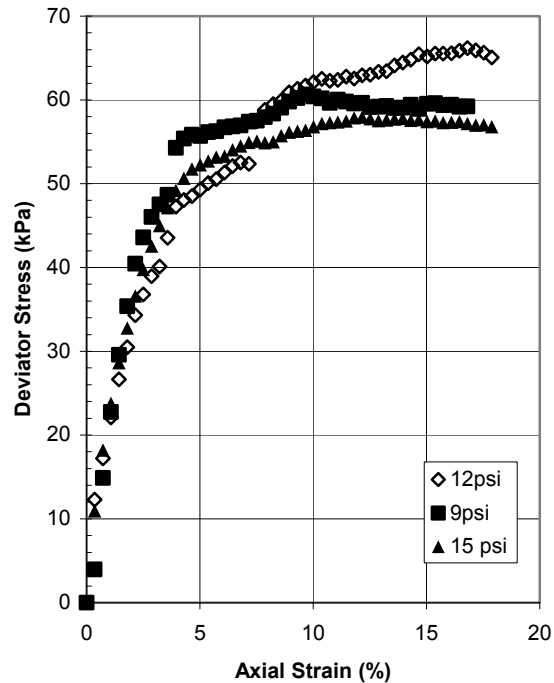


Figure 50. UU Triaxial Stress-Strain Behavior of Alluvial Clay

Confined Compression (Oedometer) Consolidation Test Results

One-dimensional confined compression tests were conducted to determine the compressibility of the alluvial clay layer. Results were used to provide an estimate of primary consolidation settlement and the time-rate of settlement. Tests were performed on Shelby tube samples obtained from depths of 3.7 m and 4.0 m. The samples were prepared with height to diameter ratio of 0.4. Each stress increment was maintained until primary consolidation was complete. During the consolidation process, the change in specimen height was recorded as a function of time.

For rate of settlement analysis the square root of time compression curves (compression vs. square root of time) were plotted for several pressure increments. The coefficient of consolidation, c_v , was calculated and time-settlement relationships were established. Table 12 presents a summary of consolidation parameter values. Coefficient of consolidation averaged $0.07 \pm 0.03 \text{ m}^2/\text{day}$ and was used to estimate time-settlement relationships.

Consolidation test results were also analyzed by plotting void ratio, e , versus the logarithm of applied effective pressure. Results are presented in Figure 51 and show that the alluvial clay layer is normally consolidated.

Table 12. Summary of Consolidation Parameter Values for Alluvial Clay

Test No.	Depth (m)	Initial Void Ratio, e_0	Average Compression Index	OCR
1	3.74	1.127	0.318	0.92
2	4.04	1.031	0.324	1.07
Average	3.9	1.08	0.32	1.0

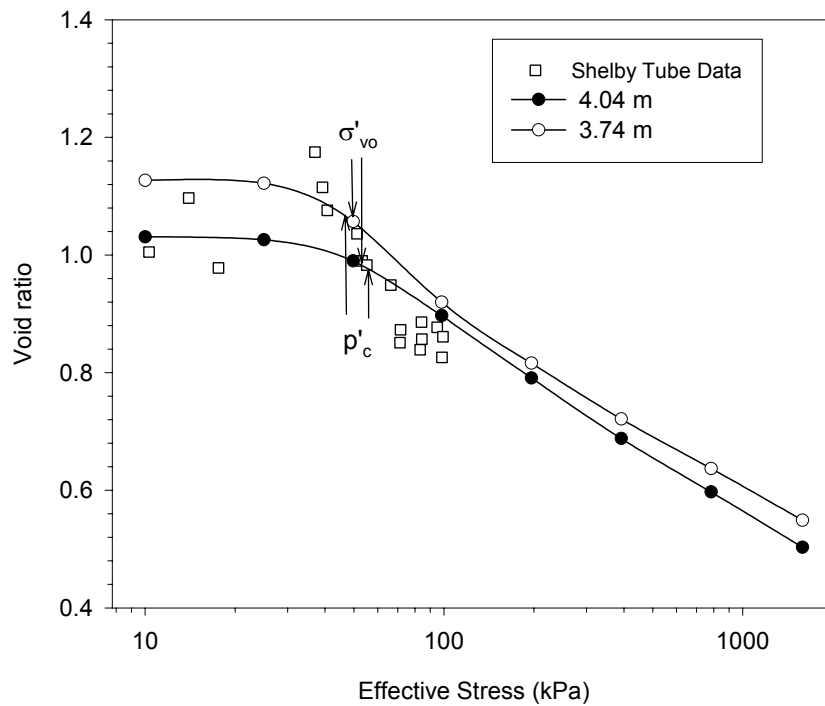


Figure 51. e - $\log(p)$ Curves including Void Ratio Measurements from Several Field Samples

Soil Index Test Results

Atterberg limits tests, natural water content and dry density measurements were performed on samples obtained at CPT1. The depth of sampling ranged from 0 to 9 m. Figure 52 presents the plastic limit, moisture content, and liquid limit determined at each depth. Average liquid limit and plasticity index values are 44 percent and 16 percent, respectively. In situ moisture content decreased with depth from about 42 percent to 32 percent—resulting in an average liquidity index of about 0.8. Hydrometer analysis shows that the alluvial clay is composed of about 74 percent silt size particles and about 26 percent clay size particles and classifies as CL according to the Unified Soil Classification System.

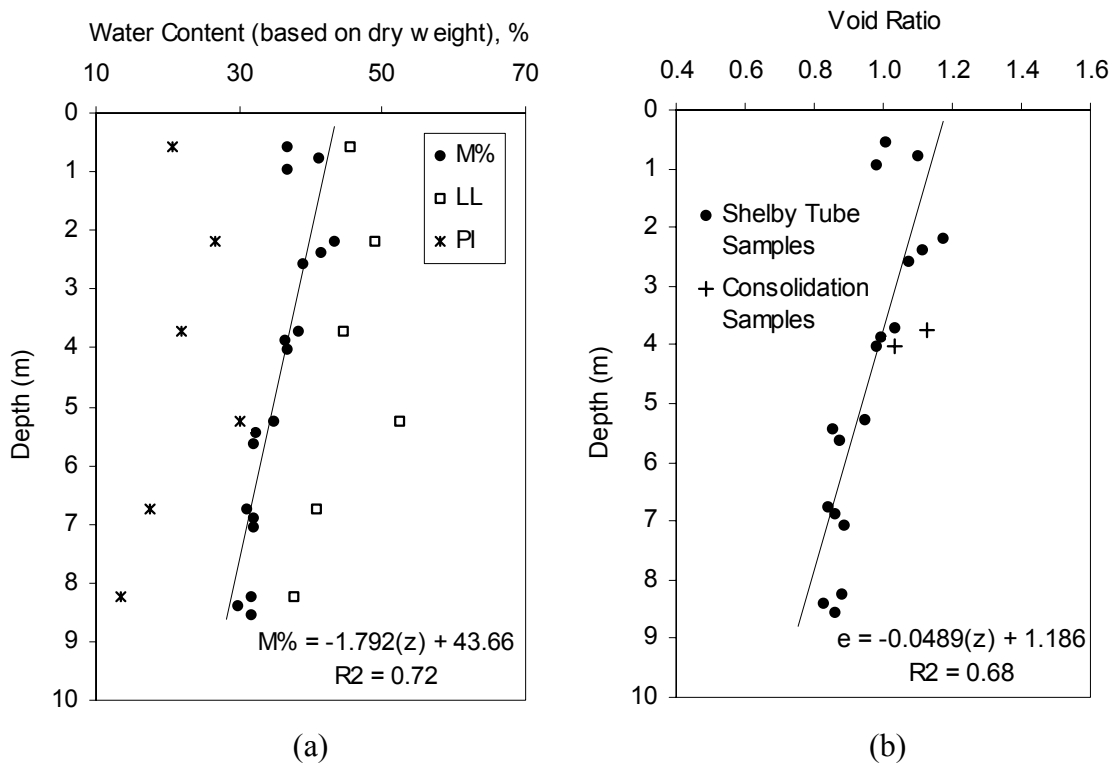


Figure 52. (a) Soil Index Properties and (b) Void Ratio Versus Depth for Alluvial Clay

Full-Scale Modulus Load Test Results

Following the in situ testing and laboratory investigations, a full-scale load test program was designed and carried out at the southwest corner of the production site. Load tests were performed on individual and groups of Geopier elements of varying lengths. Three tests were performed on individual piers and two tests on pier groups of four each. The group load tests were capped with a square reinforced concrete footing. The purpose of the load test program was to compare and contrast the behavior of individual pier elements with a group of uniformly loaded piers within a grid, as is the case beneath the box culvert, and to verify parameter values used in design.

To further investigate pier and matrix soil behavior under vertical load, instrumentation devices were installed and measured during loading. Total stress cells were installed in one of the individual pier tests and one of the group pier tests and were strategically placed within the piers and also between piers on the matrix soil. The intent was to monitor stress distribution through the piers during loading and stress concentration at the top of piers and matrix soil. Inclinator casings were also installed near one of the individual load test piers, and one of the group test piers. The inclinometer device was pulled through the inclinometer casing in 60 cm increments to develop lateral displacement profiles in matrix soil adjacent to a pier. This measurement revealed pier bulging under high load levels.

Individual Load Test Results

Individual load tests were performed on three Geopier elements of 0.76 m diameter. The installations were located in the test area on the southwest corner of the project site. Pier No. 1 was installed to a depth of 2.97 m and included stress cell and inclinometer instrumentation. Pier No. 2 was installed to a depth of 2.74 m. Pier No. 3 was installed to a depth of 5.05 m. Pier No. 1 and No. 2 were spaced 3.05 m apart and Pier No. 2 and No. 3 were spaced 4.57 m apart to minimize any interaction effects.

Pier No. 1 was fitted with four stress cells, one telltale, and two inclinometer casings. Figure 53 shows locations of the instrumentation. Figure 54 shows the constructed pier elements with a concrete cap and the two inclinometer-casing tubes in the background. Figure 55 shows the load-settlement relationship for the top of pier and the telltale. Loading was discontinued at a top of pier stress of about 880 kPa, which corresponds to about 21 mm settlement at top of pier and 4 mm at the telltale elevation. The difference in settlement is attributed to pier bulging. Figure 56 shows the pier stiffness in terms of applied stress/displacement. Results indicate that stiffness is a function of applied stress and ranges from about 87 to 41 kPa/mm (also MN/m³).

Figure 57 shows the total stress cell readings in Pier No. 1 during the load test. Results are provided for applied stress increments from 24 kPa to 714 kPa. The total stress cell located at 1.3 m was not included in the regression because the readings appear to be spurious. Measurements show that only about 20 percent of the applied stress reached the bottom of Pier No. 1 at high stress levels.

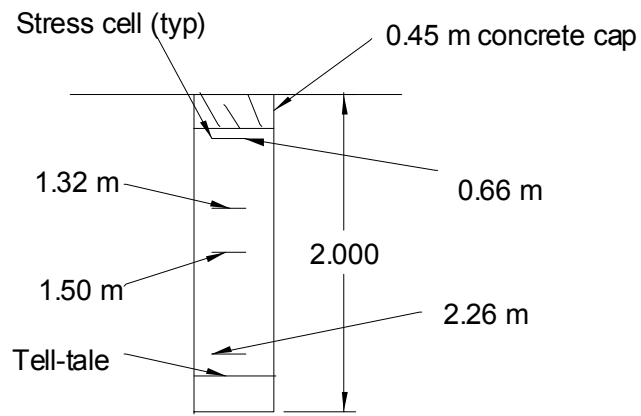


Figure 53. Plan of Individual Pier No. 1 with Instrumentation Locations (Dimensions Shown are in Meters)



Figure 54. Test Pier No. 1

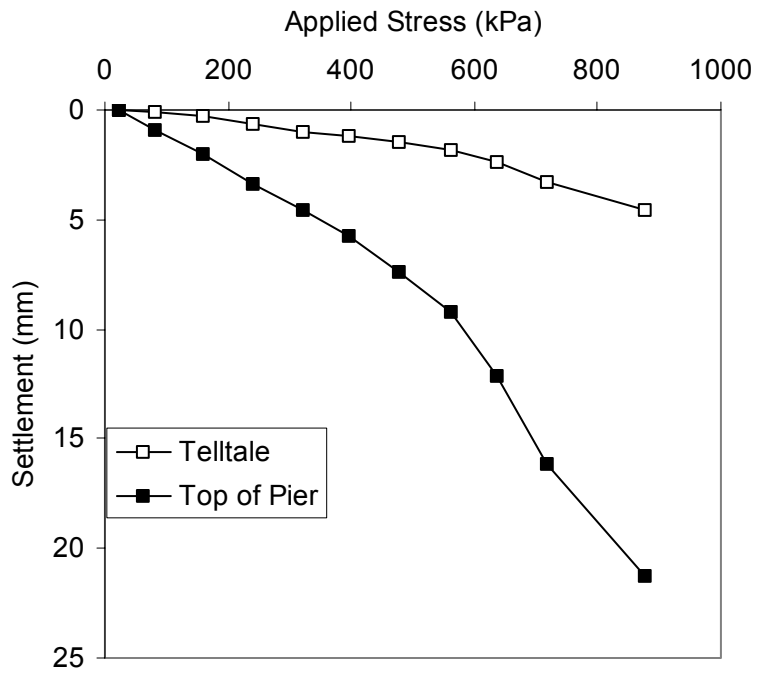


Figure 55. Load-Settlement Results for Pier No. 1

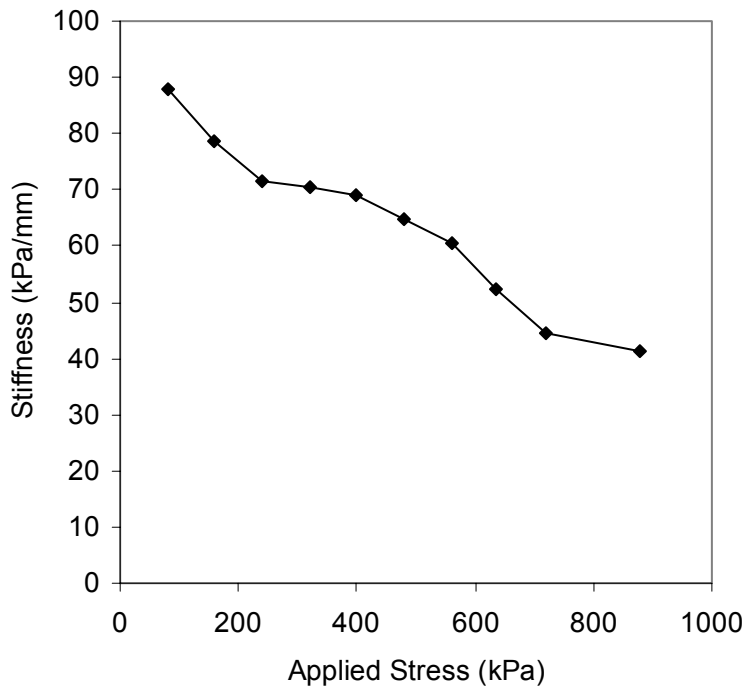


Figure 56. Stiffness Results for Pier No. 1

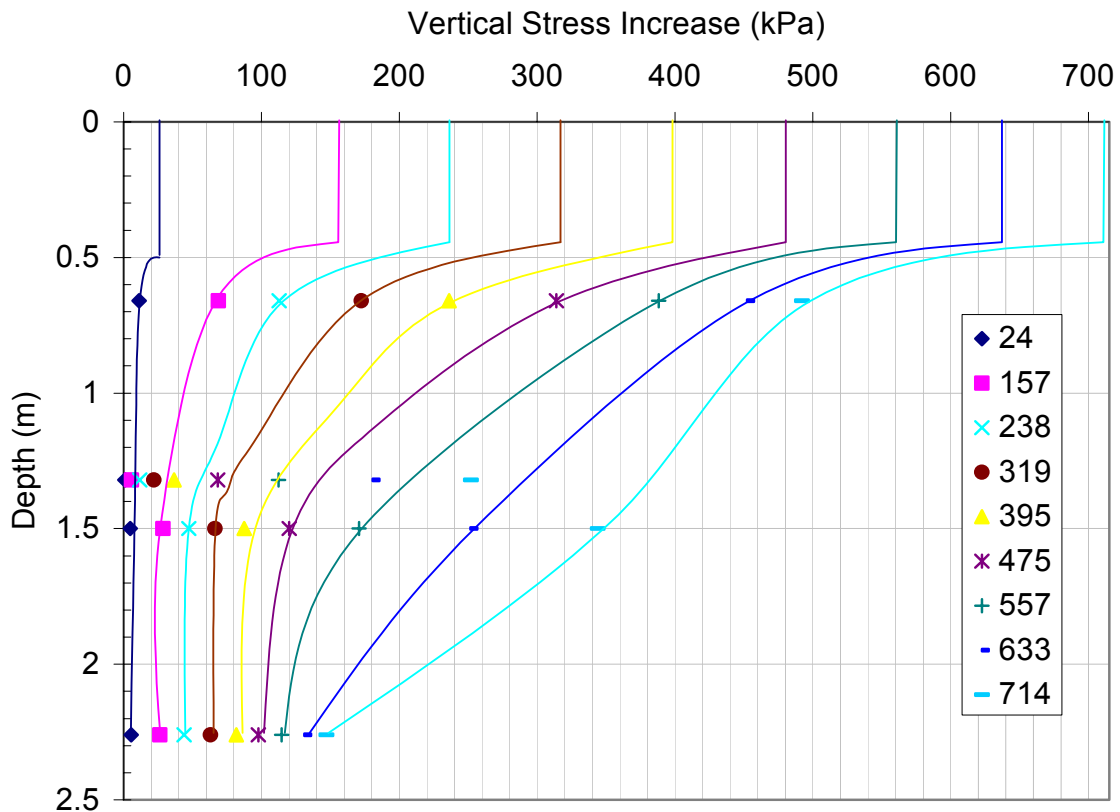


Figure 57. Vertical Stress Distribution from Total Stress Cell Readings in Pier No. 1 (Legend Indicates Applied Stress at Top of Pier)

Inclinometer Casing No. 1 and No. 2 were located about 16.5 cm and 38.1 cm from the edge of Pier No. 1, respectively. Figure 58 presents the lateral deformation measurements immediately after pier installation. Results show deflections up to 9 mm in Casing No. 1 at a depth of 3.2 m and about 1.5 mm in Casing No. 2 near the ground surface. Figures 59 and 60 show the profile at successive load increments for each casing relative to the profile of the casing after pier construction (graph shows only the deflection associated with loading). Each casing shows an area of deflection extending from about 1 to 3 m in the soil profile, with a maximum of 4 mm at a depth of 1.5 m. This movement suggests pier bulging at high loads. Smaller deflections were observed for Casing No. 2, located farther from the pier. The effects of lateral prestraining during construction are observed by the greater deflection magnitude that occurred during construction versus during loading.

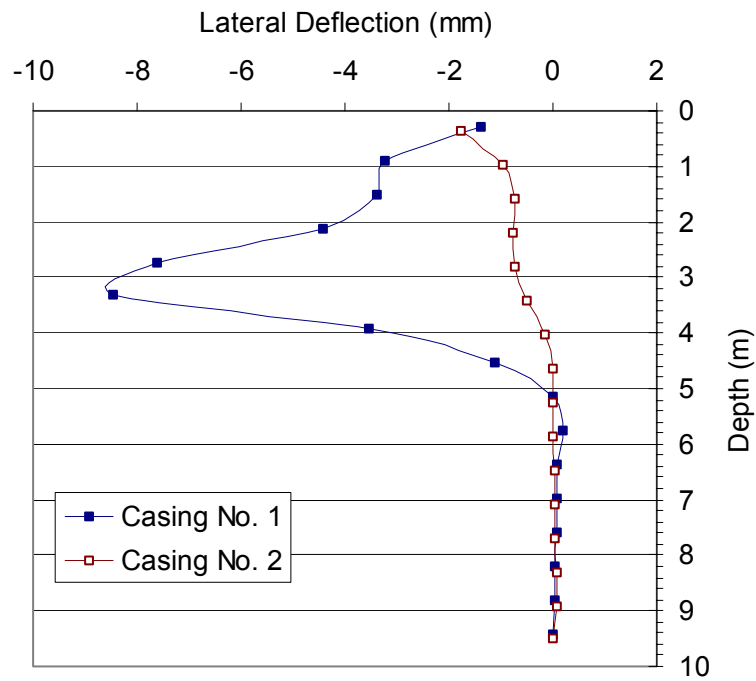


Figure 58. Incliner Casing Profiles after Pier No. 1 Installation

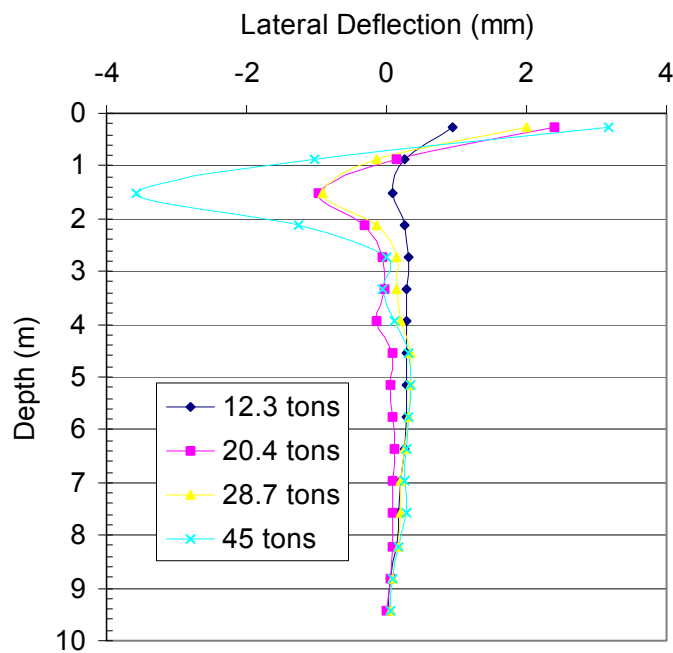


Figure 59. Incliner Casing No. 1 Profiles during Pier No. 1 Loading

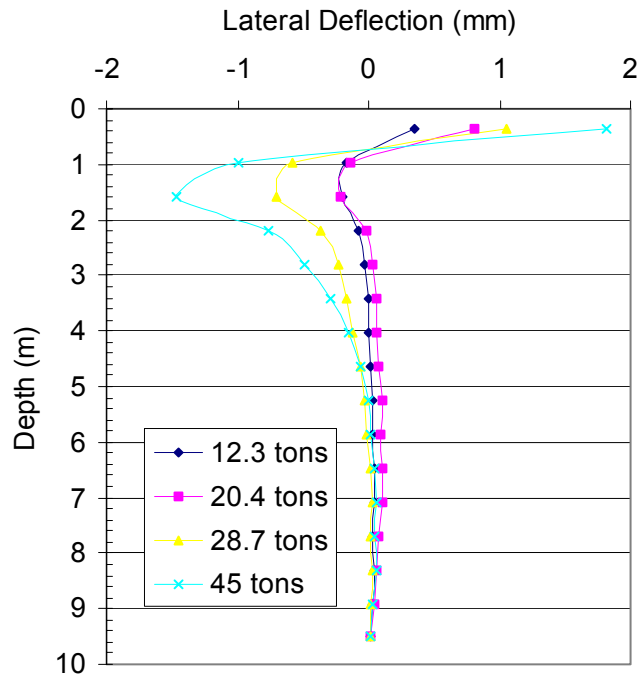


Figure 60. Inclinometer Casing No. 2 Profiles during Pier No. 1 Loading

Pier No. 2 was drilled to a depth of 2.74 m. A telltale was installed above the bottom bulb. Figures 61 and 62 show the settlement and stiffness measurements. Loading was aborted at a stress of about 560 kPa. Top of pier settlement reached 48 mm at this point while the telltale settled about 30 mm. Stiffness varied from about 105 to 10 kPa/mm (also MN/m³) over the applied stress range. Compared with Pier No. 1, No. 2 was not as stiff at high levels of load. Further, telltale movement in Pier No. 2 was about 26 mm more than in Pier No. 1. It is speculated that the total stress cells in Pier No. 1 may have affected its load-settlement behavior.

Pier No. 3 was drilled to a depth of 5.05 m. A telltale was installed prior to construction of the bottom bulb. Figures 63 and 64 display the settlement and stiffness characteristics. Loading was aborted at a stress of about 640 kPa. Top of pier settlement reached 22 mm while the telltale settled only 1.4 mm. The difference in top of pier settlement and telltale settlement suggests pier bulging. Stiffness varied from about 164 to 28 kPa/mm (also MN/m³) and was generally higher than Pier No. 1 and No. 2.

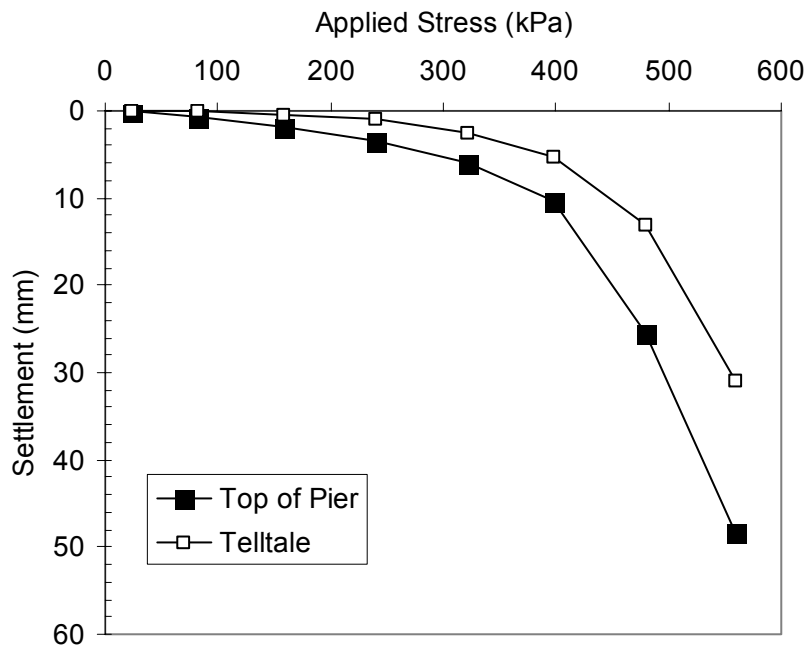


Figure 61. Load-Settlement Results for Pier No. 2

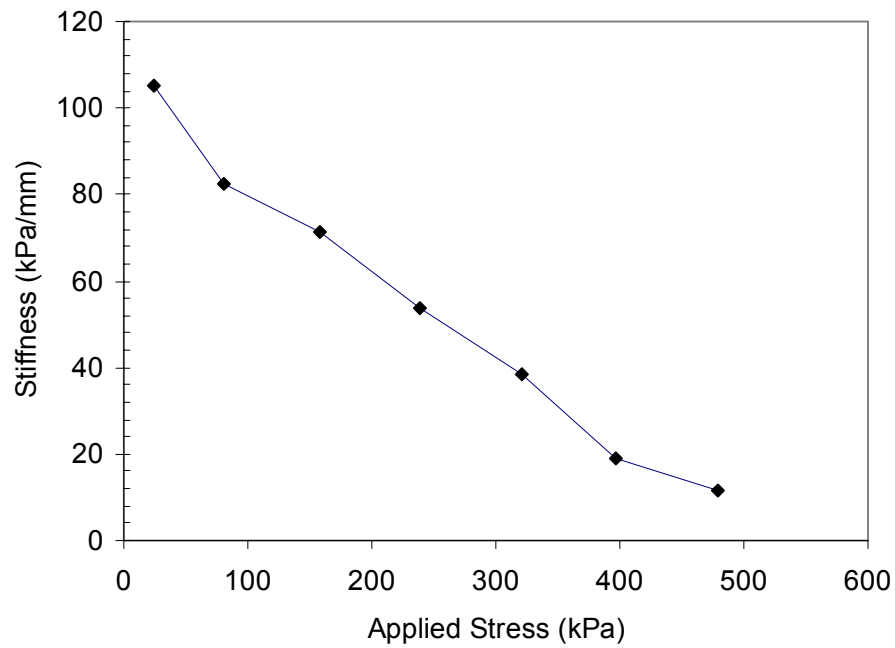


Figure 62. Stiffness Results for Pier No. 2

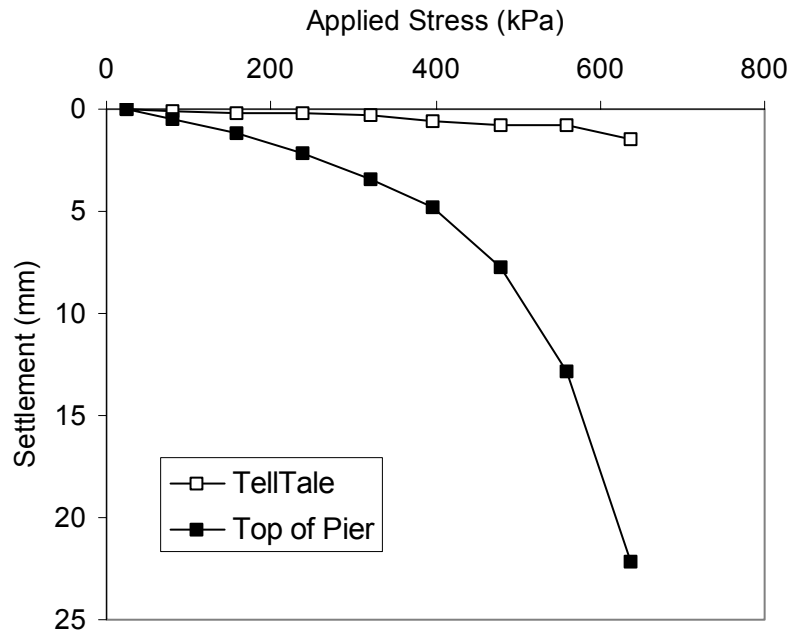


Figure 63. Load-Settlement Results for Pier No. 3

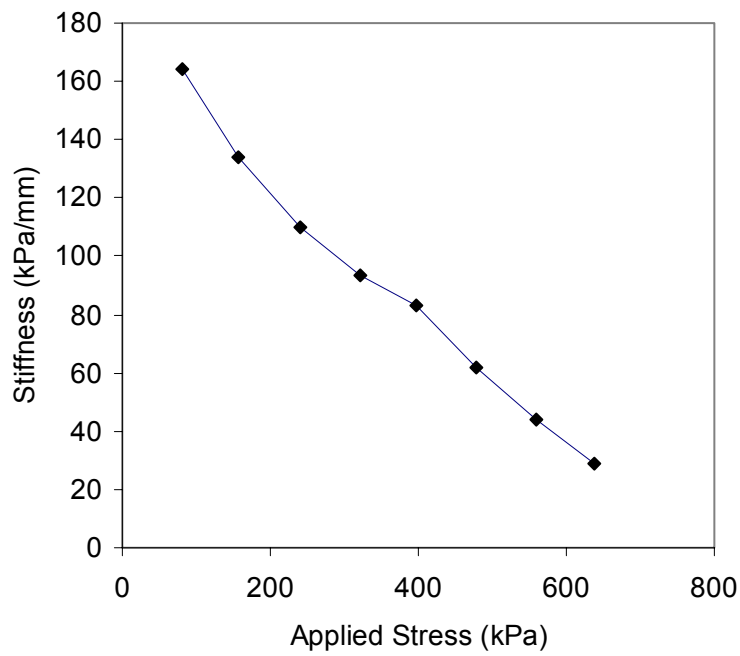


Figure 64. Stiffness Results for Pier No. 3

Group Load Test Results

Two group load tests were performed with footing width (B) to pier depth (D) ratios of 1 and 2 for Group No. 1 and No. 2, respectively. Each consisted of four 0.76 m diameter piers installed in a square pattern with 1.07 m center-to-center spacing and a 0.46 m thick by 2.3 m square reinforced concrete footing. Figures 65 and 66 show the plan and profile views of the installation. Telltales were installed in two of the four piers for both load tests. Total stress cells and inclinometer measurements were available for Group No. 1 only.

Figure 67 shows the construction of Group No. 1 and the load frame setup. Sixteen helical anchors screwed into the underlying weathered shale layer provided uplift anchoring. Figure 68 shows settlement versus load applied at the top of footing for Group No. 1 and No. 2. For Group No. 1, testing was aborted at a load of about 1250 kN because load could no longer be maintained. Over the full range of load increments, the top of footing and the telltales settled similar amounts, which suggests that the Geopier elements were not bulging significantly. Again, the telltales were positioned at 1.9 m below top of footing. Group No. 2 top of footing settlement was similar to Group No. 1 up to a load of about 1000 kN, but showed less settlement between loads of 1000 and 1750 kN. As indicated by the telltale measurements, the Group No. 2 Geopier elements bulged during loading.

As a comparison to the individual load test results, Figure 69 shows the single pier “equivalent” (S_g) load-settlement results for both group load tests. The average applied load was determined by dividing the total group load by four. Figure 70 shows that at high loads the group load-settlement behavior is slightly more efficient than individual pier (S_i) load-settlement behavior.

Group No. 1 was instrumented with 8 total stress cells and shows stress development in the piers, on top of the piers, and on top of the matrix soil between piers. Figure 65 lists the location of each stress cell and shows their locations. Four cells were placed within Geopier elements, one on top of a pier, and three on the matrix soil just beneath the footing. Figure 71 shows the total stress cell measurements. Previous studies show that stress concentrates on the stiffer Geopier elements, rather than the softer matrix soil (Fox and Lawton 1994). Stress cell #662, located on top of a pier, showed the largest stress increase at 400 kPa. Figure 72 shows that stress concentration ratio peaked at about 4, which is calculated as the stress reading at cell #662 (on top of pier) divided by the average matrix soil reading given by cells #657, #661, and #666.

Inclinometer measurements (51 cm from edge of a pier) were recorded before and after pier installation and then during three subsequent loadings as shown in Figure 73. Maximum lateral deflection of 0.5, 2.5, and 6.6 mm were observed for loads of about 424, 836, and 1247 kN, respectively. The zone of bulging extended from about 1.5 m to 6.0 m below grade. The depth of each pier was only 2.7 m below grade. Lateral movement at depths up to 6 m suggests a punching-type bearing capacity failure. No ground heave was observed.

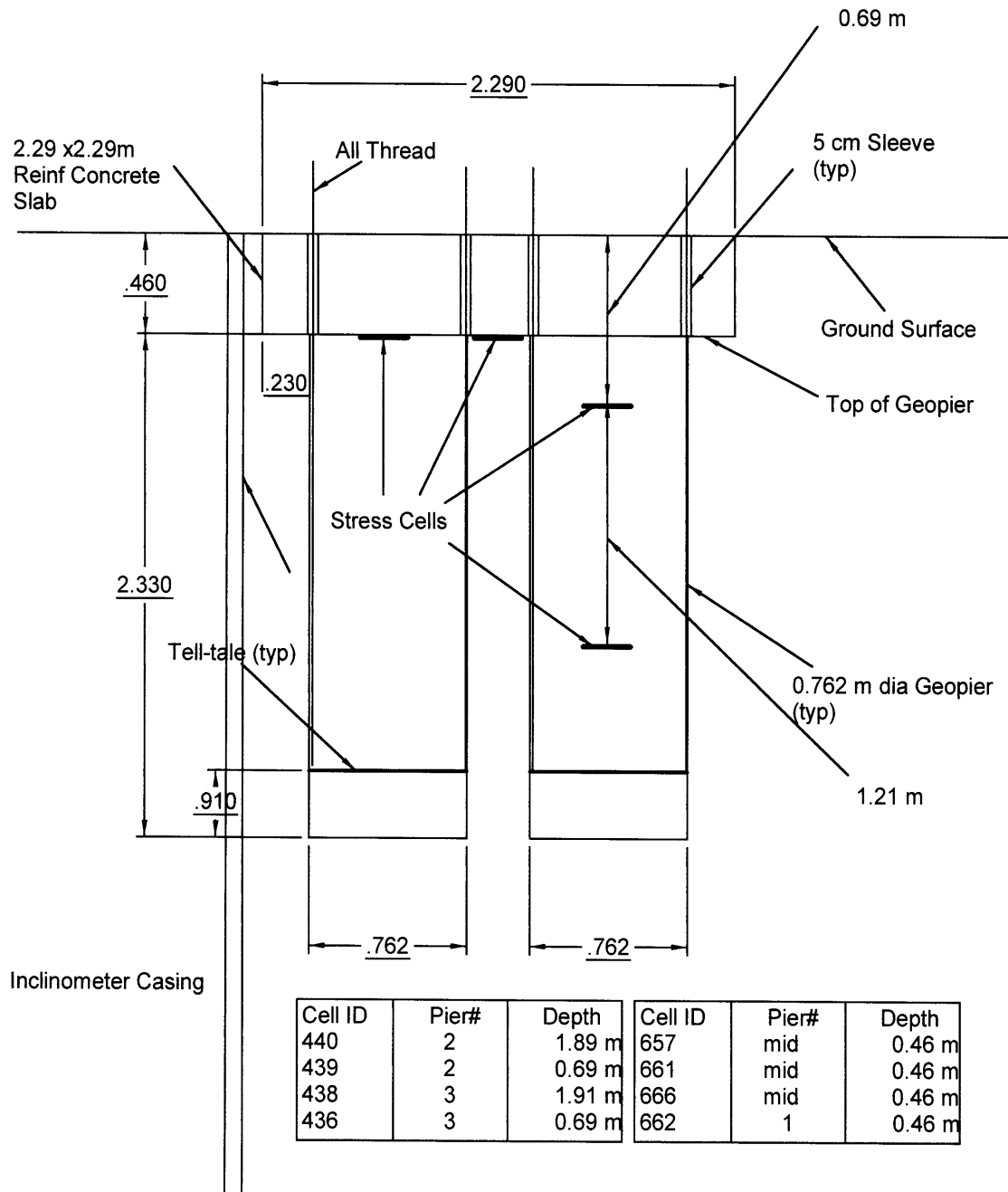
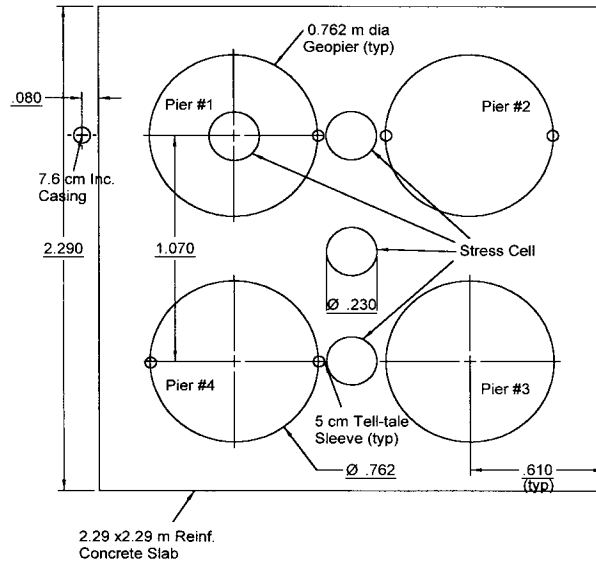


Figure 65. Group Load Test No. 1 Profile View Showing Instrumentation Locations (Dimensions Shown in Meters Unless Indicated)



**Figure 66. Group Load T No. 1 Instrumentation Plan
(Dimensions Shown in Meters Unless Indicated)**



Figure 67. Group Load Test No. 1 Construction and Load Frame

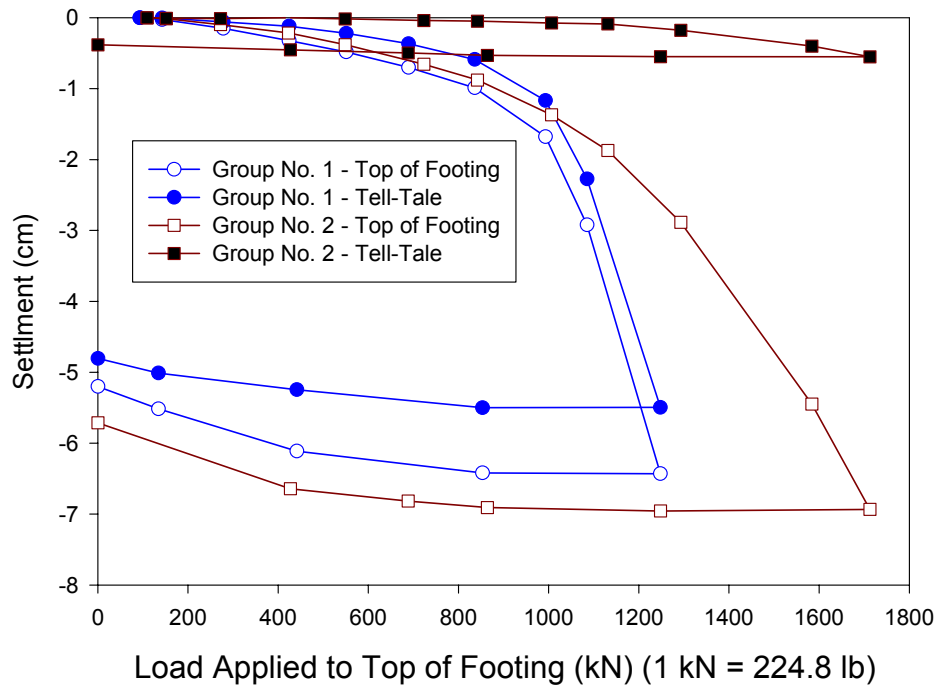


Figure 68. Settlement vs. Applied Load at Top of Footing of Group No. 1 and 2

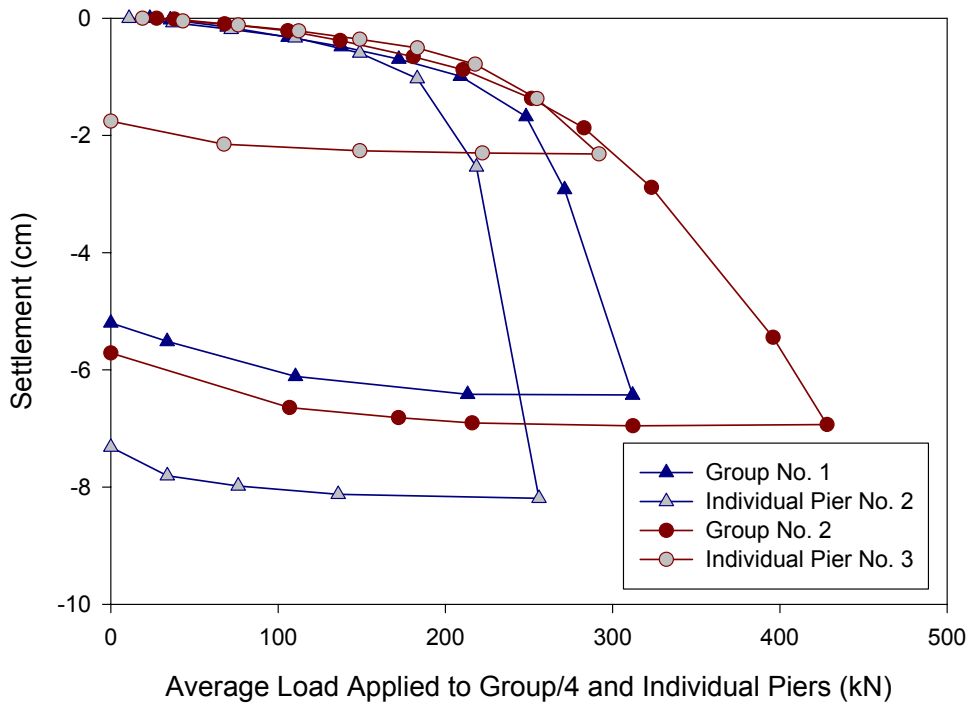


Figure 69. Comparison of Group and Individual Pier Behavior

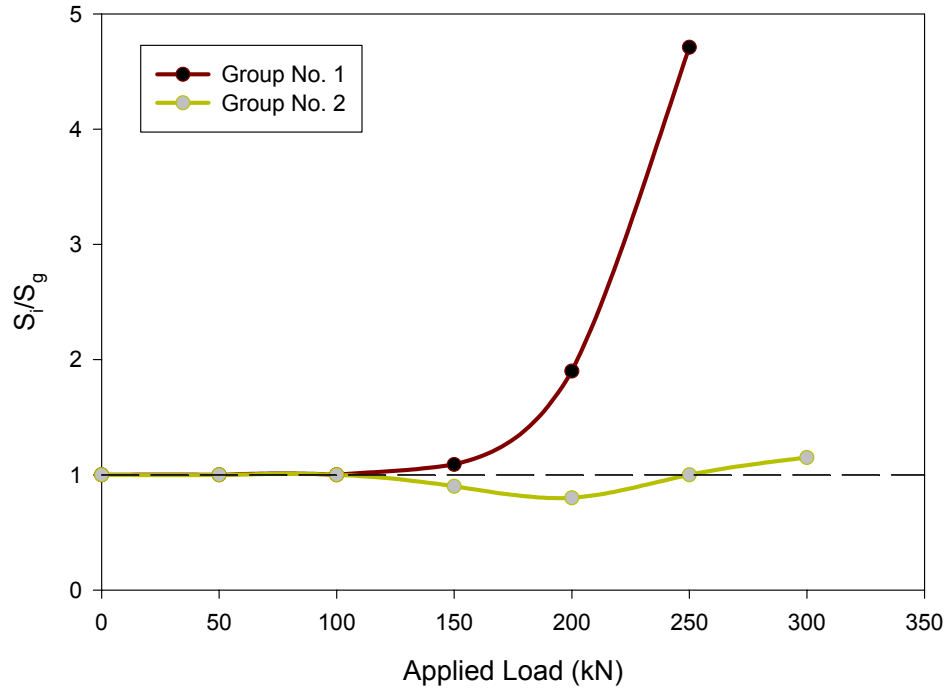


Figure 70. Group Efficiency Compared to Individual Load Tests

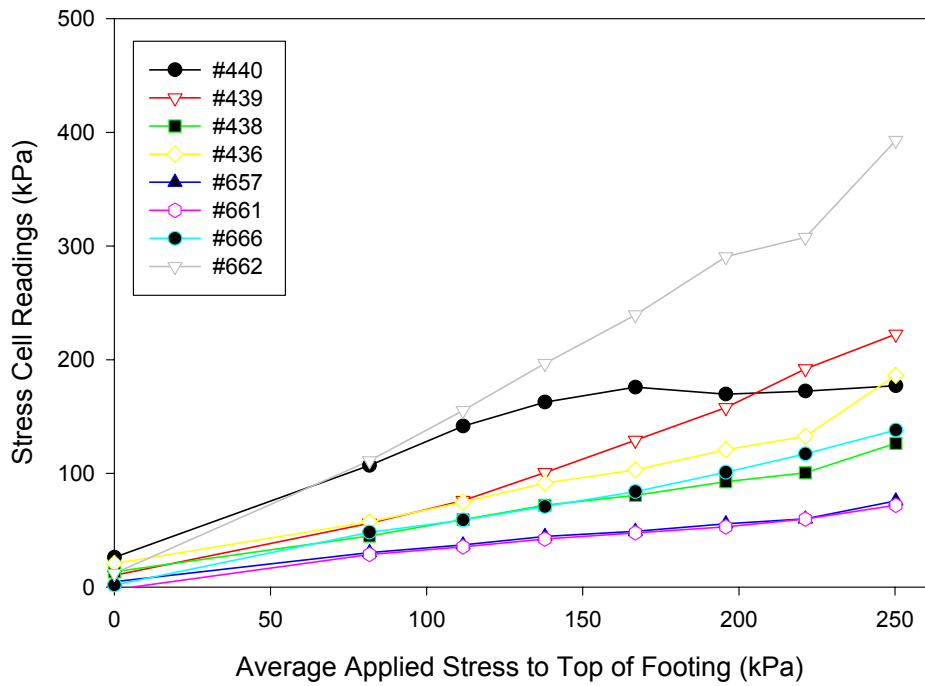


Figure 71. Total Stress Cell Readings for Group No. 1

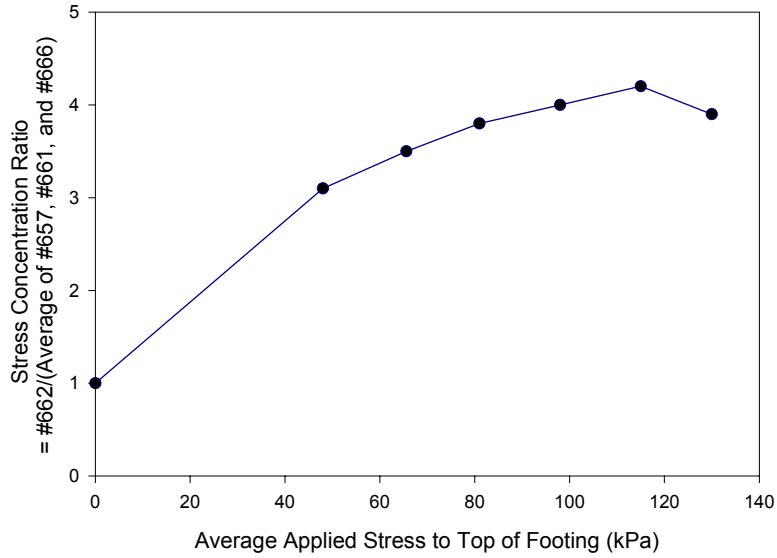


Figure 72. Stress Concentration Ratio for Group Load Test No. 1

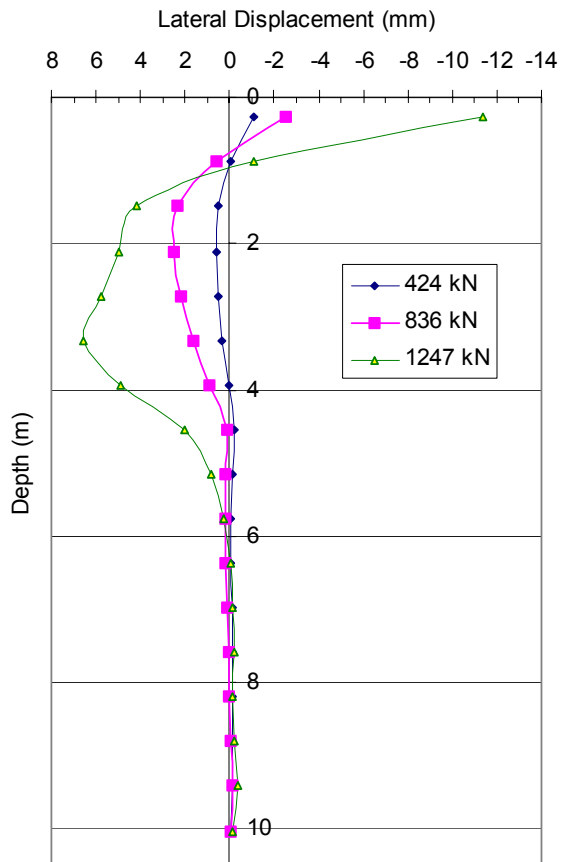


Figure 73. Inclinometer Profile for Group Load Test No. 1 during Loading

Performance Monitoring

Total and differential settlement of the box culvert and settlement of the bridge were considered during the performance-monitoring phase of this project. Optical surveys, vibrating wire total stress cells, piezometers, and settlement cells were used to monitoring the box culvert and bridge structure. Results of the performance monitoring are described below.

Instrumentation Results

Geotechnical instrumentation, including total stress cells, piezometers, and settlement cells were installed before construction of the embankment. An instrumentation console consisting of a data-logging device, memory storage, battery, and solar panel was placed at the site to provide automatic logging of data twice per day. The instrumentation plan is shown in Figure 74. Eleven settlement pins were also installed at equidistant intervals along the floor of the culvert and were surveyed optically on a regular basis before and after construction.

Piezometers

To measure pore pressure changes in the alluvial clay layer during Geopier construction and subsequent embankment construction, piezometers were installed in a single borehole at depths of 0.6 m, 2.1 m, 4.7 m and 5.9 m (see Figure 75). Wet site conditions during borehole drilling and Geopier construction are shown in Figure 76.

After establishing a baseline reading, piezometer measurements were recorded during construction of three adjacent Geopier elements. The data-logging device was programmed to log readings at four-second intervals. The time and duration of installation activities were recorded simultaneously as the installations progressed. Superposition of pore pressure measurements with construction activities is presented in Figure 77. Results initially show relatively large pore pressure decreases during drilling of the piers—presumably due to suction effects during auger extraction, which could be heard at the surface.

After drilling each pier, aggregate was placed and compacted. The first lift for each pier was a nominal 0.6 m thick and all subsequent lifts were 0.3 m thick. Each lift was compacted for about 20 seconds. During compaction, pore pressure increases were recorded. The largest peaks were observed during compaction at elevations coincident with a piezometer elevation. This is evidenced in the ramming of pier 122.

At the bottom of the piers, penetration of the glacial sand layer resulted in rapid water infiltration and caving in the hole. It was quickly decided that piers should be terminated just above the sand layer.

Long-term pore pressure measurements during and after embankment construction are shown in Figure 78. It was anticipated that pore pressure would increase as embankment fill height increased and then decrease as consolidation progressed. Results, however, indicate no significant pore pressure increase during fill operations and suggests that the closely spaced Geopier elements were acting as pore water drains.

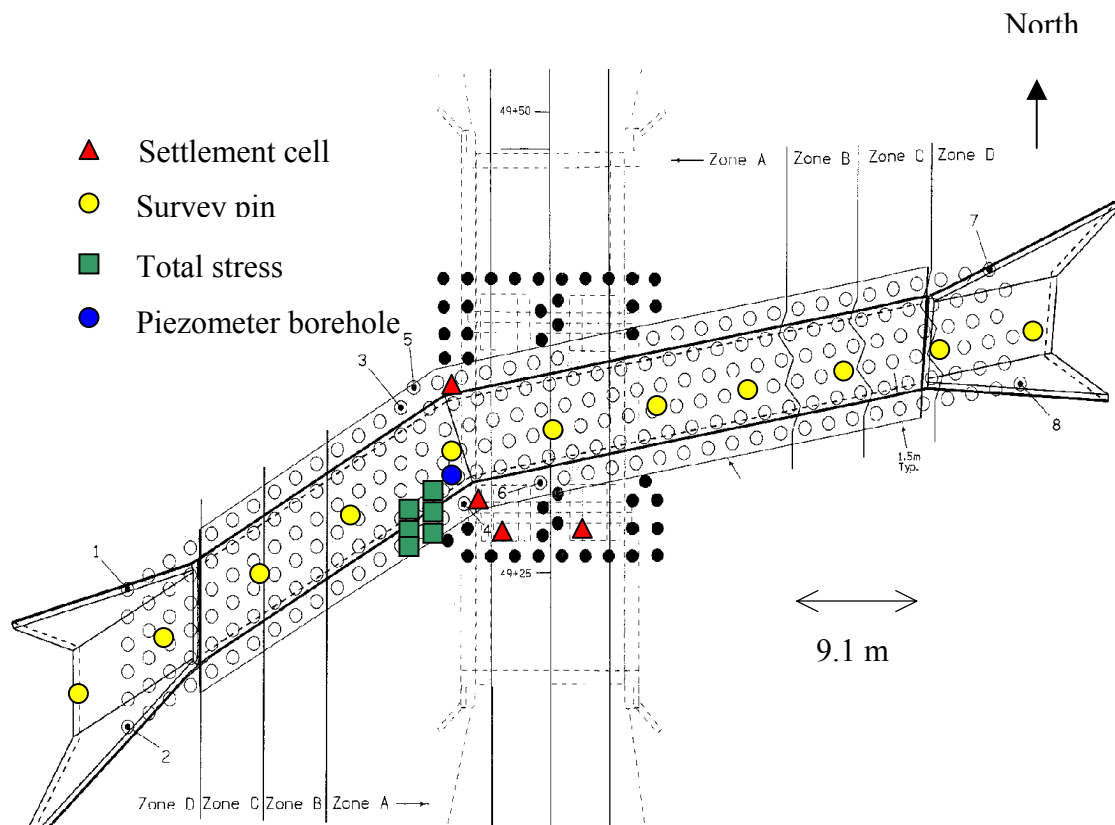


Figure 74. Locations of Instrumentation and Geopier Installation Zones

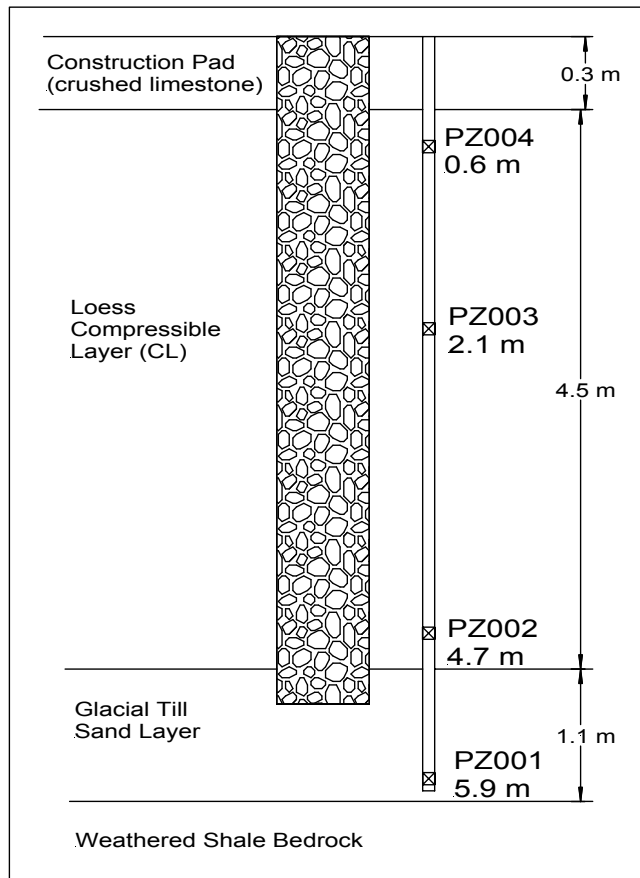
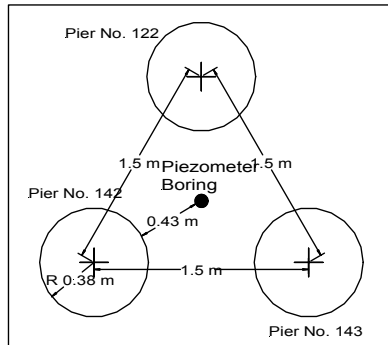


Figure 75. Piezometer Layout



Figure 76. Wet Conditions during Piezometer Borehole Installation and Geopier Construction

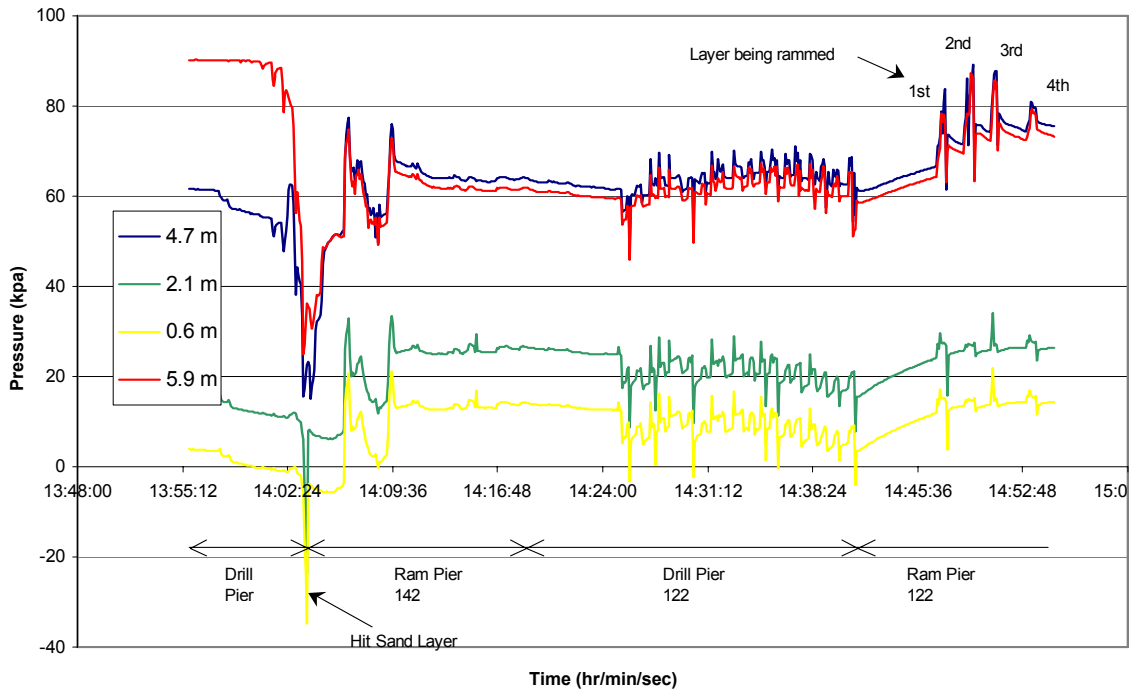
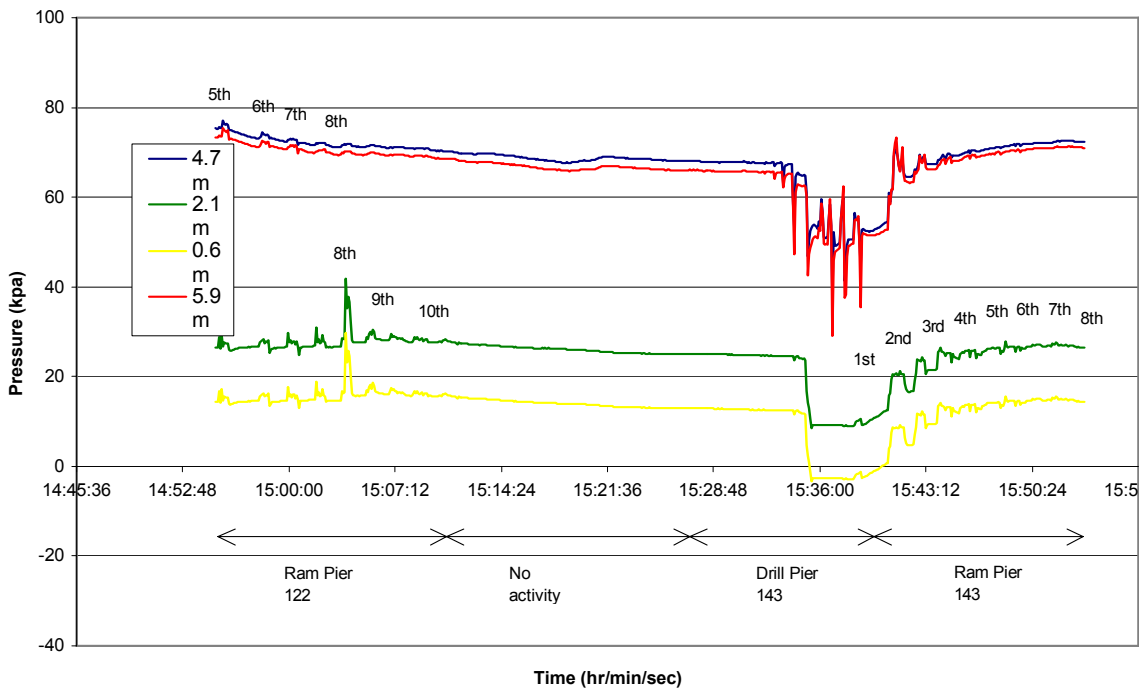


Figure 77. Piezometer Readings for First Half of Dynamic Pore Pressure Test



**Figure 77. Piezometer Readings for Second Half of Dynamic Pore Pressure Test
(continued)**

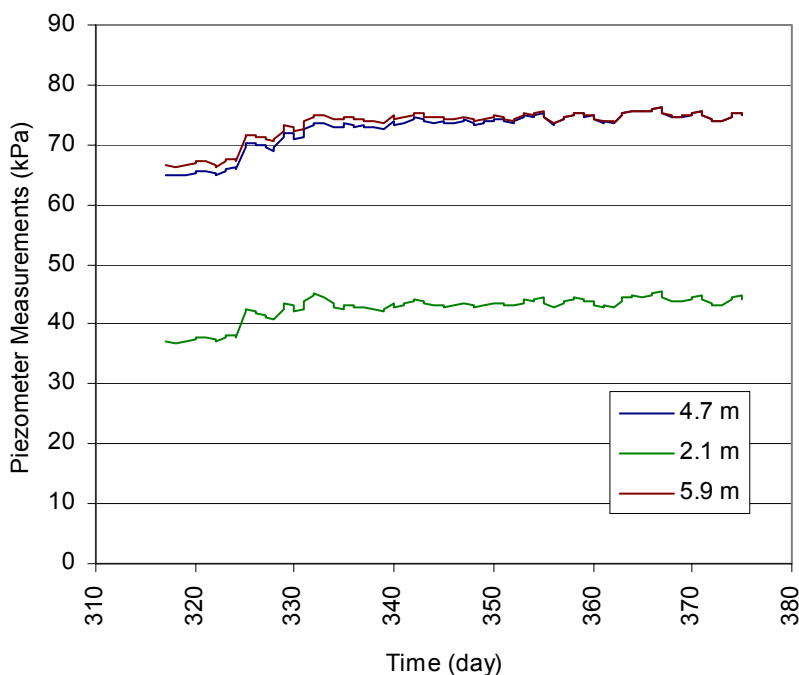


Figure 78. Piezometer Readings Before, During, and After Embankment Construction

Total Stress cells

Total stress cells were installed in two groups of three. For each group, two cells were installed at the tops of piers and one cell at the top of the matrix soil between piers. The location of individual cells is shown in Figure 74. Total stress cells were positioned to measure stress increase under the largest part of the embankment and also to measure stress concentration ratios between the pier and matrix soil.

Figure 79 shows total stress cell readings starting one-week prior and ending five-weeks after embankment construction. Stress measurements ranged from about 60 to 120 kPa. The average stress increase for cells placed at the top of Geopier elements was about 115 kPa and for cells placed on the matrix soil about 80 kPa. The average stress concentration is therefore about 1.4.

Settlement cells

The settlement cell system consisted of a liquid reservoir, liquid-filled tubing, and the settlement cell, which contained a vibrating wire pressure transducer. As settlement occurs, the transducer measures the change in pressure head. Knowing the density of the liquid in the reservoir and tubing, vertical settlement can be calculated. Figure 74 shows the settlement cell locations. Two cells were attached to bridge piers at the southern end of the bridge, and two cells were attached to the box culvert near the center of the bridge. Figure 80 presents the settlement cell readings before and after construction. Results show considerable scatter, which is believed to be a result of the data logger sampling the vibrating wire pressure transducers prior to establishing a uniform reading.

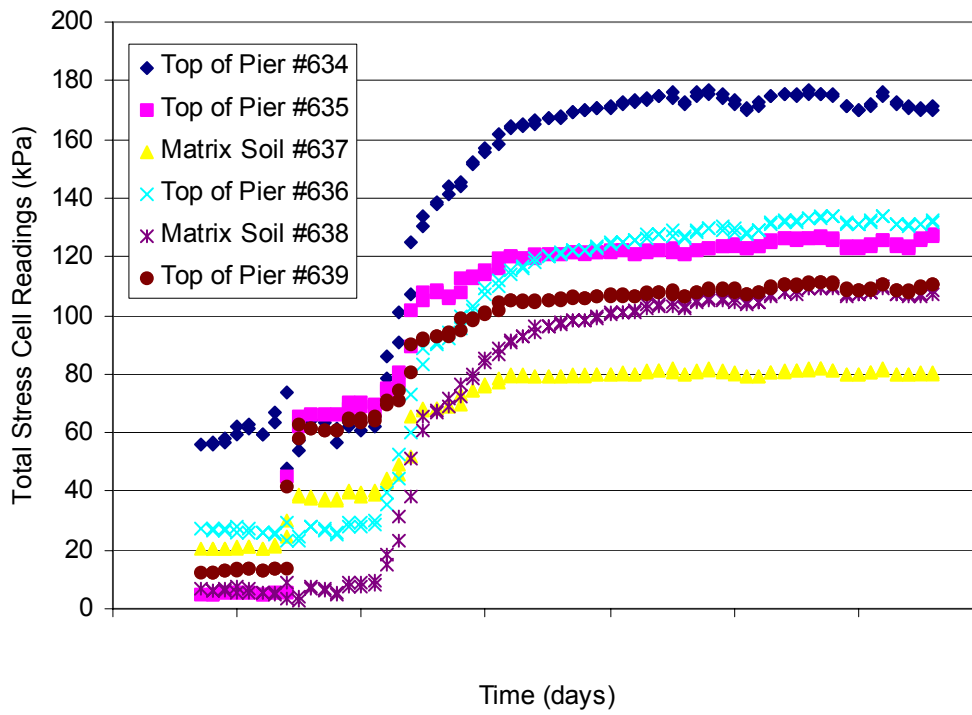


Figure 79. Stress Cell Readings Before and After Embankment Construction

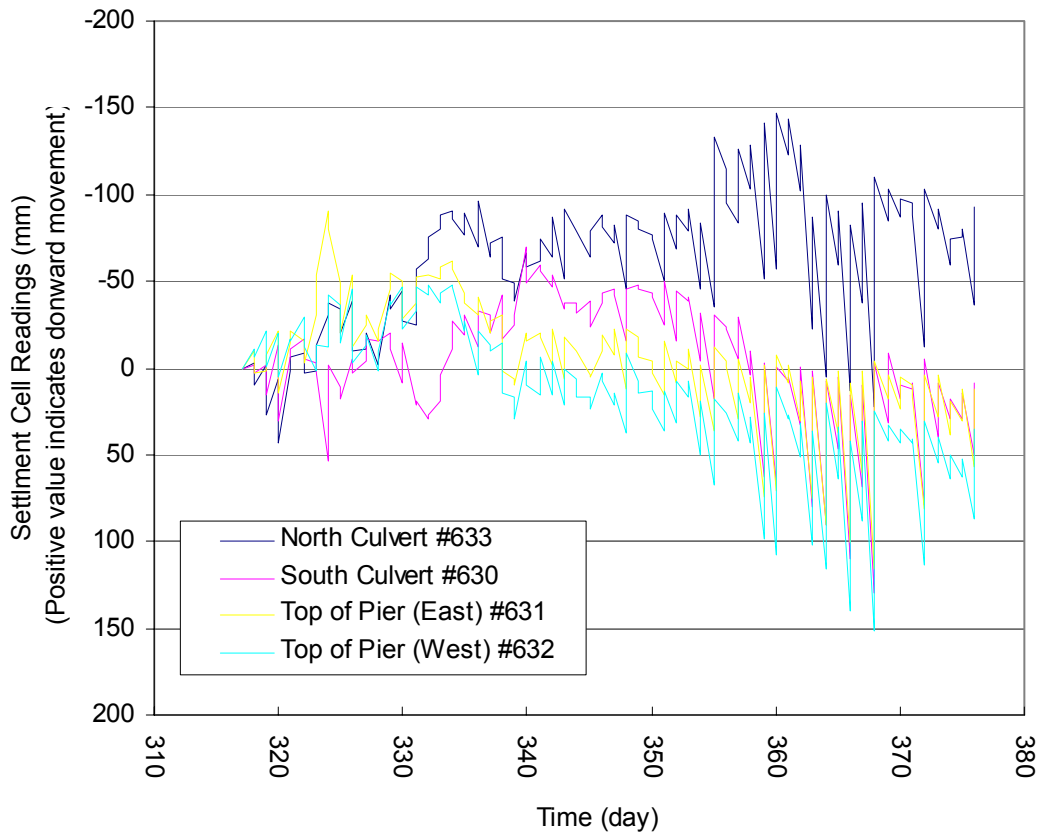


Figure 80. Settlement Cell Readings Before and After Embankment Construction

Comparison to Design Predictions

This section of the report briefly describes the assumptions used in the settlement calculations for the unreinforced culvert and for the Geopier reinforced condition. Finally, field measurements are described, which verify the predicted values.

Unreinforced Culvert

Results provided in Figure 51 and Table 12 were used to estimate the magnitude of primary consolidation settlement for the unreinforced culvert. Assumptions used in these calculations were: (1) The alluvial clay layer was normally consolidated; (2) The drainage distance equals half the thickness of the alluvial clay layer or about 3.75 — assumes glacial sand at the bottom of the alluvial clay layer would act as a drainage pathway; (3) The applied stress at the ground surface due to box culvert and embankment construction would be about 160 kPa; and (4) Based on estimates from Boussinesq theory, a stress increase of 125 kPa was estimated at the mid-height of the clay layer. Using these assumptions, it was estimated that the unreinforced culvert would settle about 50 cm. A period of 170 days was estimated to reach 90 percent primary consolidation.

Geopier Reinforced Condition

To estimate settlement for the Geopier reinforced condition, stiffness of the Geopier elements and stress concentration must be estimated. For clay soils with SPT N values of 1 to 3, Fox and Cowell (1998) recommend using a design stiffness of about 33 MN/m³. Full-scale load test results verified that this value was reasonable. Stress concentration is established with the expression (Lawton et al. 1994):

$$q_g = q [R_s / (R_s R_a - R_a + 1)] \quad (2)$$

Where q_g is the stress applied to the tops of the Geopier elements and q is the average applied stress at the bottom of the box culvert. A stiffness ratio (R_s) was established using computations derived from in situ tests. Using an area replacement ratio of 25 percent and a maximum culvert-bottom stress of 160 kPa (Zone A), a top-of-Geopier stress (q_g) of 490 kPa is computed. The settlement of the reinforced zone (s_g) is then computed as:

$$s_g = q_g / k_g = 490 \text{ kPa} / 33 \text{ MN/m}^3 = 14 \text{ mm} \quad (3)$$

Based on an assumed stress distribution and soil elastic modulus values, additional settlements on the order of 11 cm were computed to occur below the 6.7 m long elements (details are described by Fox and Cowell 1998). Calculated design lengths and anticipated settlements are provided in Table 13. Based on these calculations, the design criteria of ≥ 15 cm of total settlement and ≥ 10 cm of differential settlement would be satisfied. Design calculations performed by the authors' for Zones A through D are provided in Appendix H.

For estimating the time rate of settlement, solutions are given by Han and Ye (2001) who identify two mechanisms that contribute to settlement rate reduction: (1) The presence of the vertical drainage element, which reduce the flow distance for the dissipation of excess pore water pressure and (2) The concentration of stress to the relatively stiff Geopier elements, which reduce the consolidation settlement of the compressible matrix soils. With Geopier reinforcement, 90 percent primary consolidation was estimated at about 10 days.

Field Measurements

Figure 81 and Table 14 show the optical survey log along the length of the box culvert. The data indicate a maximum settlement of 11.5 cm at pin number 5 and a maximum differential settlement of 7.9 cm between pin numbers 5 and 11. Figure 82 shows the completed box culvert section. Figure 83 shows the settlement at pin 5 as a function of fill height. Measurements show that the culvert settled 1 cm before backfilling, which began on 11/27/01. Fill placement was completed on 12/6/01. Figure 84 shows the settlement of the culvert at pin 5 with respect to time. Future long-term (up to 5 years) settlement measurements are planned.

Table 13. Design Settlement Calculations

Design Section Zone	Shaft Length (m)	Bearing Pressure (kPa)	Upper Zone Settlement (cm)	Lower Zone Settlement (cm)	Total Settlement (cm)
A	6.71	163	1.4	10.3	12.7
B	5.79	123	1.1	12.0	13.0
C	4.27	82	0.7	11.9	12.6
D	0.91	41	0.4	10.3	10.6

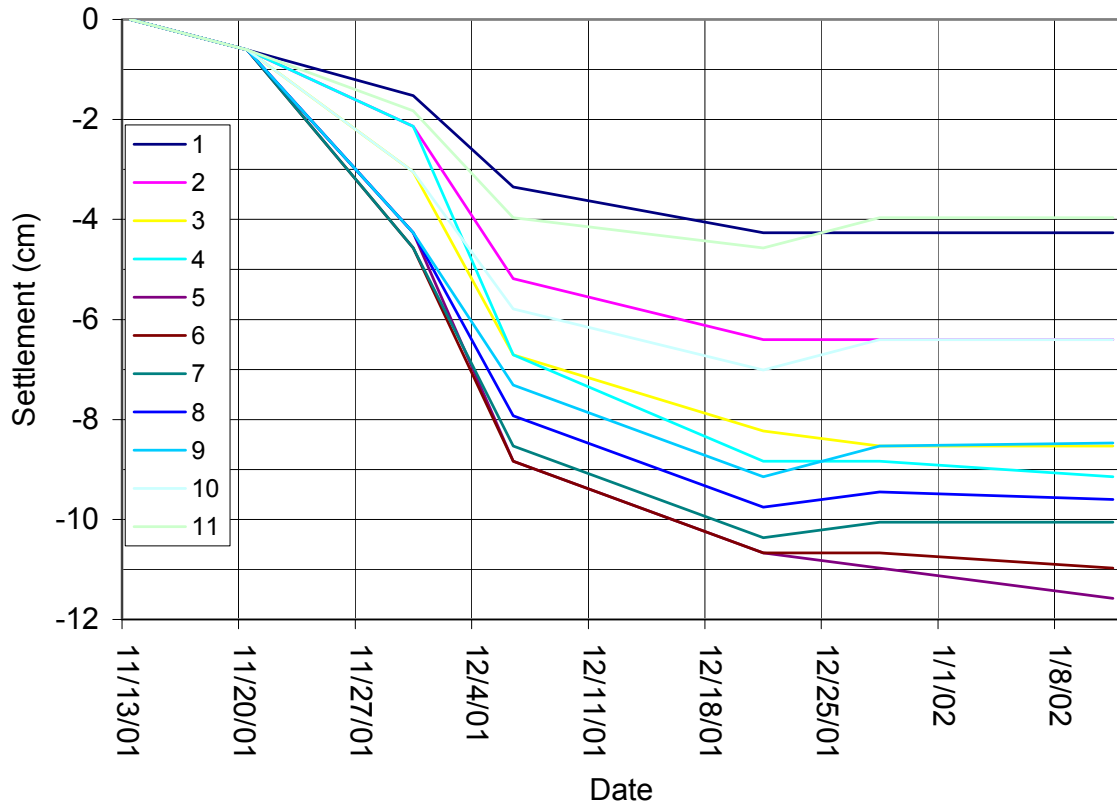


Figure 81. Settlement of Box Culvert along Survey Pins (pin 1 west to pin 11 east)

Table 14. Settlement of each Surveying Pin One-Week Prior to and Five Weeks after Embankment Construction

Date	Pin Number										
	1	2	3	4	5	6	7	8	9	10	11
	Settlement (mm)										
11/20/01	6	6	6	6	6	6	6	6	6	6	6
11/30/01	15	21	30	21	43	46	46	43	43	30	18
12/6/01	34	52	67	67	88	88	85	79	73	58	40
12/21/01	43	64	82	88	107	107	104	98	91	70	46
12/28/01	43	64	85	88	110	107	101	94	85	64	40
1/11/02	43	64	85	91	116	109	101	96	85	64	40

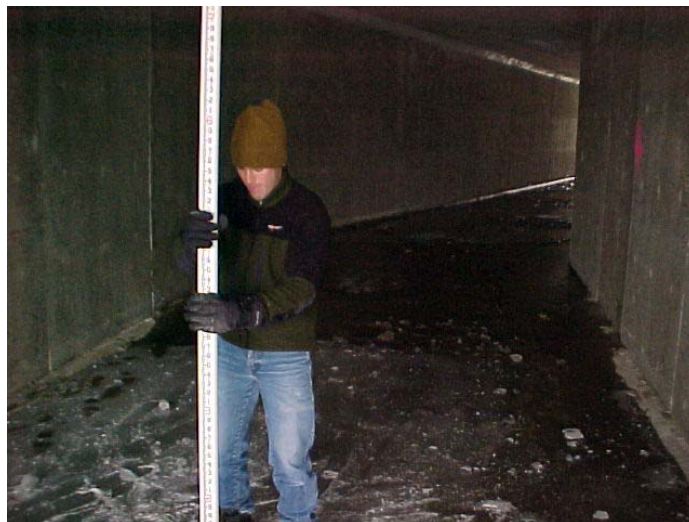


Figure 82. Completed Box Culvert

Although the project met the criterion for differential settlement, it is the authors' opinion that the Geopier elements in zone D were too long. The design called for four zones of different pier lengths. Varying the pier lengths was intended to compensate for the non-uniform fill height over the culvert, i.e., shorter piers where there is less overburden. Figure 74 shows the pier zones and Table 13 lists design pier lengths for each zone. Review of the pier installation as-built records reveals that piers in zones A, B, and C were drilled as specified in the original design documents. However, zone D piers were constructed to an average length of 2.3 m, which is more than twice the design length of 0.9 m. Zone D was designed to settle about 10.6 cm, but with longer than specified piers it only settled about 4 cm, contributing to increased differential settlement. In effect, the box culvert curled up at the ends, which is believed to have contributed to opening of small gaps along construction joints (see Fig. 85). The gaps are larger at the bottom of the culvert than the top, confirming the "curled up" behavior described above.



Figure 85. Crack Opening at Construction Joints in Box Culvert

Summary and Conclusions

The following conclusions are based on the information gathered throughout the course of this investigation:

- Group load tests of Geopier elements indicate that the ultimate capacity of groups of four piers loaded beneath a rigid foundation is similar to the sum of individual capacities.
- Telltale measurements for the group load tests indicate that the footing width (B) to pier length (D) ratio of 1 resulted in a punching type failure. Bulging failure was observed for the $B/D = 2$ group load test.
- Stress concentrations on the Geopier elements during full-scale load testing of Group No. 1 measured about 4 relative to the matrix soil.
- The vertical stress distribution within individual Pier No. 1 indicates that about 20 percent of the applied stress of at the top of pier reaches the bottom of the pier at high load levels.
- Pore pressure measurements adjacent to piers during construction show that pore pressure increases during ramming and quickly dissipates.
- The box culvert settled about 12 cm relative to the predicted unreinforced settlement of about 50 cm.
- Measured settlement is lower than the criteria of 15 cm of total settlement and 10 cm of differential settlement.
- The increase in pier construction length in *Zone D* likely resulted in an additional 2 to 3 cm of differential settlement.
- Settlement rate calculations within the alluvial clay layer revealed that Geopier reinforcement could increase the time rate to reach 90 percent primary consolidation from 170 days to about 10 days. Field monitoring indicates that about 90 percent was reached somewhere between 7 and 14 days.

Project No. 3: Bridge Approach Embankment Reinforcement at US Hwy 18/218 (Charles City, IA)

The third application for Geopier soil reinforcement evaluated in this study is controlling or preventing formation of the “bump at the end of the bridge.” As is the case in Iowa, many state DOTs consider bridge approach settlement a problem of significant cost that requires regular maintenance. Settlement of the natural foundation soils and compression of the embankment fill material are the two most significant factors contributing to the formation of the bump (see Briaud 1997). This project provided the opportunity to monitor bridge approach settlement for adjacent Geopier reinforced and non-reinforced embankments. The project was established through Iowa DOT Offices of Bridge and Soil Design with cooperation from Peterson Contracting, Inc., and the ISU Spangler Geotechnical Laboratory. Geopier® Foundation Company, Inc., provided partial financial support for monitoring.

Project Conditions

30 Geopier elements of varying length were installed on each side of a new bridge to support the reinforced concrete approach slabs. The new bridge deck is pile-supported and both the east and west (plan view) approach slabs were constructed of fill soil. The top of the embankment is about 12 m wide and the roadway is about 8 m wide. Based on initial site borings, the embankment fills consist of about 8 m to 9 m of clay fill overlying native medium stiff to stiff glacial clay. Results of the unconfined compression tests for the fill material at each side of the bridge indicate average undrained shear strength of about 65 kPa.

Design

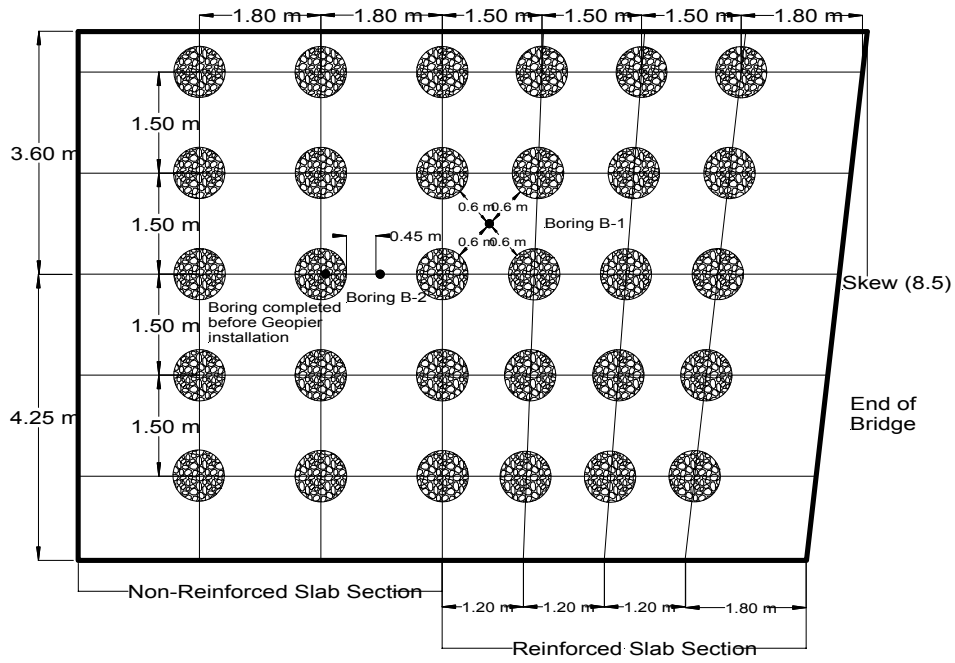
The Geopier design is shown in Figure 92 and includes a total of 30 Geopier elements spaced 1.8 m on-center in both directions. Six rows of Geopier elements were planned with the edge of the first row located parallel to and approximately 1.2 m from the edge of the driven H-piles. Each row contains 5 Geopier elements. Table 17 lists the design drill lengths for the Geopier elements.

Table 15. Geopier Design Drill Lengths

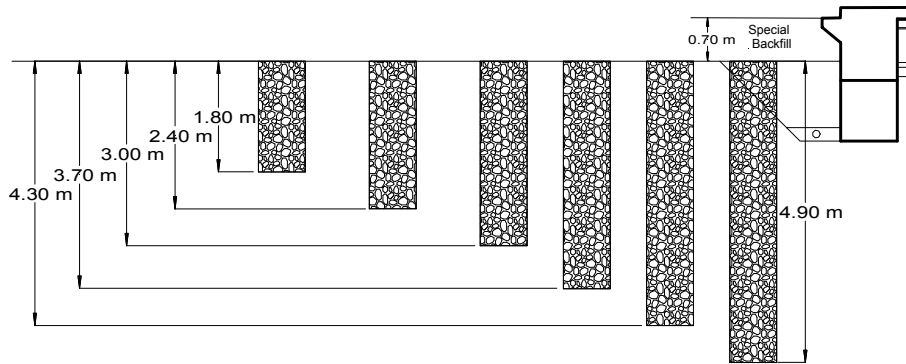
Row number	Geopier Element Length (m)
1 (Closest to bridge)	4.9
2	4.9
3	3.7
4	2.4
5	2.4
6	1.8

Performance Monitoring

Figures 93 through 95 show the performance monitoring results, which consist of optical settlement surveys recorded every 6 months. As shown there is little difference at this time between the reinforced and unreinforced sections. The South abutment of the Geopier reinforced section, however, shows less settlement from about 40 to 60 ft than the non-reinforced section. Additional settlement monitoring (up to five years) is planned at this site. Future projects could consider increasing the length of the Geopier elements to penetrate the underlying embankment foundation soils.



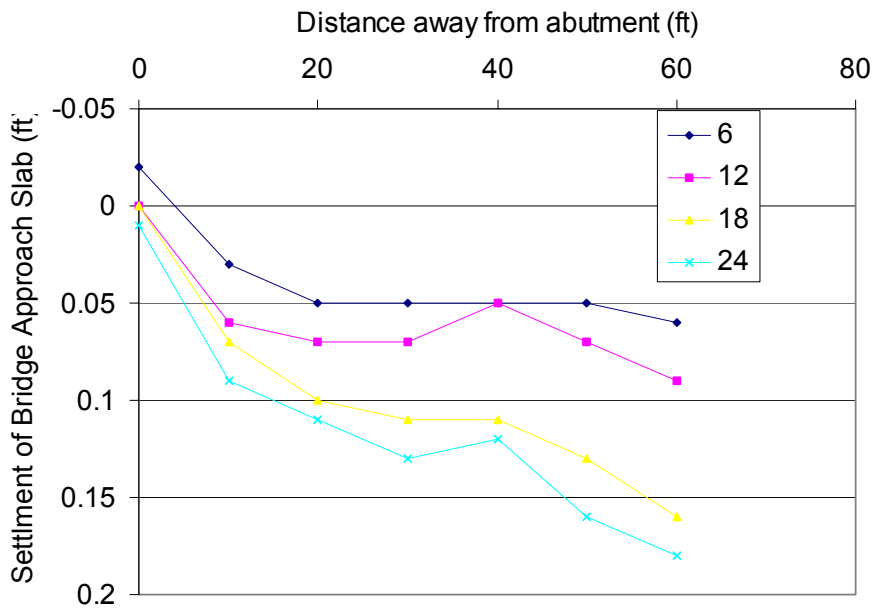
PLAN VIEW OF GEOPIER INSTALLATIONS SOUTH APPROACH



PROFILE OF GEOPIER DRILL DEPTHS SOUTH APPROACH

Figure 86. Design Details for Geopier Installation

NBL North Abutment - Geopier Reinforced



NBL South Abutment - Geopier Reinforced

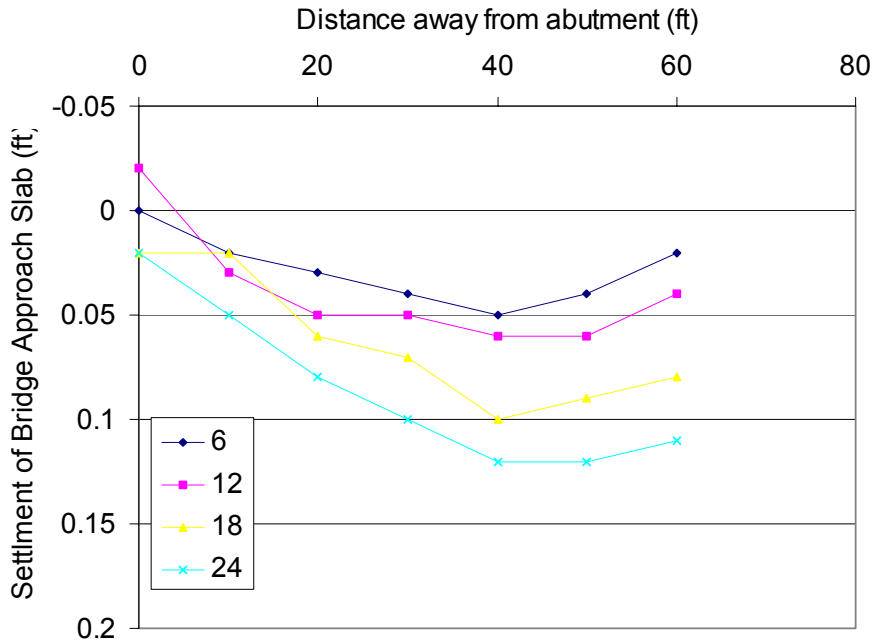


Figure 87. Approach Slab Settlement for Geopier Reinforced Section

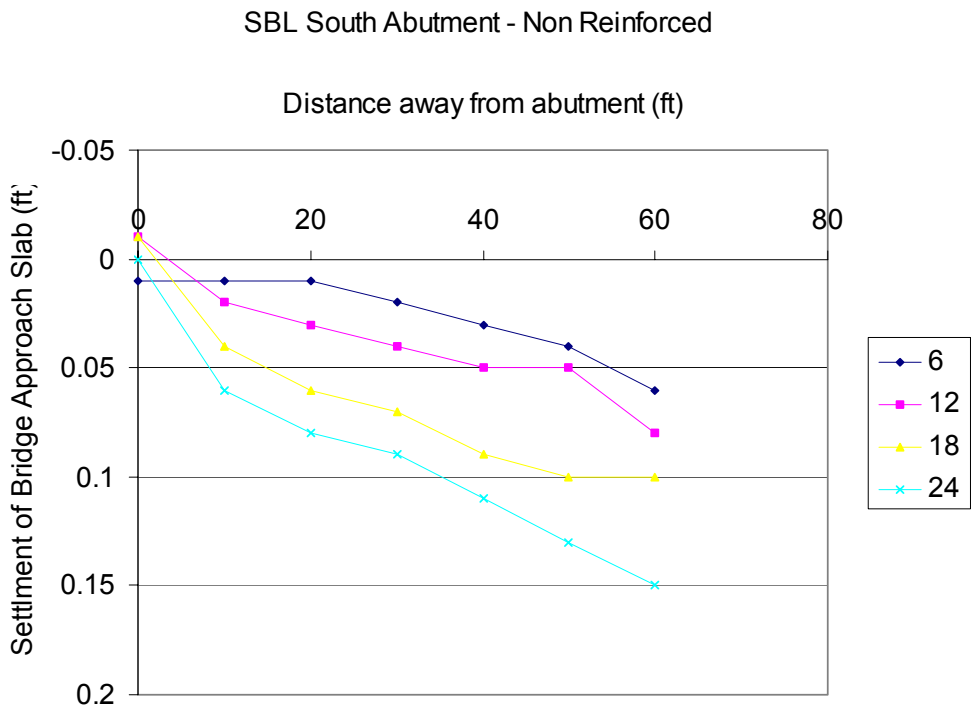
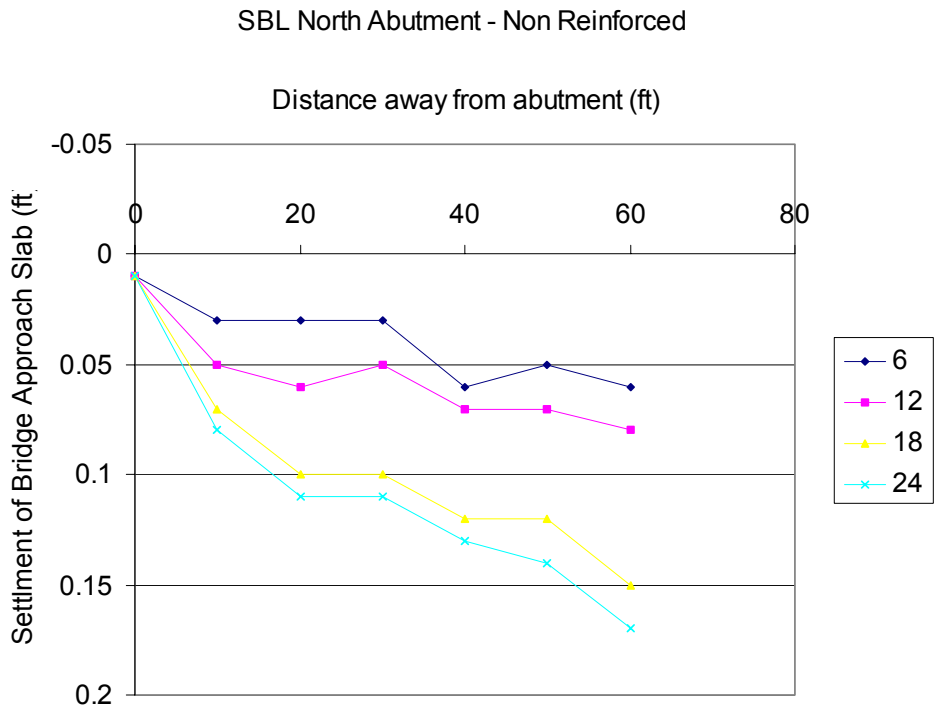


Figure 88. Approach Slab Settlement for Non-Reinforced Section

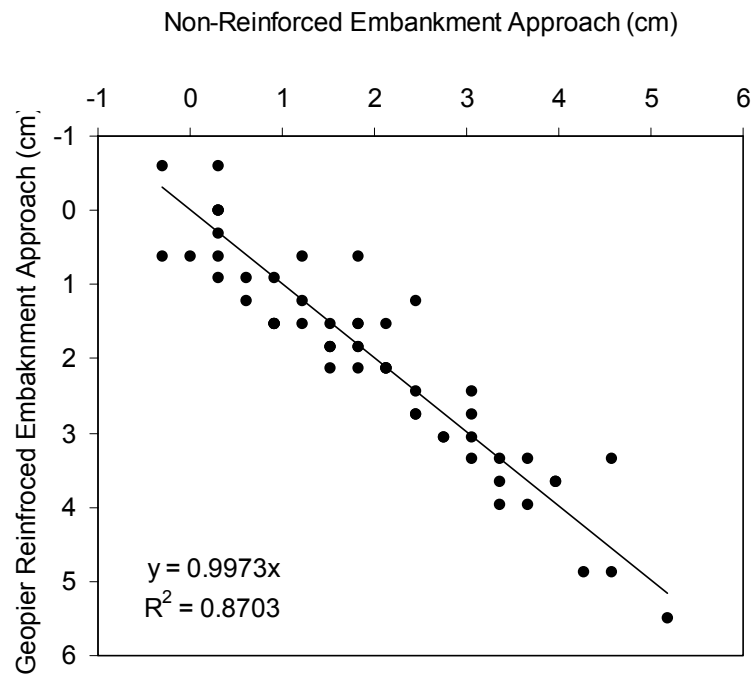


Figure 89. Comparison between Geopier Reinforced Section and the Non-Reinforced Section

SUMMARY AND CONCLUSIONS

The major conclusions derived from these studies are as follows:

Project No. 1: Embankment Foundation Reinforcement at US Hwy 5/I-35 (Des Moines, IA)

- The subsurface conditions at the stone column site were slightly stiffer and less cohesive than the subsurface conditions at the Geopier site, based on interpretation of CPT data.
- Element spacings at both sites were 1.8 m on-center. The greater diameters of the stone column elements and application of a triangular spacing pattern result in a greater area replacement ratio.
- SPT results for tests performed within the elements indicate an average N-value of 11 for the stone columns and an average N-value of 17 for the Geopier elements.
- PBP tests before Geopier construction and 7 and 73 days after construction do not show significant changes in pressuremeter modulus or limit pressure..
- The ratio of post-installation matrix soil lateral stress for the Geopier elements to the post-installation matrix soil lateral stress for the stone columns is about 2.
- Load test results indicate that the ratio of pre-bulging compressive strength for the Geopier element to the pre-bulging compressive strength for the stone column is about 4.
- Load test results indicate that the ratio of Geopier stiffness to stone column stiffness ranges from about 2 to 9 as a function of applied stress.
- Settlement of matrix soils surrounding the stone columns was about three times as large as the settlement of matrix soil surrounding the Geopier elements.
- Settlement cell instrumentation yielded uncertain results in terms of magnitude, but supports the observation that the Geopier matrix soils are settling similarly to the Geopier elements.
- Stress cell instrumentation show that stress concentrations for Geopier elements and stone columns is in the range of 2 to 7.

The stone column site has performed its intended function for global slope reinforcement. This is evidenced by the fact that the embankment has not failed. The Geopier installations also have performed as intended by reducing settlement and the construction delay between embankment completion and abutment construction from the original 120 days to just 30 days. In short, advantages of the stone columns at this site include larger diameter and shaft length, whereas the Geopier elements were smaller but stiffer. Future comparative investigations are highly encouraged with emphasis on documenting the influence of lateral stress on the load-settlement behavior.

Project No. 2: Box Culvert Foundation Reinforcement at IA Hwy 191 (Neola, IA)

- Group load tests of Geopier elements indicate that the ultimate capacity of groups of four piers loaded beneath a rigid foundation is similar to the sum of individual capacities.
- Telltale measurements for the group load tests indicate that the footing width (B) to pier length (D) ratio of 1 resulted in a punching type failure. Bulging failure was observed for the B/D = 2 group load test.

- Stress concentrations on the Geopier elements during full-scale load testing of Group No. 1 measured about 4 relative to the matrix soil.
- The vertical stress distribution within individual Pier No. 1 indicates that about 20 percent of the applied stress of at the top of pier reaches the bottom of the pier at high load levels.
- Pore pressure measurements adjacent to piers during construction show that pore pressure increases during ramming and quickly dissipates.
- The box culvert settled about 12 cm relative to the predicted unreinforced settlement of about 50 cm.
- Measured settlement is lower than the criteria of 15 cm of total settlement and 10 cm of differential settlement.
- The increase in pier construction length in *Zone D* likely resulted in an additional 2 to 3 cm of differential settlement.
- Settlement rate calculations within the alluvial clay layer revealed that Geopier reinforcement could increase the time rate to reach 90 percent primary consolidation from 170 days to about 10 days. Field monitoring indicates that about 90 percent was reached somewhere between 7 and 14 days.

Project No. 3: Bridge Approach Embankment Reinforcement at US Hwy 18/218 (Charles City, IA)

- Settlement monitoring to date indicates little difference between the Geopier reinforced sections and the unreinforced sections.
- Future projects should consider increasing the length of the Geopier elements to penetrate compressible embankment foundation materials.
- Monitoring at this site will continue for a period of five years.

REFERENCES

- Barksdale, R.D. and Bachus, R.C. (1983). *Design and Construction of Stone Columns: Vol. I*. Report No. 1 FHWA/RD 83/026. Federal Highway Administration, Washington, D.C., 210 pp.
- Bergado, D.T., Anderson, L.R., Miura, N., and Balasubramaniam, A.S. (1996) *Soft ground improvement in lowland and other environments*. ASCE Press, New York, N.Y., 1996.
- Bergado, D.T., Lam, F.L. (1987). “Full scale load tests of granular piles with different densities and different proportions of gravel and sand on soft Bangkok clay,” *Soils and Foundations*, Vol. 27, No. 1, p. 86-93.
- Bergado, D.T., Miura, N., Panichayatum, B., and Sampaco, C.L. (1988). “Reinforcement of soft Bangkok clay using granular piles,” *Proc. Intl. Geotechnical Symposium on Theory and Practice of Earth Reinforcement*, Fukuoka, Japan, p. 179-184.
- Briaud, Jean-Louis. (1989). *The Pressuremeter Test for Highway Applications*. Report No. FHWA –IP-89-008. Federal Highway Administration, Washington, D.C.
- Briaud, J.L., James, R.W., and Hoffman, S. B. (1997). *NCHRP Synthesis 234: Settlement of Bridge Approaches (The Bump at the End of the Bridge)*. Transportation Research Board, National Research Council, Washington, D.C., 71 pp.
- Caskey, J.M. (2001). “Uplift Capacity of Rammed Aggregate Pier Soil Reinforcing Elements.” Masters Thesis. University of Memphis. December.
- Douglas, B., and R. Olsen. (1981). *Soil Classification Using Cone Penetrometer. Symposium on Cone Penetration Testing and Experience*. Geotechnical Engineering Division, ASCE, St. Louis, pp. 209-227.
- Elias, V., Welsh, J., Warren, J., and R. Lukas. (2000). Ground Improvement Technical Summaries. Publication No. FHWA-SA-98-068. Federal Highway Administration, Washington, D.C.
- FitzPatrick, B.T. and Wissmann, K.J. (2002). “Technical Bulletin No. 5 – Geopier Shear Reinforcement for Global Stability and Slope Stability.” Geopier Foundation Company, Inc. Blacksburg, Virginia.
- Fox, N.S. and Cowell, M.J. (1998). *Geopier Foundation and Soil Reinforcement Manual*. Geopier Foundation Company, Inc., Scottsdale, Arizona.
- Gaul, A.J. (2001). “Embankment foundation reinforcement using rammed aggregate piers in Iowa soils.” Masters Thesis. Iowa State University.
- Goughnour, R., and R. Barksdale. (1984). “Performance of a Stone Column Supported Embankment.” *International Conference on Case Histories in Geotechnical Engineering*, Vol. 2, St Louis, pp. 735-742.

- Greewood, D. A. (1970). "Mechanical Improvement of Soils Below Ground Surface." *Ground Engineering*, pp.11-22.
- Hall, K.M., Wissmann, K.J., Caskey, J.M., and FitzPatrick, B.T. (2002). "Soil reinforcement used to arrest bearing capacity failure at a steel mill." *Proceedings, 4th International Conference on Ground Improvement*. Kuala Lumpur, Malaysia, 26–28 March.
- Han, J., and Ye, S.L. (2001). "Simplified Method for Consolidated Rate of Stone Column Reinforced Foundations." *ASCE Journal of Geotechnical and Geoenvironmental Engineering*. Vol. 127, No. 7.
- Handy, R.L. (1976). "Discussion: Measurement of in-situ shear strength, in-situ measurement of soil properties." *ASCE*, Vol. II, p. 143-149.
- Handy, R. L. (2001). "Does Lateral Stress Really Influence Settlement." *ASCE Journal of Geotechnical and Geoenvironmental Engineering*, Vol. 127, No. 7.
- Handy, R.L., White, D.J., and Wissmann, K.J. (2002). "Concentric Stress Zones near Rammed Aggregate Piers." (Manuscript in preparation – draft to be provided upon request.)
- Hoewelkamp, K.K. (2002). "Rammed aggregate pier soil reinforcement: group load tests and settlement monitoring of large box culvert." Masters Thesis. Iowa State University.
- Hughes, J.M.O. and N.J. Withers. (1974). "Reinforcing Soft Cohesive Soil with Stone Columns." *Ground Engineering*, May, pp. 42-49.
- Hughes, J.M.O., Withers, N.J., Greenwood, D.A. (1975). "A field trial of the reinforcing effect of a stone column in soil," *Geotechnique*, Vol. 25, No. 1, p. 31-44.
- Jebe, W., and K. Bartels. (1983). "The Development of Compaction Methods with Vibrators from 1976 to 1982." *8th European Conference on Soil Mechanics and Foundation Engineering*, A.A. Balkema, Helsinki.
- Lambe, T. W. and Whitman, Robert V. (1969). *Soil mechanics*. John Wiley & Sons, New York, New York.
- Lawton, E.C., and Fox, N.S. (1994). "Settlement of structures supported on marginal or inadequate soils stiffened with short aggregate piers." *Vertical and Horizontal Deformations of Foundations and Embankments*, A.T. Yeung and G.Y. Fello (Editors), American Society of Civil Engineers, 2, 962-74.
- Lawton, E.C., Fox, N.S. Fox, and Handy, R.L. (1994). "Control of settlement and uplift of structures using short aggregate piers." *In-Situ Deep Soil Improvement*, Proc. ASCE National Convention, Atlanta, Georgia. 121-132.
- Lawton, E.C. and Merry, S.M. (2000). *Performance of Geopier Supported Foundations During Simulated Seismic Tests on Northbound Interstate 15 Bridge Over South Temple, Salt Lake City*. Final Report No. UUCVEEN 00-03. University of Utah. December.

- Madhav, M.R., Vitkar, R.P. (1978). "Strip footing on weak clay stabilized with granular trench or pile." *Canadian Geotechnical Journal*, Vol.15, No. 4, p. 605-609.
- Marchetti, S. (1980). "In-situ tests by flat dilatometer." *Journal of Geotechnical Engineering Division, ASCE*, Vol. 106, GT 3, p. 299-321.
- Minks, A.G., Wissmann, K.J., Caskey, J.M., and Pando, M.A. (2001). "Distribution of Stresses and Settlements Below Floor Slabs Supported by Rammed Aggregate Piers." *Proceedings, 54th Canadian Geotechnical Conference*. Calgary, Alberta. September 16–19.
- Mitchell, J.K. (1981). "Soil Improvement: State of the Art." *Tenth International Conference on Soil Mechanics and Foundation Engineering. Session 12*. Stockholm, Sweden. June 15–19.
- Munfakh, G., Abramson, L., Barksdale, R., and M. Juran. (1987). "In-Situ Ground Improvement. Soil Improvement." *Geotechnical Special Publication No. 12*. ASCE, New York, pp. 1-17.
- Rathgeb, E., and C. Kutzner. (1975). "Some Application of the Vibro-Replacement Process." *Geotechnique*, Vol. 25, No. 1, pp. 45-50.
- Robertson, P.K, and Campanella, R.G. (1986). *Guidelines for use, interpretation, and application of the CPT and CPTU*. 3rd ed., Hogentogler and Co., Inc.
- Schmertmann, J.H. (1976). "Measurement of in-situ shear strength, in-situ measurement of soil properties." *ASCE*, Vol. II, p. 57-138.
- Shioi, Y., and J. Fukui. (1982). "Application of N-value to Design of Foundations," *JACI*, Vol. 81, No. 5, Sept-Oct., pp. 469-475.
- Terzaghi, K., Peck, R.B. (1967). *Soil mechanics in engineering practice*. 2nd edition, John Wiley and Sons, New York.
- White, D.J., Lawton, E.C., and Pitt, J.M. (2000). "Lateral Earth Pressure Induced by Rammed Aggregate Piers." *Proceedings, 54th Annual Canadian Geotechnical Conference*. Montreal.
- White, D.J., Wissmann, K.J., and Lawton, E.C. (2001). "Geopier Soil Reinforcement for Transportation Applications." *Geotechnical News*. Vol. 19, No. 4.
- White, D.J., Wissmann, K.J., Barnes, A.G., and Gaul, A.J. (2002a). "Embankment Support: A Comparison of Stone Column and Rammed Aggregate Pier Soil Reinforcement." *Presented, Transportation Research Board. 81st Meeting*, Washington, D.C. January 13–17.
- White, D.J., Suleiman, H.T Pham, and Bigelow, J. (2002b). *Shear Strength Envelopes for Aggregate used in Geopier Foundation Construction: Final Report*. Iowa State University. September.
- Wineland, J.D. (1976). "Borehole shear device, in-situ measurement of soil properties." *ASCE*, Vol. II, p. 57-138.

- Wissmann, K.J., Lawton, E.C., and Farrell, T.M. (1999). “Technical Bulletin No. 1 – Behavior of Geopier-Supported Foundation Systems During Seismic Events.” Geopier Foundation Company, Inc. Scottsdale, Arizona.
- Wissmann, K.J. (2000). “Technical Bulletin No. 2 – Bearing Capacity of Geopier-Supported Foundation Systems.” Geopier Foundation Company, Inc. Scottsdale, Arizona.
- Wissmann, K.J., Fox, N.S., and Martin, J.P. (2000). “Rammed Aggregate Piers Defeat 75-foot Long Driven Piles.” *Proceedings, Performance Confirmation of Constructed Geotechnical Facilities. ASCE Special Publication No. 194*. Amherst, Massachusetts. April 9 to 12.
- Wissmann, K.J., and FitzPatrick, B.T., and Lawton, E.C. (2001b). “ Technical Bulletin No. 4 – Geopier Lateral Resistance.” Geopier Foundation Company, Inc. Scottsdale, Arizona.
- Wissmann, K.J., FitzPatrick, B.T., White, D.J., and Lien, B.H. (2002). “Improving global stability and controlling settlement with Geopier soil reinforcing elements.” *Proceedings, 4th International Conference on Ground Improvement*. Kuala Lumpur, Malaysia, 26–28 March.

APPENDIX A: PROJECT NO. 1 CPT RESULTS

Table A1. Piezocone Penetration Data for CPTU-1

Depth (m)	q_T (kPa)	f_s (kPa)	R_f (%)	f_s/σ'_{vo}	Q
0.15	331	14.6	4.63	7.38	169.0
0.40	421	21.6	5.23	2.88	53.7
0.65	529	20.3	4.68	1.56	40.7
0.90	421	20.1	4.79	1.16	23.4
1.15	355	12.1	3.41	0.54	15.0
1.40	259	12.4	4.82	0.46	8.6
1.65	399	14.4	3.62	0.45	11.6
1.90	685	21.1	3.08	0.59	18.2
2.15	764	23.4	3.06	0.62	19.1
2.40	885	41.0	4.61	1.02	21.0
2.65	1271	78.1	6.09	1.84	28.8
2.90	2193	155.9	7.09	3.51	48.1
3.15	1955	121.0	6.16	2.60	40.8
3.40	1248	59.9	4.79	1.23	24.3
3.65	1097	41.8	3.81	0.82	20.2
3.90	765	23.0	2.99	0.43	13.0
4.15	797	19.5	2.45	0.35	13.0
4.40	777	18.6	2.39	0.32	12.1
4.65	1118	42.3	3.72	0.71	17.3
4.90	1058	46.2	4.36	0.75	15.6
5.15	820	19.3	2.37	0.30	11.3
5.40	940	31.0	3.29	0.47	12.7
5.65	881	30.6	3.42	0.45	11.4
5.90	657	12.4	1.88	0.18	7.8
6.15	704	13.8	1.95	0.19	8.1
6.40	961	10.5	1.22	0.14	11.2
6.65	1864	19.5	1.32	0.25	22.7
6.90	3256	16.5	0.79	0.21	39.5
7.15	5226	30.6	0.59	0.38	63.1
7.40	4631	38.3	0.87	0.46	54.3
7.65	4407	27.6	0.64	0.33	50.3
7.90	6479	37.9	0.58	0.44	73.1
8.15	5446	32.9	0.61	0.37	59.8
8.40	6611	41.9	0.63	0.46	71.3
8.65	6791	47.3	0.70	0.51	71.7
8.90	7141	51.1	0.72	0.54	73.9
9.15	4732	28.7	0.60	0.30	47.4
9.40	4158	17.8	0.43	0.18	40.6
9.65	4466	23.0	0.51	0.23	42.7
9.90	4589	28.9	0.63	0.28	43.2
10.15	4472	27.6	0.62	0.26	41.2
10.40	4095	22.2	0.55	0.21	36.8
10.65	4828	32.8	0.71	0.30	42.8
10.90	13102	79.3	0.60	0.72	116.6
11.15	14891	98.6	0.66	0.87	129.3
11.40	13281	101.7	0.77	0.88	112.5
11.65	10916	70.9	0.69	0.59	89.7
11.90	18005	144.6	0.81	1.19	145.9

Table A1. (continued)

Depth (m)	μ (kPa)	σ_{vo} (kPa)	μ_o (kPa)	σ'_{vo} (kPa)	B_q
0.15	-3.4	2.94	0.0	2.94	-0.01
0.40	-1.5	7.84	0.0	7.84	0.00
0.65	-17.4	12.74	0.0	12.74	-0.03
0.90	-29.8	17.63	0.0	17.63	-0.07
1.15	-23.6	22.32	0.0	22.32	-0.07
1.40	-15.3	26.95	0.0	26.95	-0.07
1.65	-5.7	31.57	0.0	31.57	-0.02
1.90	14.2	36.20	0.6	35.61	0.02
2.15	35.3	40.82	2.9	37.88	0.04
2.40	40.5	45.45	5.4	40.06	0.04
2.65	45.9	50.07	7.8	42.23	0.03
2.90	86.9	54.70	10.3	44.41	0.04
3.15	75.4	59.32	12.7	46.58	0.03
3.40	71.2	63.95	15.2	48.76	0.05
3.65	75.4	68.57	17.6	50.93	0.06
3.90	81.1	73.20	20.1	53.11	0.09
4.15	107.4	77.82	22.5	55.28	0.12
4.40	120.2	82.45	25.0	57.46	0.14
4.65	121.6	87.07	27.4	59.63	0.09
4.90	128.7	91.70	29.9	61.81	0.10
5.15	114.3	96.32	32.3	63.98	0.11
5.40	132.4	100.95	34.8	66.16	0.12
5.65	134.2	105.57	37.2	68.33	0.13
5.90	142.6	110.20	39.7	70.51	0.19
6.15	160.8	114.82	42.1	72.68	0.20
6.40	152.2	119.44	44.6	74.85	0.13
6.65	90.5	123.89	47.0	76.85	0.02
6.90	48.5	128.29	49.5	78.80	0.00
7.15	-2.6	132.69	51.9	80.75	-0.01
7.40	-2.8	137.09	54.4	82.70	-0.01
7.65	-2.6	141.49	56.8	84.65	-0.01
7.90	-3.9	145.89	59.3	86.60	-0.01
8.15	-5.0	150.29	61.7	88.55	-0.01
8.40	-3.7	154.69	64.2	90.50	-0.01
8.65	-3.4	159.09	66.6	92.45	-0.01
8.90	-3.0	163.49	69.1	94.40	-0.01
9.15	-3.2	167.89	71.5	96.35	-0.02
9.40	1.5	172.29	74.0	98.30	-0.02
9.65	5.1	176.69	76.4	100.25	-0.02
9.90	7.3	181.09	78.9	102.20	-0.02
10.15	9.2	185.49	81.3	104.15	-0.02
10.40	12.3	189.89	83.8	106.10	-0.02
10.65	14.8	194.32	86.2	108.08	-0.02
10.90	17.1	199.37	88.7	110.68	-0.01
11.15	19.2	204.62	91.1	113.48	0.00
11.40	21.8	209.87	93.6	116.28	-0.01
11.65	24.7	215.12	96.0	119.08	-0.01
11.90	26.8	220.37	98.5	121.88	0.00

Table A1. (continued)

Depth (m)	F (%)	I_c	φ (Degrees)	D_r (%)
0.15	4.44	2.35	31.7	52.8
0.40	5.24	2.61	30.5	45.7
0.65	3.93	2.60	30.5	45.3
0.90	4.98	2.85	28.6	34.1
1.15	3.62	2.90	27.2	25.8
1.40	5.36	3.20	25.3	14.1
1.65	3.91	3.01	27.0	24.2
1.90	3.25	2.81	29.3	37.9
2.15	3.23	2.79	29.6	40.2
2.40	4.88	2.87	30.2	43.6
2.65	6.40	2.85	31.8	53.2
2.90	7.29	2.74	34.3	68.1
3.15	6.38	2.75	33.6	64.2
3.40	5.06	2.84	31.4	50.6
3.65	4.06	2.83	30.7	46.3
3.90	3.32	2.93	28.8	35.4
4.15	2.72	2.88	28.9	36.0
4.40	2.68	2.90	28.7	34.7
4.65	4.11	2.89	30.4	44.6
4.90	4.78	2.96	30.0	42.5
5.15	2.67	2.92	28.7	34.7
5.40	3.70	2.97	29.3	38.1
5.65	3.95	3.02	28.9	35.8
5.90	2.28	3.02	27.4	27.0
6.15	2.34	3.01	27.7	28.5
6.40	1.25	2.75	29.1	37.0
6.65	1.12	2.47	32.2	55.6
6.90	0.53	2.09	34.8	71.3
7.15	0.60	1.95	37.0	84.5
7.40	0.85	2.08	36.4	80.7
7.65	0.65	2.05	36.1	78.9
7.90	0.60	1.89	37.9	89.6
8.15	0.62	1.97	37.0	84.3
8.40	0.65	1.92	37.9	89.6
8.65	0.71	1.94	37.9	90.0
8.90	0.73	1.93	38.1	91.2
9.15	0.63	2.06	36.1	79.1
9.40	0.45	2.06	35.4	75.1
9.65	0.54	2.07	35.7	76.9
9.90	0.66	2.11	35.8	77.4
10.15	0.64	2.12	35.7	76.4
10.40	0.57	2.14	35.2	73.6
10.65	0.71	2.13	35.9	78.0
10.90	0.61	1.73	40.6	106.3
11.15	0.67	1.71	41.2	109.6
11.40	0.78	1.80	40.6	106.0
11.65	0.66	1.84	39.6	100.0
11.90	0.81	1.73	41.9	114.0

Table A2. Piezocone Penetration Data for CPTU-2

Depth (m)	q_T (kPa)	f_s (kPa)	R_f (%)	f_s/σ'_{vo}	Q
0.15	985	50.9	5.19	20.26	398.1
0.40	679	37.0	5.47	5.09	92.2
0.65	395	14.9	3.76	1.15	30.3
0.90	291	15.7	5.44	0.91	15.9
1.15	260	14.6	5.61	0.66	10.8
1.40	520	28.2	5.39	1.05	18.4
1.65	748	37.2	4.98	1.19	22.9
1.90	804	43.5	5.41	1.23	21.8
2.15	984	68.4	6.89	1.81	25.0
2.40	1361	120.9	8.94	3.04	33.2
2.65	1303	89.6	6.93	2.14	29.9
2.90	1081	65.7	6.08	1.49	23.3
3.15	846	55.5	6.55	1.20	17.0
3.40	653	32.8	5.00	0.68	12.2
3.65	541	20.9	3.86	0.41	9.3
3.90	540	18.4	3.40	0.35	8.8
4.15	551	30.3	5.27	0.55	8.6
4.40	723	46.9	6.48	0.82	11.2
4.65	572	31.8	5.57	0.54	8.2
4.90	551	32.4	5.88	0.53	7.5
5.15	440	20.5	4.66	0.32	5.4
5.40	407	15.5	3.81	0.24	4.6
5.65	436	12.8	2.99	0.19	4.8
5.90	852	16.3	2.40	0.23	10.5
6.15	4096	17.0	0.42	0.24	55.1
6.40	4983	27.0	0.54	0.36	65.6
6.65	3352	42.1	1.54	0.55	42.5
6.90	3861	19.7	0.51	0.25	47.8
7.15	5477	34.5	0.63	0.43	66.8
7.40	6680	50.9	0.76	0.62	79.8
7.65	6783	55.4	0.82	0.66	79.2
7.90	5979	42.7	0.72	0.50	67.9
8.15	6983	56.5	0.81	0.64	77.8
8.40	4925	39.8	0.80	0.44	53.2
8.65	3604	19.2	0.53	0.21	37.6
8.90	3312	15.9	0.48	0.17	33.6
9.15	3788	24.9	0.66	0.26	37.9
9.40	3401	20.9	0.62	0.21	33.1
9.65	2693	19.9	0.94	0.20	25.3
9.90	5770	46.5	0.81	0.46	55.0
10.15	8497	58.2	0.69	0.56	79.9
10.40	13552	76.8	0.56	0.72	124.9
10.65	17301	121.4	0.70	1.11	155.9
10.90	14291	105.3	0.75	0.94	125.4
11.15	17451	113.0	0.65	0.98	149.5
11.40	23696	68.0	0.31	0.58	198.6

Table A2. (continued)

Depth (m)	μ (kPa)	σ_{vo} (kPa)	μ_o (kPa)	σ'_{vo} (kPa)	B_q
0.15	0.6	2.94	0.0	2.94	0.00
0.40	-45.4	7.84	0.0	7.84	-0.07
0.65	-41.1	12.73	0.0	12.73	-0.11
0.90	-29.9	17.42	0.0	17.42	-0.11
1.15	-22.3	22.05	0.0	22.05	-0.09
1.40	-4.0	26.67	0.0	26.67	-0.01
1.65	43.2	31.30	0.0	31.30	0.06
1.90	66.3	35.92	0.6	35.33	0.09
2.15	82.3	40.55	2.9	37.61	0.08
2.40	100.4	45.17	5.4	39.78	0.07
2.65	99.2	49.80	7.8	41.96	0.07
2.90	98.0	54.42	10.3	44.13	0.09
3.15	112.7	59.05	12.7	46.31	0.13
3.40	124.8	63.67	15.2	48.48	0.19
3.65	129.6	68.30	17.6	50.66	0.24
3.90	143.0	72.92	20.1	52.83	0.26
4.15	150.4	77.55	22.5	55.01	0.27
4.40	148.0	82.17	25.0	57.18	0.19
4.65	157.3	86.80	27.4	59.36	0.27
4.90	180.6	91.42	29.9	61.53	0.33
5.15	180.2	96.05	32.3	63.71	0.43
5.40	204.4	100.67	34.8	65.88	0.55
5.65	243.3	105.30	37.2	68.06	0.62
5.90	276.4	109.91	39.7	70.22	0.32
6.15	13.7	114.37	42.1	72.23	-0.01
6.40	-0.6	118.77	44.6	74.18	-0.01
6.65	0.3	123.17	47.0	76.13	-0.01
6.90	0.3	127.57	49.5	78.08	-0.01
7.15	-1.7	131.97	51.9	80.03	-0.01
7.40	-2.2	136.37	54.4	81.98	-0.01
7.65	-4.4	140.77	56.8	83.93	-0.01
7.90	-3.6	145.17	59.3	85.88	-0.01
8.15	-2.9	149.57	61.7	87.83	-0.01
8.40	-3.7	153.97	64.2	89.78	-0.01
8.65	-0.6	158.37	66.6	91.73	-0.02
8.90	3.2	162.77	69.1	93.68	-0.02
9.15	5.7	167.17	71.5	95.63	-0.02
9.40	8.0	171.57	74.0	97.58	-0.02
9.65	11.0	175.97	76.4	99.53	-0.03
9.90	13.5	180.40	78.9	101.51	-0.01
10.15	15.9	185.45	81.3	104.11	-0.01
10.40	18.5	190.70	83.8	106.91	0.00
10.65	19.2	195.95	86.2	109.71	0.00
10.90	23.4	201.20	88.7	112.51	0.00
11.15	25.5	206.45	91.1	115.31	0.00
11.40	27.6	211.70	93.6	118.11	0.00

Table A2. (continued)

Depth (m)	F (%)	I_c	φ (Degrees)	D_r (%)
0.15	5.19	2.15	36.9	84.1
0.40	5.51	2.49	32.8	59.4
0.65	3.91	2.69	29.1	36.9
0.90	5.74	3.01	26.9	23.7
1.15	6.12	3.16	25.8	17.0
1.40	5.71	2.96	28.6	34.2
1.65	5.18	2.86	30.0	42.3
1.90	5.66	2.91	30.0	42.7
2.15	7.25	2.94	30.9	47.5
2.40	9.19	2.93	32.3	56.0
2.65	7.15	2.88	31.9	54.0
2.90	6.40	2.92	30.9	47.9
3.15	7.06	3.05	29.6	40.2
3.40	5.56	3.09	28.3	32.2
3.65	4.42	3.12	27.3	26.1
3.90	3.94	3.11	27.2	25.5
4.15	6.39	3.24	27.2	25.5
4.40	7.32	3.19	28.4	32.7
4.65	6.56	3.27	27.2	25.4
4.90	7.04	3.32	26.9	23.9
5.15	5.96	3.39	25.8	16.9
5.40	5.07	3.40	25.3	14.2
5.65	3.89	3.32	25.5	15.7
5.90	2.19	2.90	28.7	34.5
6.15	0.43	1.93	36.1	79.1
6.40	0.56	1.91	37.0	84.3
6.65	1.31	2.28	35.0	72.6
6.90	0.53	2.02	35.6	76.3
7.15	0.64	1.94	37.3	85.9
7.40	0.78	1.92	38.1	91.3
7.65	0.83	1.94	38.2	91.4
7.90	0.73	1.96	37.5	87.4
8.15	0.83	1.95	38.2	91.6
8.40	0.83	2.08	36.5	81.2
8.65	0.56	2.13	34.9	72.0
8.90	0.50	2.15	34.5	69.3
9.15	0.69	2.17	35.1	72.8
9.40	0.65	2.21	34.5	69.4
9.65	0.79	2.35	33.3	62.5
9.90	0.83	2.07	36.9	84.0
10.15	0.70	1.90	38.7	94.8
10.40	0.57	1.69	40.9	107.8
10.65	0.71	1.67	42.0	114.4
10.90	0.75	1.75	41.0	108.5
11.15	0.66	1.66	41.9	113.9
11.40	0.29	1.36	43.3	122.3

Table A3. Piezocone Penetration Data for CPTU-3

Depth (m)	q_T (kPa)	f_s (kPa)	R_f (%)	f_s/σ'_{vo}	Q
0.15	1610	78.0	5.10	31.91	641.2
0.40	1669	59.9	3.71	8.02	226.7
0.65	970	41.9	4.32	3.40	77.6
0.90	783	32.2	4.13	1.90	45.3
1.15	730	31.4	4.30	1.44	32.5
1.40	1094	50.8	4.64	1.92	40.4
1.65	1335	72.2	5.40	2.32	42.1
1.90	1389	86.6	6.23	2.47	38.6
2.15	1205	83.5	7.01	2.24	31.2
2.40	1350	83.7	6.19	2.12	33.1
2.65	1224	60.9	5.00	1.46	28.2
2.90	1015	54.2	5.35	1.24	21.9
3.15	836	39.1	4.67	0.85	16.9
3.40	582	25.1	4.34	0.52	10.8
3.65	614	21.5	3.49	0.43	10.9
3.90	802	40.4	5.00	0.77	13.9
4.15	880	47.3	5.39	0.87	14.7
4.40	607	28.3	4.71	0.50	9.2
4.65	440	14.7	3.37	0.25	6.0
4.90	511	15.3	3.03	0.25	6.9
5.15	3588	20.9	0.87	0.33	55.1
5.40	4059	17.0	0.42	0.26	60.7
5.65	5454	20.3	0.37	0.30	79.7
5.90	4058	18.6	0.47	0.27	57.2
6.15	4864	47.3	1.06	0.66	66.9
6.40	4167	32.2	0.93	0.44	55.4
6.65	3561	38.9	1.16	0.52	45.9
6.90	5433	30.1	0.55	0.39	69.0
7.15	4808	27.4	0.57	0.35	59.3
7.40	6503	43.3	0.67	0.54	78.8
7.65	6292	39.1	0.62	0.47	74.4
7.90	4446	51.5	1.23	0.61	50.9
8.15	3050	11.5	0.38	0.13	33.5
8.40	2610	11.3	0.44	0.13	27.7
8.65	3000	18.8	0.63	0.21	31.4
8.90	5406	35.4	0.67	0.38	56.6
9.15	8528	51.7	0.62	0.54	88.0
9.40	12399	75.7	0.61	0.77	125.2
9.65	13829	67.6	0.49	0.67	136.0
9.90	15059	87.5	0.58	0.85	144.1
10.15	18788	143.3	0.76	1.35	175.4
10.40	17986	106.9	0.58	0.98	163.6

Table A3. (continued)

Depth (m)	μ (kPa)	σ_{vo} (kPa)	μ_0 (kPa)	σ'_{vo} (kPa)	B_q
0.15	-11.4	2.94	0.0	2.94	-0.01
0.40	-36.4	7.83	0.0	7.83	-0.02
0.65	-51.0	12.52	0.0	12.52	-0.05
0.90	-49.1	17.15	0.0	17.15	-0.06
1.15	-44.5	21.77	0.0	21.77	-0.06
1.40	-35.9	26.40	0.0	26.40	-0.03
1.65	-20.0	31.02	0.0	31.02	-0.02
1.90	-6.9	35.65	0.6	35.06	-0.01
2.15	2.1	40.27	2.9	37.33	0.00
2.40	7.2	44.90	5.4	39.51	0.00
2.65	18.5	49.52	7.8	41.68	0.01
2.90	36.5	54.15	10.3	43.86	0.03
3.15	42.7	58.77	12.7	46.03	0.04
3.40	47.3	63.40	15.2	48.21	0.06
3.65	55.0	68.02	17.6	50.38	0.07
3.90	65.6	72.65	20.1	52.56	0.06
4.15	69.1	77.27	22.5	54.73	0.06
4.40	64.3	81.90	25.0	56.91	0.07
4.65	62.9	86.52	27.4	59.08	0.10
4.90	65.5	91.14	29.9	61.25	0.08
5.15	33.5	95.59	32.3	63.25	0.00
5.40	2.5	99.99	34.8	65.20	-0.01
5.65	-3.6	104.39	37.2	67.15	-0.01
5.90	-2.8	108.79	39.7	69.10	-0.01
6.15	-3.4	113.19	42.1	71.05	-0.01
6.40	6.1	117.59	44.6	73.00	-0.01
6.65	-5.8	121.99	47.0	74.95	-0.02
6.90	-4.8	126.39	49.5	76.90	-0.01
7.15	-5.9	130.79	51.9	78.85	-0.01
7.40	-5.9	135.19	54.4	80.80	-0.01
7.65	-6.8	139.59	56.8	82.75	-0.01
7.90	-5.2	143.99	59.3	84.70	-0.01
8.15	-5.9	148.39	61.7	86.65	-0.02
8.40	-1.2	152.79	64.2	88.60	-0.03
8.65	1.9	157.19	66.6	90.55	-0.02
8.90	4.3	161.59	69.1	92.50	-0.01
9.15	7.3	166.33	71.5	94.79	-0.01
9.40	9.4	171.58	74.0	97.59	-0.01
9.65	11.4	176.83	76.4	100.39	0.00
9.90	14.3	182.08	78.9	103.19	0.00
10.15	16.7	187.33	81.3	105.99	0.00
10.40	18.9	192.58	83.8	108.79	0.00

Table A3. (continued)

Depth (m)	F (%)	I_c	φ (Degrees)	D_r (%)
0.15	4.85	2.04	39.3	98.2
0.40	3.61	2.11	37.1	85.2
0.65	4.38	2.45	33.4	62.9
0.90	4.20	2.59	31.6	52.3
1.15	4.43	2.70	30.7	46.8
1.40	4.75	2.66	32.2	55.7
1.65	5.54	2.70	32.8	59.1
1.90	6.40	2.77	32.7	58.4
2.15	7.17	2.87	31.8	53.5
2.40	6.41	2.81	32.3	55.9
2.65	5.19	2.80	31.7	52.3
2.90	5.64	2.90	30.6	46.2
3.15	5.03	2.95	29.6	40.0
3.40	4.84	3.09	27.8	28.9
3.65	3.93	3.04	27.9	29.9
3.90	5.54	3.05	29.1	36.9
4.15	5.90	3.04	29.4	39.0
4.40	5.40	3.18	27.6	27.8
4.65	4.18	3.26	25.9	18.0
4.90	3.65	3.18	26.6	21.8
5.15	0.60	1.99	35.8	77.2
5.40	0.43	1.89	36.3	80.3
5.65	0.38	1.76	37.7	88.3
5.90	0.47	1.93	36.2	79.4
6.15	1.00	2.05	37.0	84.2
6.40	0.79	2.06	36.2	79.4
6.65	1.13	2.21	35.4	74.5
6.90	0.57	1.90	37.3	86.3
7.15	0.59	1.96	36.7	82.4
7.40	0.68	1.89	38.1	90.7
7.65	0.64	1.90	37.8	89.4
7.90	1.20	2.19	36.1	79.1
8.15	0.40	2.11	34.3	68.0
8.40	0.46	2.21	33.5	63.2
8.65	0.66	2.23	34.1	66.9
8.90	0.68	2.01	36.8	83.5
9.15	0.62	1.83	39.0	96.2
9.40	0.62	1.70	40.7	106.5
9.65	0.50	1.62	41.1	109.2
9.90	0.59	1.64	41.5	111.3
10.15	0.77	1.65	42.5	117.2
10.40	0.60	1.60	42.2	115.6

Table A4. Piezocone Penetration Data for CPTU-4

Depth (m)	q_T (kPa)	f_s (kPa)	R_f (%)	f_s/σ'_{vo}	Q
0.15	1248	52.7	4.24	18.96	452.6
0.40	2261	96.1	4.26	12.80	298.2
0.65	2358	99.0	4.26	7.80	183.0
0.90	3774	157.4	4.16	8.93	214.7
1.15	3404	191.5	5.64	8.65	153.3
1.40	2722	160.7	5.91	6.03	101.1
1.65	1913	127.0	6.66	4.06	60.2
1.90	1700	114.3	6.73	3.22	46.9
2.15	2502	110.3	4.63	2.92	65.0
2.40	1488	75.7	5.19	1.90	36.2
2.65	1004	48.8	4.90	1.16	22.7
2.90	849	38.9	4.59	0.88	18.0
3.15	716	36.6	5.03	0.78	14.1
3.40	889	64.5	7.33	1.33	17.0
3.65	831	47.5	5.66	0.94	15.0
3.90	3195	33.9	1.98	0.64	58.6
4.15	3509	44.4	1.29	0.81	62.5
4.40	4991	36.6	0.74	0.64	86.4
4.65	2560	27.8	1.23	0.47	42.2
4.90	2333	16.1	0.74	0.26	36.9
5.15	1226	29.3	2.53	0.47	18.1
5.40	2300	28.3	1.30	0.44	34.1
5.65	2403	16.7	0.69	0.25	34.5
5.90	4614	32.0	0.70	0.47	65.6
6.15	4625	53.1	1.21	0.75	64.0
6.40	5026	34.1	0.67	0.47	67.8
6.65	4842	28.7	0.59	0.39	63.4
6.90	5776	37.3	0.64	0.49	74.0
7.15	5582	45.0	0.81	0.57	69.6
7.40	5081	34.5	0.68	0.43	61.7
7.65	4252	24.3	0.58	0.30	50.1
7.90	2417	13.8	0.56	0.16	27.1
8.15	1293	9.8	0.75	0.11	13.3
8.40	4665	29.5	0.68	0.33	51.1
8.65	10921	73.2	0.67	0.81	118.6
8.90	13955	89.4	0.65	0.96	147.7
9.15	10826	74.9	0.69	0.78	110.7
9.40	10490	82.0	0.80	0.83	104.3

Table A4. (continued)

Depth (m)	μ (kPa)	σ_{vo} (kPa)	μ_0 (kPa)	σ'_{vo} (kPa)	B_q
0.15	45.6	2.94	0.0	2.94	0.04
0.40	-44.0	7.84	0.0	7.84	-0.02
0.65	-45.8	12.74	0.0	12.74	-0.02
0.90	-25.6	17.57	0.0	17.57	-0.01
1.15	-43.0	22.21	0.0	22.21	-0.01
1.40	-47.9	26.84	0.0	26.84	-0.02
1.65	-47.6	31.46	0.0	31.46	-0.03
1.90	-41.6	36.09	0.6	35.50	-0.03
2.15	-23.0	40.71	2.9	37.77	-0.01
2.40	0.1	45.34	5.4	39.95	0.00
2.65	10.2	49.96	7.8	42.12	0.00
2.90	23.0	54.59	10.3	44.30	0.02
3.15	47.9	59.21	12.7	46.47	0.05
3.40	51.6	63.84	15.2	48.65	0.04
3.65	55.6	68.46	17.6	50.82	0.05
3.90	41.8	73.03	20.1	52.94	0.01
4.15	1.0	77.44	22.5	54.90	-0.01
4.40	-3.3	81.84	25.0	56.85	-0.01
4.65	-3.4	86.24	27.4	58.80	-0.01
4.90	2.6	90.64	29.9	60.75	-0.01
5.15	1.1	95.04	32.3	62.70	-0.03
5.40	-1.5	99.44	34.8	64.65	-0.02
5.65	-2.2	103.84	37.2	66.60	-0.02
5.90	-1.2	108.24	39.7	68.55	-0.01
6.15	-1.9	112.64	42.1	70.50	-0.01
6.40	0.4	117.04	44.6	72.45	-0.01
6.65	-1.4	121.44	47.0	74.40	-0.01
6.90	-1.7	125.84	49.5	76.35	-0.01
7.15	-2.8	130.24	51.9	78.30	-0.01
7.40	-2.6	134.64	54.4	80.25	-0.01
7.65	-0.6	139.04	56.8	82.20	-0.01
7.90	1.2	143.44	59.3	84.15	-0.03
8.15	3.3	147.84	61.7	86.10	-0.05
8.40	7.4	152.27	64.2	88.08	-0.01
8.65	9.4	157.32	66.6	90.68	-0.01
8.90	12.3	162.57	69.1	93.48	0.00
9.15	14.8	167.82	71.5	96.28	-0.01
9.40	17.0	173.07	74.0	99.08	-0.01

Table A4. (continued)

Depth (m)	F (%)	I_c	φ (Degrees)	D_r (%)
0.15	4.23	2.03	38.1	90.9
0.40	4.27	2.11	38.6	93.9
0.65	4.22	2.20	37.6	88.1
0.90	4.19	2.17	39.1	97.0
1.15	5.66	2.36	38.0	90.7
1.40	5.96	2.48	36.5	81.6
1.65	6.75	2.66	34.5	69.2
1.90	6.87	2.73	33.6	64.1
2.15	4.48	2.50	35.3	74.2
2.40	5.24	2.72	32.7	58.5
2.65	5.12	2.86	30.7	46.5
2.90	4.89	2.93	29.8	41.0
3.15	5.57	3.04	28.8	35.4
3.40	7.82	3.08	29.8	41.0
3.65	6.23	3.05	29.3	38.4
3.90	1.09	2.11	35.7	76.4
4.15	1.29	2.14	36.0	78.6
4.40	0.75	1.88	37.6	88.2
4.65	1.12	2.24	34.4	68.6
4.90	0.72	2.19	33.8	65.4
5.15	2.59	2.75	30.7	46.5
5.40	1.29	2.35	33.6	64.1
5.65	0.72	2.21	33.8	65.0
5.90	0.71	1.97	36.8	83.2
6.15	1.18	2.11	36.8	82.9
6.40	0.69	1.95	37.1	84.9
6.65	0.61	1.95	36.8	83.4
6.90	0.66	1.91	37.6	88.1
7.15	0.83	1.98	37.4	86.8
7.40	0.70	1.99	36.9	83.7
7.65	0.59	2.03	36.0	78.3
7.90	0.61	2.27	33.2	61.8
8.15	0.85	2.61	30.2	43.5
8.40	0.65	2.04	36.3	80.0
8.65	0.68	1.75	40.3	103.9
8.90	0.65	1.66	41.4	110.5
9.15	0.70	1.78	40.1	102.8
9.40	0.79	1.83	39.9	101.5

Table A5. Piezocone Penetration Data for CPTU-5

Depth (m)	q_T (kPa)	f_s (kPa)	R_f (%)	f_s/σ'_{vo}	Q
0.15	4455	63.6	1.46	26.99	2055.1
0.40	4465	47.5	1.17	6.35	565.4
0.65	4751	14.0	0.32	1.24	401.6
0.90	4840	63.0	1.61	3.52	281.3
1.15	3770	103.0	2.84	4.53	164.9
1.40	2998	97.3	3.30	3.58	109.9
1.65	6153	71.1	1.76	2.18	185.0
1.90	9916	145.0	1.55	3.88	266.0
2.15	3695	150.7	4.10	3.59	87.2
2.40	5910	118.0	2.26	2.52	123.7
2.65	2858	105.1	3.89	2.03	54.5
2.90	1936	93.7	4.88	1.65	33.1
3.15	2590	82.2	3.17	1.34	41.2
3.40	2273	80.3	3.53	1.22	33.5
3.65	2008	85.2	4.25	1.21	27.5
3.90	2199	106.5	4.84	1.41	28.2
4.15	2281	92.3	4.06	1.18	28.1
4.40	2607	114.2	4.38	1.42	31.3
4.65	2601	120.5	4.63	1.46	30.4
4.90	2198	111.7	5.10	1.31	24.8
5.15	2114	127.0	6.01	1.46	23.1
5.40	2002	112.6	5.61	1.26	21.3
5.65	1670	75.7	4.54	0.83	17.1
5.90	1239	50.8	4.15	0.54	12.1
6.15	939	43.5	4.70	0.45	8.6
6.40	1007	40.2	3.97	0.41	9.0
6.65	1024	22.6	2.35	0.23	9.0
6.90	666	12.8	1.92	0.13	5.2
7.15	575	12.8	2.24	0.12	4.2
7.40	547	12.6	2.32	0.12	3.8
7.65	589	8.2	1.44	0.08	4.1
7.90	1053	21.6	2.26	0.19	8.2
8.15	695	22.8	3.35	0.20	4.8
8.40	838	15.3	1.94	0.13	5.9
8.65	704	12.8	1.82	0.11	4.6
8.90	595	10.5	1.80	0.09	3.6
9.15	726	14.4	1.98	0.12	4.5
9.40	774	18.2	2.35	0.15	4.8
9.65	959	27.4	2.85	0.22	6.2
9.90	1110	34.1	3.08	0.27	7.2
10.15	961	27.2	2.83	0.21	5.9
10.40	916	29.9	3.28	0.23	5.4
10.65	963	30.3	3.14	0.22	5.7
10.90	906	21.1	2.34	0.15	5.1
11.15	934	17.6	1.88	0.13	5.2
11.40	885	14.4	1.63	0.10	4.7
11.65	934	12.6	1.36	0.09	5.0
11.90	2860	55.4	3.08	0.38	18.0
12.15	6969	109.0	1.80	0.74	45.6

Table A5. (continued)

Depth (m)	μ (kPa)	σ_{vo} (kPa)	μ_o (kPa)	σ'_{vo} (kPa)	B_q
0.15	0.1	2.94	0.0	2.94	0.00
0.40	0.3	7.84	0.0	7.84	0.00
0.65	-5.4	12.74	0.0	12.74	0.00
0.90	-0.7	17.64	0.0	17.64	0.00
1.15	15.6	22.54	0.0	22.54	0.00
1.40	11.3	27.44	0.0	27.44	0.00
1.65	13.5	32.34	0.0	32.34	0.00
1.90	3.0	37.24	0.0	37.24	0.00
2.15	12.3	42.14	0.0	42.14	0.00
2.40	16.5	47.04	0.0	47.04	0.00
2.65	9.9	51.94	0.0	51.94	0.00
2.90	10.2	56.73	0.0	56.73	0.01
3.15	4.8	61.36	0.0	61.36	0.00
3.40	-0.8	65.98	0.0	65.98	0.00
3.65	-4.7	70.61	0.0	70.61	0.00
3.90	-7.9	75.23	0.0	75.23	0.00
4.15	7.9	79.86	1.5	78.39	0.00
4.40	29.5	84.48	3.9	80.56	0.01
4.65	37.8	89.11	6.4	82.74	0.01
4.90	64.8	93.73	8.8	84.91	0.03
5.15	53.0	98.36	11.3	87.09	0.02
5.40	49.8	102.98	13.7	89.26	0.02
5.65	58.6	107.61	16.2	91.44	0.03
5.90	68.4	112.23	18.6	93.61	0.04
6.15	70.7	116.86	21.1	95.79	0.06
6.40	74.3	121.48	23.5	97.96	0.06
6.65	80.9	126.11	26.0	100.14	0.06
6.90	92.4	130.73	28.4	102.31	0.12
7.15	109.1	135.36	30.9	104.49	0.18
7.40	121.2	139.98	33.3	106.66	0.22
7.65	128.8	144.61	35.8	108.84	0.21
7.90	142.5	149.23	38.2	111.01	0.12
8.15	160.1	153.86	40.7	113.19	0.22
8.40	167.1	158.48	43.1	115.36	0.18
8.65	178.2	163.11	45.6	117.54	0.25
8.90	226.0	167.73	48.0	119.71	0.42
9.15	267.7	172.36	50.5	121.89	0.39
9.40	288.1	176.98	52.9	124.06	0.39
9.65	305.9	181.61	55.4	126.24	0.32
9.90	312.8	186.23	57.8	128.41	0.28
10.15	323.0	190.86	60.3	130.59	0.34
10.40	327.0	195.48	62.7	132.76	0.37
10.65	340.9	200.11	65.2	134.94	0.36
10.90	352.5	204.73	67.6	137.11	0.41
11.15	371.9	209.36	70.1	139.29	0.42
11.40	383.2	213.98	72.5	141.46	0.46
11.65	389.2	218.61	75.0	143.64	0.44
11.90	164.9	223.23	77.4	145.81	0.03
12.15	-20.3	227.86	79.9	147.99	-0.01

Table A5. (continued)

Depth (m)	F (%)	I_c	φ (Degrees)	D_r (%)
0.15	1.43	1.41	44.2	127.4
0.40	1.07	1.44	41.8	113.4
0.65	0.30	1.13	41.0	108.2
0.90	1.31	1.69	40.3	104.1
1.15	2.75	2.08	38.5	93.4
1.40	3.28	2.25	36.9	84.0
1.65	1.16	1.75	40.0	102.3
1.90	1.47	1.74	41.9	113.9
2.15	4.13	2.39	36.9	83.8
2.40	2.01	2.05	38.9	95.7
2.65	3.75	2.50	35.2	73.5
2.90	4.98	2.73	33.1	61.1
3.15	3.25	2.54	34.3	68.3
3.40	3.64	2.64	33.5	63.5
3.65	4.40	2.76	32.8	59.0
3.90	5.01	2.79	33.0	60.7
4.15	4.19	2.74	33.1	61.1
4.40	4.53	2.72	33.7	64.6
4.65	4.80	2.75	33.6	64.1
4.90	5.31	2.84	32.8	58.9
5.15	6.30	2.92	32.5	57.4
5.40	5.93	2.93	32.2	55.5
5.65	4.84	2.94	31.3	50.0
5.90	4.50	3.04	29.8	41.1
6.15	5.29	3.20	28.4	32.8
6.40	4.54	3.14	28.7	34.5
6.65	2.52	2.99	28.7	34.6
6.90	2.40	3.18	26.6	22.0
7.15	2.92	3.31	25.9	17.5
7.40	3.10	3.36	25.6	15.8
7.65	1.85	3.22	25.9	17.6
7.90	2.39	3.02	28.6	34.0
8.15	4.21	3.35	26.6	21.8
8.40	2.26	3.12	27.4	26.9
8.65	2.37	3.23	26.5	21.6
8.90	2.47	3.33	25.7	16.5
9.15	2.60	3.25	26.6	22.0
9.40	3.05	3.27	26.9	23.6
9.65	3.52	3.21	27.8	29.5
9.90	3.69	3.17	28.5	33.4
10.15	3.53	3.23	27.8	29.0
10.40	4.15	3.30	27.5	27.4
10.65	3.97	3.27	27.7	28.6
10.90	3.01	3.24	27.4	26.6
11.15	2.43	3.19	27.5	27.3
11.40	2.14	3.20	27.2	25.5
11.65	1.77	3.14	27.4	26.9
11.90	2.10	2.70	32.7	58.7
12.15	1.62	2.31	36.9	84.0

APPENDIX B: PROJECT NO. 1 BST RESULTS

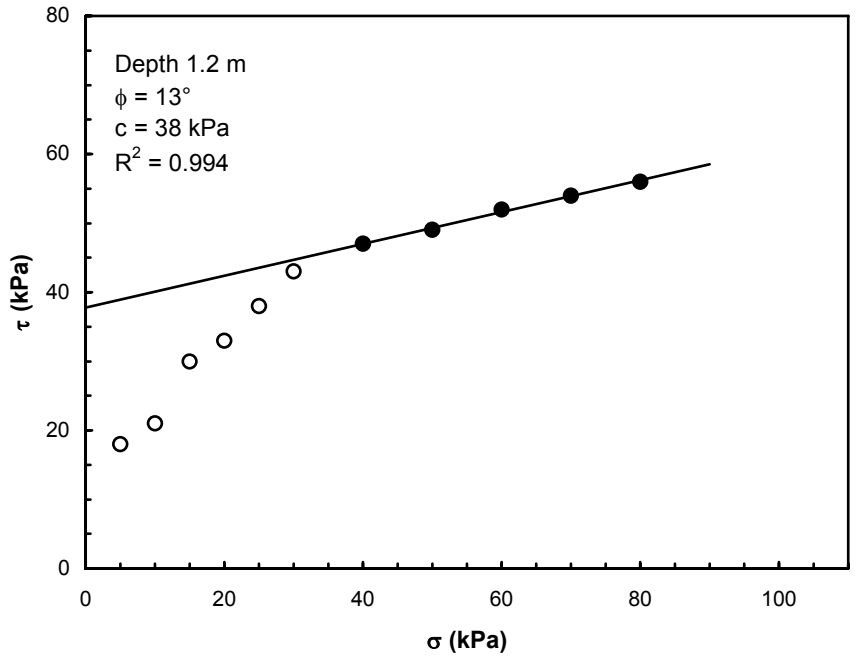


Figure B1. BHST-1 at depth 1.2 m

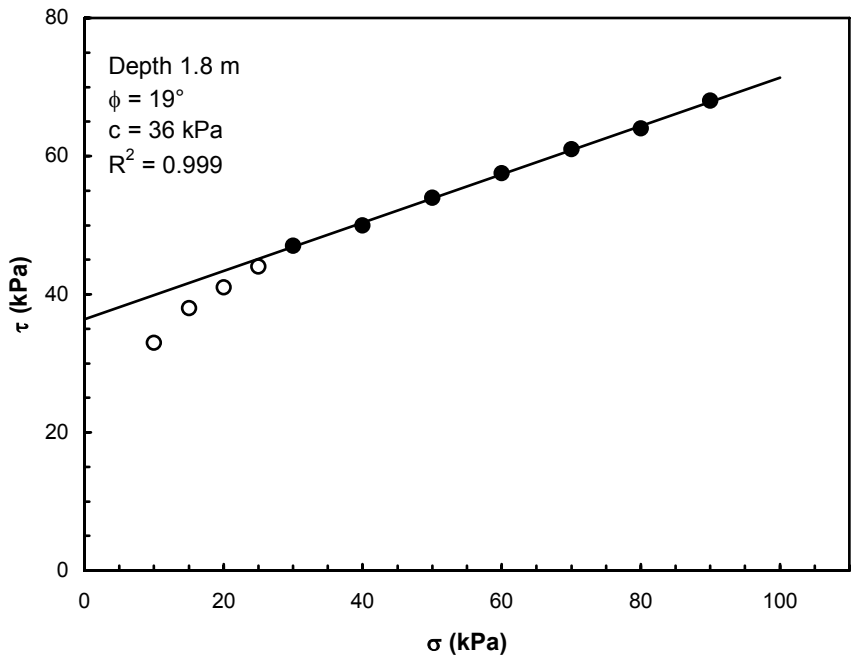


Figure B2. BHST-1 at depth 1.8 m

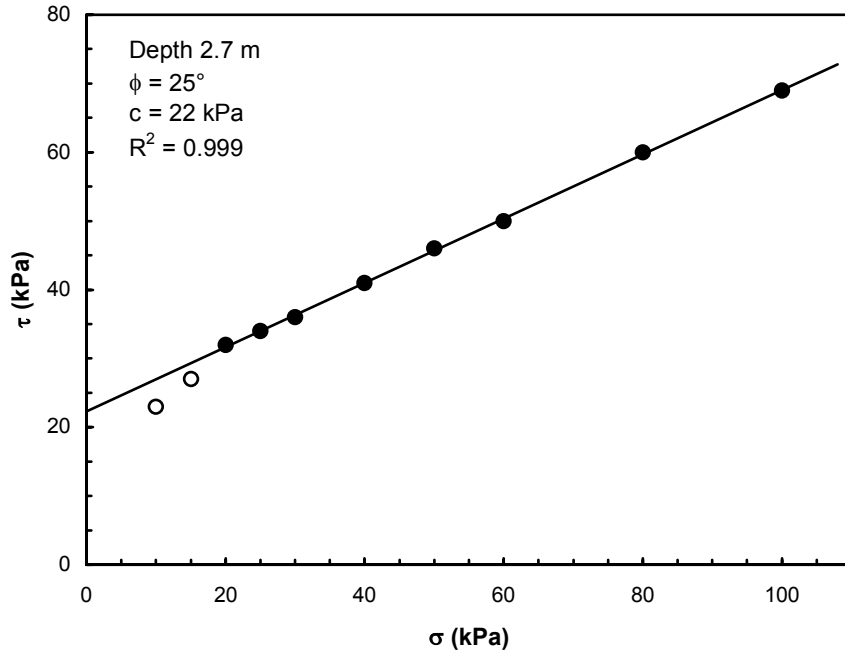


Figure B3. BHST-1 at depth 2.7 m

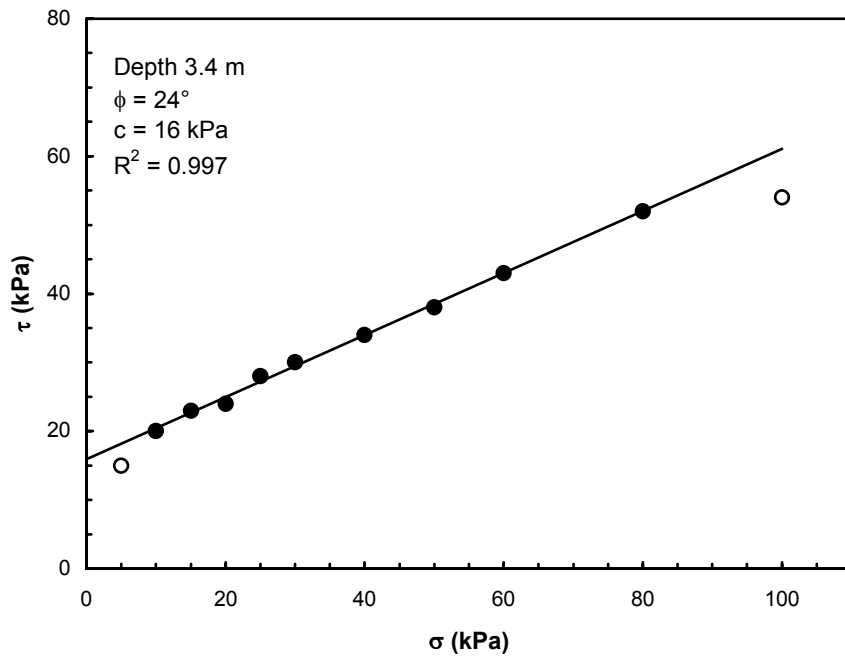


Figure B4. BHST-1 at depth 3.4 m

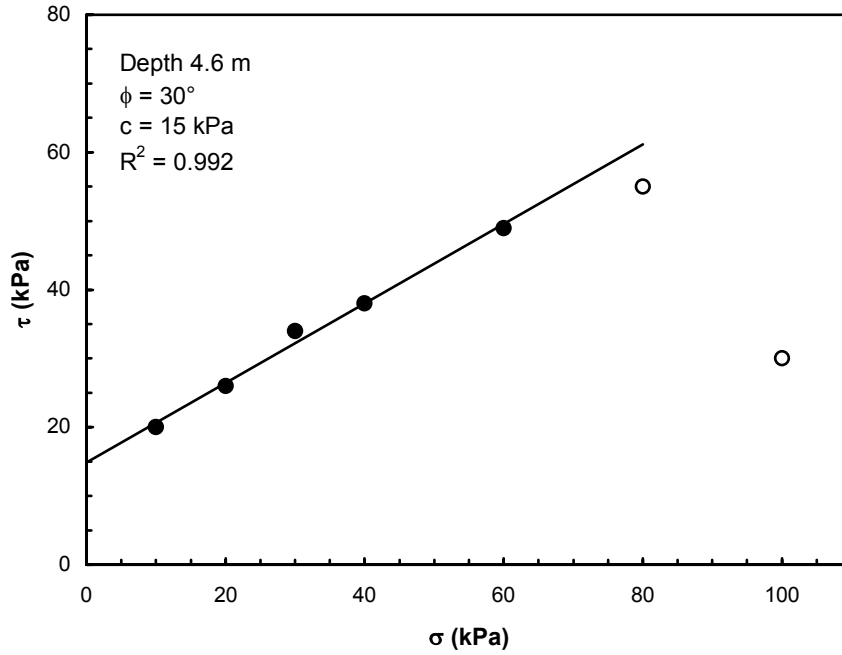


Figure B5. BHST-1 at depth 4.6 m

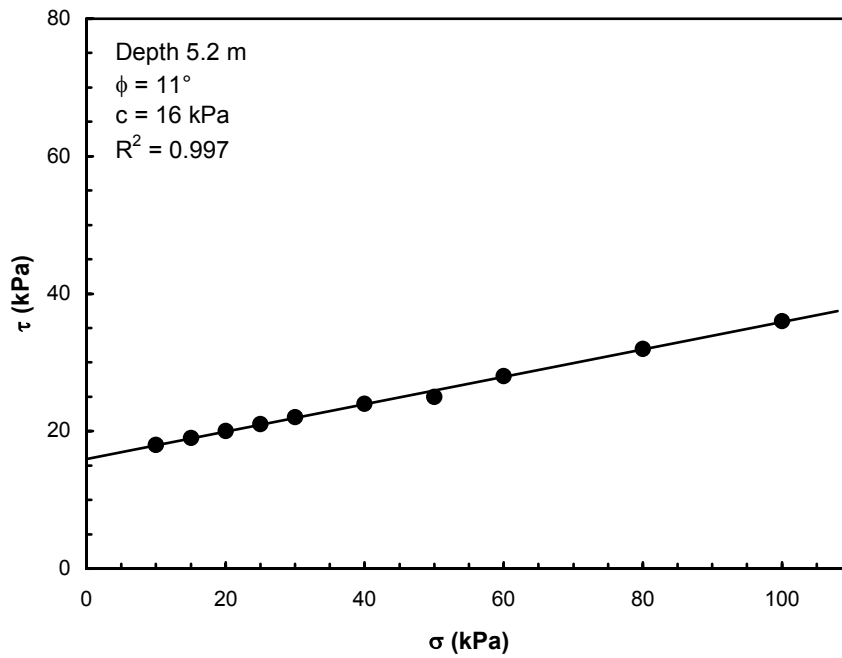


Figure B6. BHST-1 at depth 5.2 m

APPENDIX C: PROJECT NO. 1 PMT RESULTS

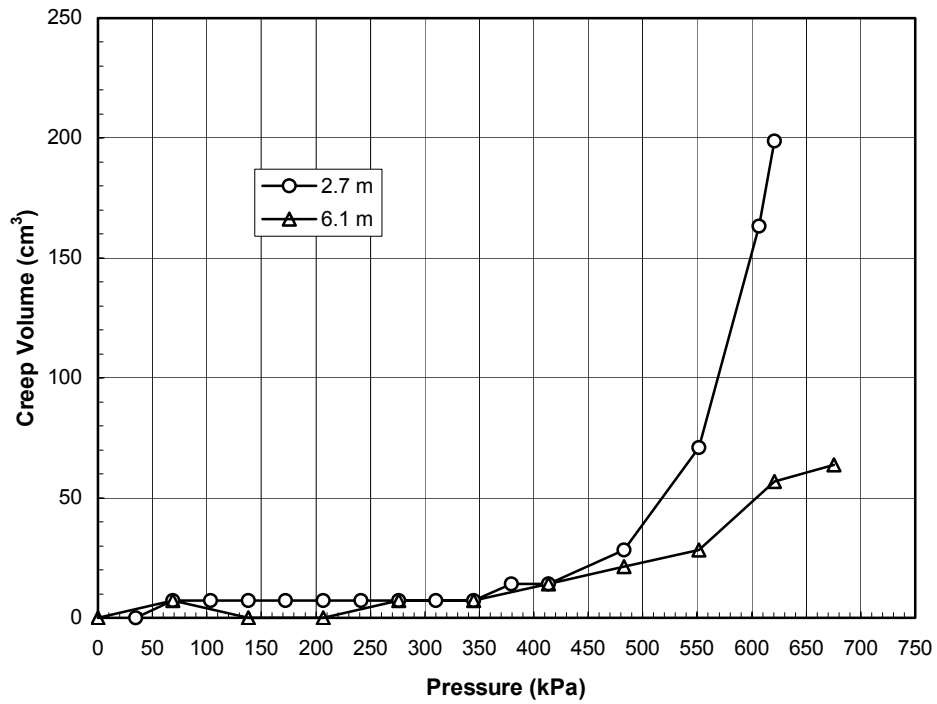
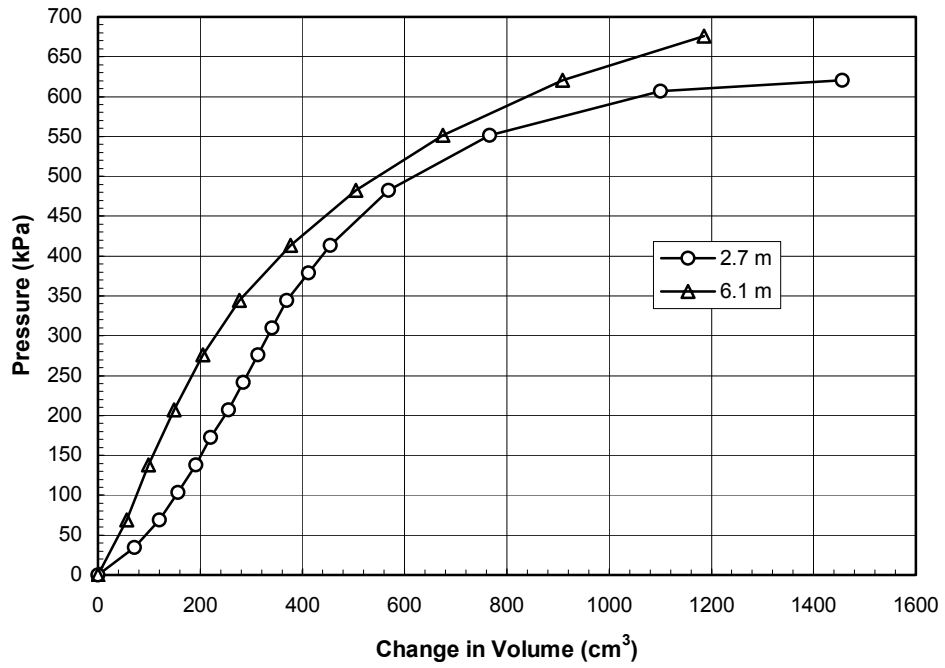


Figure C1. PMT-1 (prior to rammed aggregate pier installation) (top) pressuremeter curve, (bottom) creep curve

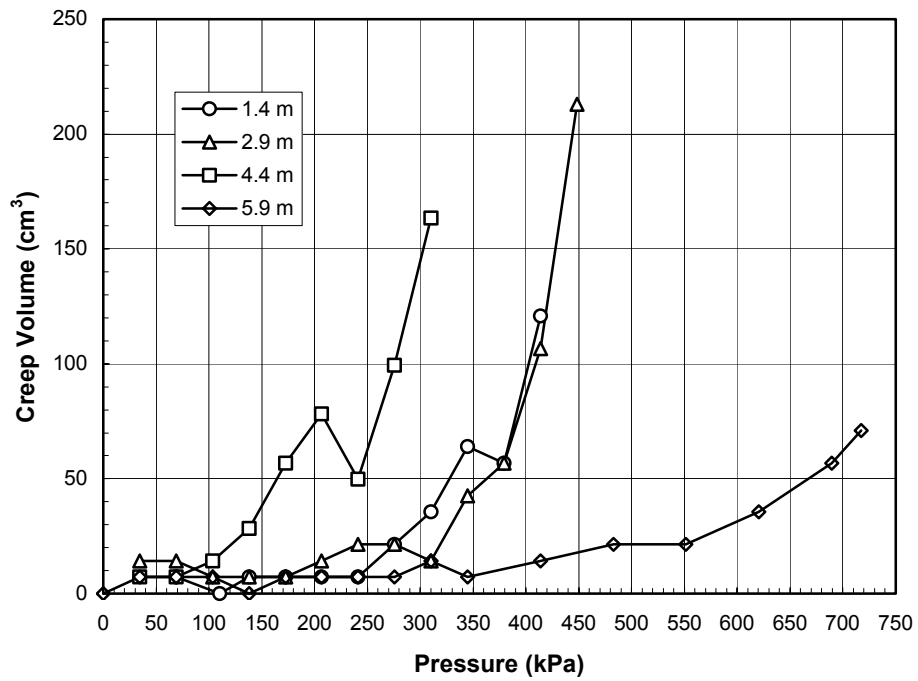
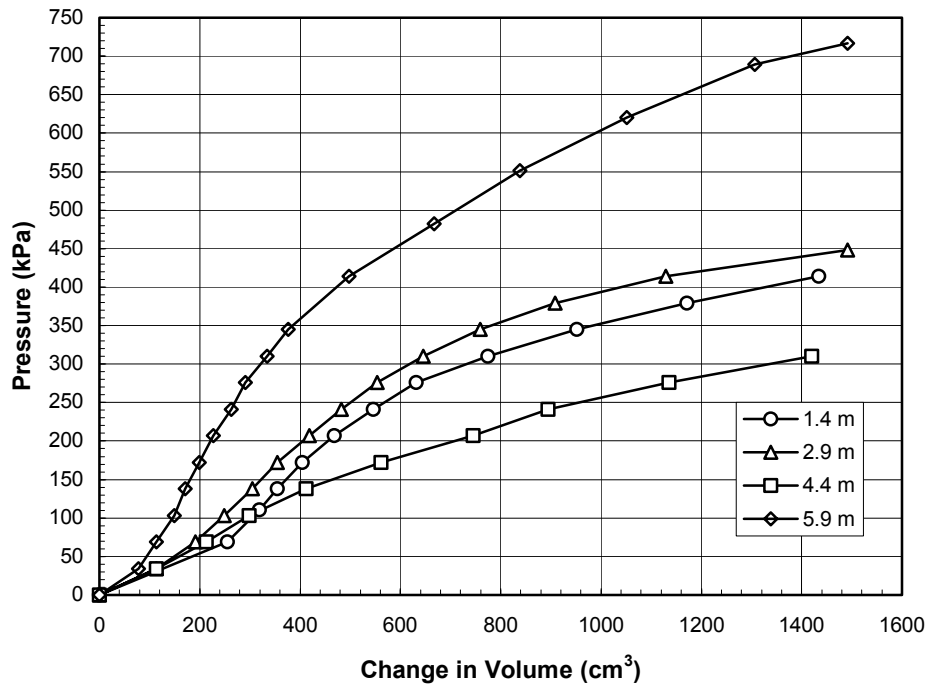


Figure C2. PMT-2 (prior to rammed aggregate pier installation) (top) pressuremeter curve, (bottom) creep curve

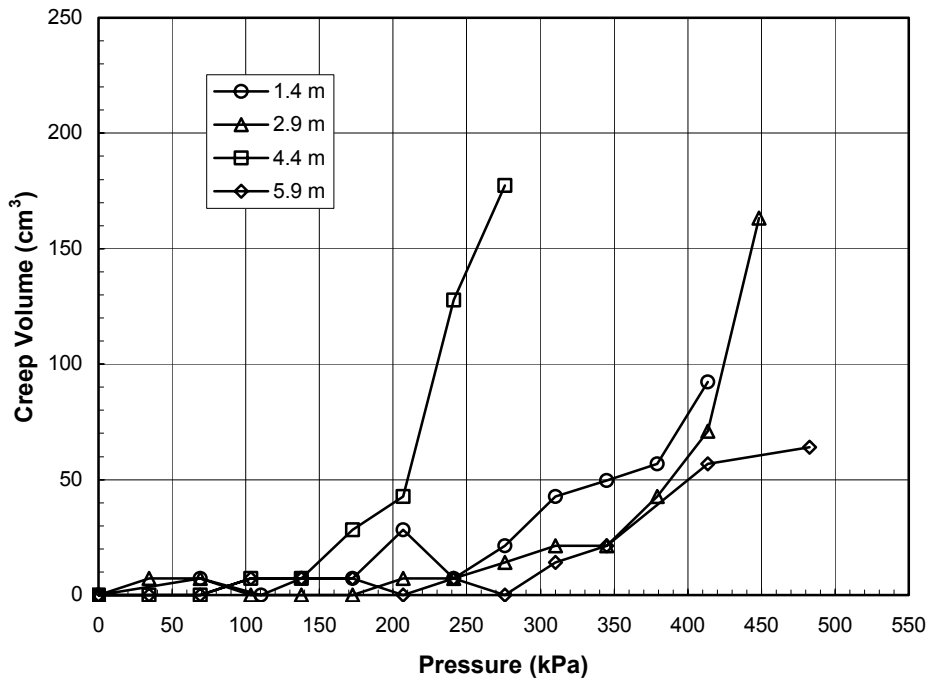
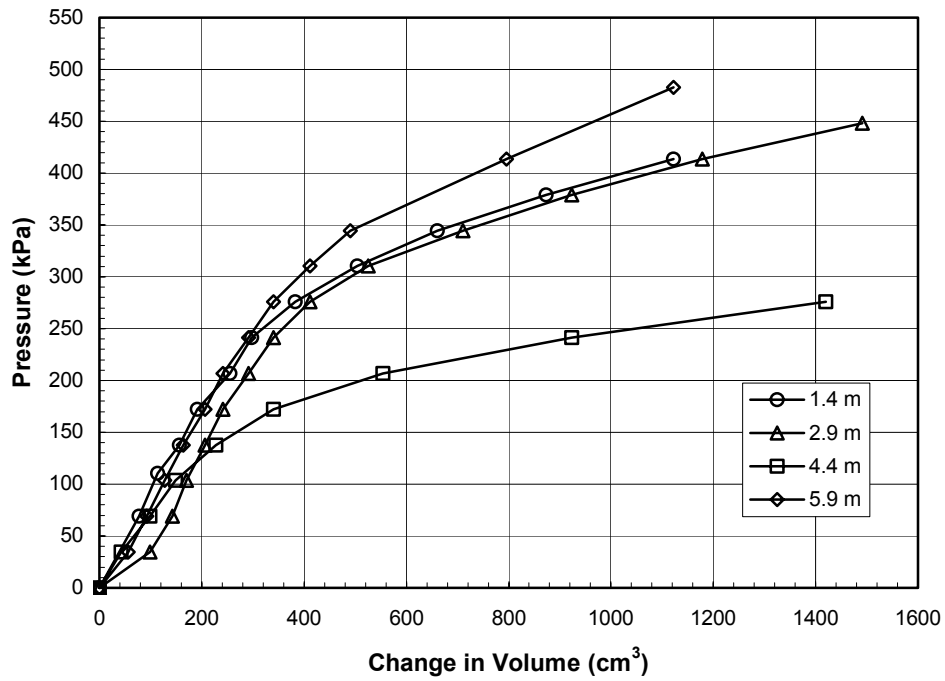


Figure C3. PMT-3 (seven days after installation of rammed aggregate piers) (top) pressuremeter curve, (bottom) creep curve

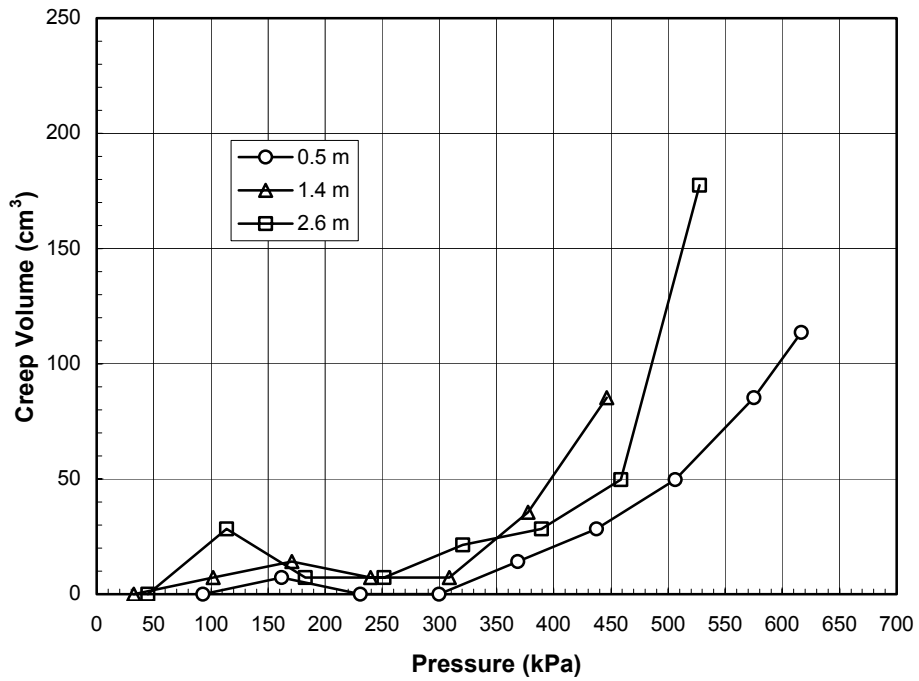
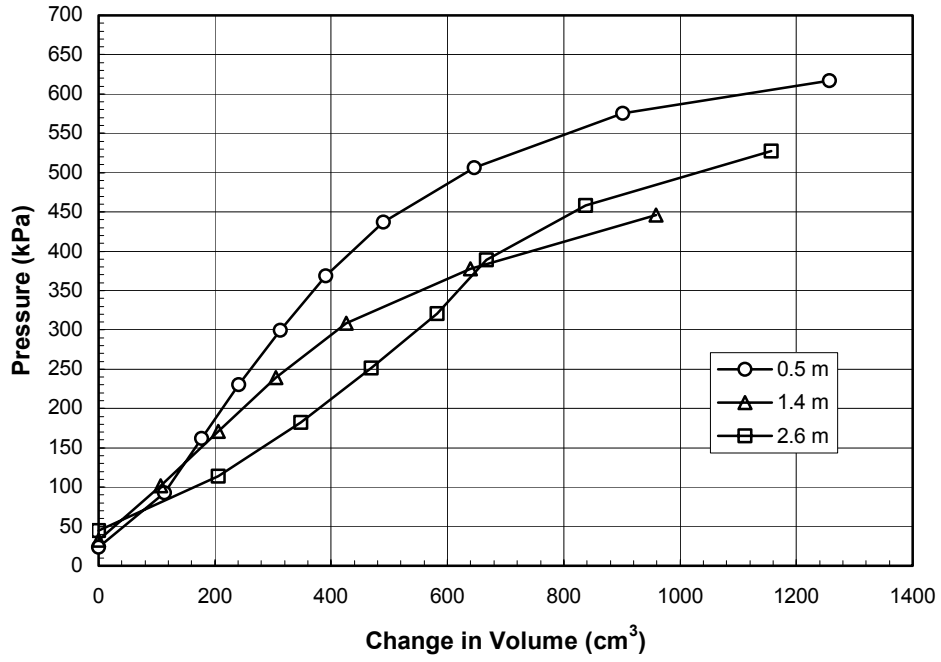


Figure C4. PMT-4 (73 days after installation of rammed aggregate piers) (top) pressuremeter curve, (bottom) creep curve

Table C1. Results of Pressuremeter Tests 1-4

Depth (m)	Test No.	Time of test	E_o (kPa)	p_L (kPa)
0.5	PMT-4	73 days after piers	5387	620
1.4	PMT-2	Prior to piers	4053	425
1.4	PMT-3	7 days after piers	4288	440
1.4	PMT-4	73 days after piers	3478	475
2.6	PMT-4	73 days after piers	2594	550
2.7	PMT-1	Prior to piers	6508	620
2.9	PMT-2	Prior to piers	3194	475
2.9	PMT-3	7 days after piers	4789	480
4.4	PMT-2	Prior to piers	1884	325
4.4	PMT-3	7 days after piers	3640	300
5.9	PMT-2	Prior to piers	6044	750
5.9	PMT-3	7 days after piers	4667	530
6.1	PMT-1	Prior to piers	7790	700

APPENDIX D: PROJECT NO. 2 CPT RESULTS

Table D1. Piezocone Penetration Data for CPTU-1

Depth (m)	q_T (kPa)	f_s (kPa)	R_f (%)	f_s/σ'_{vo}	Q	μ (kPa)	σ_{vo} (kPa)	μ_o (kPa)	σ'_{vo} (kPa)	B_q
0.15	755	29.4	4.14	12.75	300.6	-6.9	2.73	0.0	2.73	-0.01
0.40	885	38.7	4.39	5.39	122.2	-34.9	7.28	0.0	7.28	-0.04
0.65	1063	43.1	4.07	3.75	89.9	-30.3	11.83	0.0	11.83	-0.03
0.90	602	23.7	3.99	1.47	36.3	-18.1	16.38	0.0	16.38	-0.03
1.15	288	13.3	4.71	0.64	12.9	-17.4	20.93	0.0	20.93	-0.07
1.40	180	9.9	5.58	0.39	6.1	-15.6	25.48	0.0	25.48	-0.10
1.65	143	7.9	5.59	0.26	3.8	-8.7	30.03	0.0	30.03	-0.08
1.90	164	6.9	4.22	0.20	3.7	-2.3	34.58	0.0	34.58	-0.02
2.15	250	10.2	4.15	0.26	5.5	4.4	39.13	0.6	38.54	0.02
2.40	193	8.1	4.44	0.20	3.7	14.2	43.68	2.9	40.74	0.08
2.65	324	18.4	6.38	0.43	6.4	14.8	48.23	5.4	42.84	0.03
2.90	413	22.9	5.70	0.51	8.0	-14.8	52.78	7.8	44.94	-0.06
3.15	294	12.6	4.44	0.27	5.1	-1.0	57.33	10.3	47.04	-0.05
3.40	174	6.0	3.55	0.12	2.3	4.6	61.88	12.7	49.14	-0.07
3.65	200	6.7	3.54	0.13	2.6	16.1	66.43	15.2	51.24	0.01
3.90	151	5.4	3.67	0.10	1.5	19.9	70.98	17.6	53.34	0.03
4.15	165	5.0	3.07	0.09	1.6	25.9	75.53	20.1	55.44	0.07
4.40	242	5.9	2.46	0.10	2.8	33.1	80.08	22.5	57.54	0.07
4.65	347	16.4	4.63	0.27	4.4	43.4	84.63	25.0	59.64	0.07
4.90	256	6.7	2.60	0.11	2.7	53.8	89.18	27.4	61.74	0.16
5.15	221	5.6	2.53	0.09	2.0	57.6	93.73	29.9	63.84	0.22
5.40	240	5.7	2.62	0.09	2.1	61.9	98.28	32.3	65.94	0.21
5.65	232	4.6	2.07	0.07	1.9	65.5	102.83	34.8	68.04	0.24
5.90	293	9.5	3.17	0.13	2.6	67.2	107.38	37.2	70.14	0.16
6.15	432	16.0	3.70	0.22	4.4	72.0	111.93	39.7	72.24	0.10
6.40	515	21.6	4.24	0.29	5.4	70.2	116.48	42.1	74.34	0.07
6.65	402	16.4	4.12	0.21	3.7	68.4	121.03	44.6	76.44	0.08
6.90	350	14.7	4.26	0.19	2.9	67.6	125.58	47.0	78.54	0.09
7.15	305	8.7	2.86	0.11	2.2	69.0	130.13	49.5	80.64	0.11
7.40	352	9.4	2.70	0.11	2.6	71.8	134.68	51.9	82.74	0.09
7.65	240	5.4	2.33	0.06	1.2	73.5	139.23	54.4	84.84	0.19
7.90	264	5.0	1.92	0.06	1.4	75.8	143.78	56.8	86.94	0.16
8.15	313	11.9	3.91	0.13	1.8	104.1	148.33	59.3	89.04	0.27
8.40	383	16.6	4.38	0.18	2.5	160.4	152.88	61.7	91.14	0.43
8.65	413	14.2	3.41	0.15	2.7	143.1	157.43	64.2	93.24	0.31
8.90	310	7.7	2.55	0.08	1.6	147.1	161.98	66.6	95.34	0.54
9.15	358	11.9	3.33	0.12	2.0	156.2	166.53	69.1	97.44	0.46
9.40	340	9.0	2.66	0.09	1.7	174.7	171.08	71.5	99.54	0.61
9.65	506	16.2	3.20	0.16	3.3	199.1	175.63	74.0	101.64	0.38
9.90	516	14.0	2.73	0.13	3.2	193.2	180.18	76.4	103.74	0.35
10.15	401	9.4	2.40	0.09	2.0	194.7	184.73	78.9	105.84	0.54
10.40	376	10.8	2.93	0.10	1.7	212.0	189.28	81.3	107.94	0.70
10.65	383	8.7	2.28	0.08	1.7	226.6	193.83	83.8	110.04	0.75
10.90	357	8.0	2.27	0.07	1.4	225.3	198.38	86.2	112.14	0.88
11.15	460	9.8	2.19	0.09	2.2	219.5	202.93	88.7	114.24	0.51

11.40	438	10.4	2.43	0.09	2.0	163.4	207.48	91.1	116.34	0.31
11.65	456	8.0	1.81	0.07	2.1	134.3	212.03	93.6	118.44	0.17
11.90	446	9.5	2.14	0.08	1.9	161.8	216.58	96.0	120.54	0.29
12.15	416	8.2	2.02	0.07	1.6	175.3	221.13	98.5	122.64	0.39
12.40	974	21.7	2.74	0.17	6.0	156.0	225.68	100.9	124.74	0.07
12.65	648	23.5	3.61	0.18	3.3	206.0	230.23	103.4	126.84	0.25
12.90	802	32.0	4.01	0.25	4.4	127.6	234.78	105.8	128.94	0.04
13.15	1087	50.1	4.64	0.38	6.5	121.5	239.33	108.3	131.04	0.02
13.40	2673	114.0	4.51	0.85	18.2	54.3	243.88	110.7	133.14	-0.02
13.65	2619	120.1	4.68	0.89	17.5	55.4	248.43	113.2	135.24	-0.02
13.90	2781	113.1	4.19	0.82	18.4	54.5	252.98	115.6	137.34	-0.02
14.15	4034	122.2	3.10	0.88	27.1	90.6	257.53	118.1	139.44	-0.01
14.40	3632	144.5	4.00	1.02	23.8	75.3	262.08	120.5	141.54	-0.01
14.65	3611	141.1	3.93	0.98	23.3	87.7	266.63	123.0	143.64	-0.01
14.90	5381	151.2	2.84	1.04	35.1	152.4	271.18	125.4	145.74	0.01
15.15	6271	253.3	4.10	1.71	40.5	281.5	275.73	127.9	147.84	0.03
15.40	5799	208.4	3.71	1.39	36.8	571.9	280.28	130.3	149.94	0.08

Table D2. Piezocone Penetration Data for CPTU-2

Depth (m)	q_T (kPa)	f_s (kPa)	R_f (%)	f_s/σ'_{vo}	Q	μ (kPa)	σ_{vo} (kPa)	μ_0 (kPa)	σ'_{vo} (kPa)	B_q
0.15	755	29.4	4.14	12.75	300.6	-6.9	2.73	0.0	2.73	-0.01
0.40	885	38.7	4.39	5.39	122.2	-34.9	7.28	0.0	7.28	-0.04
0.65	1063	43.1	4.07	3.75	89.9	-30.3	11.83	0.0	11.83	-0.03
0.90	602	23.7	3.99	1.47	36.3	-18.1	16.38	0.0	16.38	-0.03
1.15	288	13.3	4.71	0.64	12.9	-17.4	20.93	0.0	20.93	-0.07
1.40	180	9.9	5.58	0.39	6.1	-15.6	25.48	0.0	25.48	-0.10
1.65	143	7.9	5.59	0.26	3.8	-8.7	30.03	0.0	30.03	-0.08
1.90	164	6.9	4.22	0.20	3.7	-2.3	34.58	0.0	34.58	-0.02
2.15	250	10.2	4.15	0.26	5.5	4.4	39.13	0.6	38.54	0.02
2.40	193	8.1	4.44	0.20	3.7	14.2	43.68	2.9	40.74	0.08
2.65	324	18.4	6.38	0.43	6.4	14.8	48.23	5.4	42.84	0.03
2.90	413	22.9	5.70	0.51	8.0	-14.8	52.78	7.8	44.94	-0.06
3.15	294	12.6	4.44	0.27	5.1	-1.0	57.33	10.3	47.04	-0.05
3.40	174	6.0	3.55	0.12	2.3	4.6	61.88	12.7	49.14	-0.07
3.65	200	6.7	3.54	0.13	2.6	16.1	66.43	15.2	51.24	0.01
3.90	151	5.4	3.67	0.10	1.5	19.9	70.98	17.6	53.34	0.03
4.15	165	5.0	3.07	0.09	1.6	25.9	75.53	20.1	55.44	0.07
4.40	242	5.9	2.46	0.10	2.8	33.1	80.08	22.5	57.54	0.07
4.65	347	16.4	4.63	0.27	4.4	43.4	84.63	25.0	59.64	0.07
4.90	256	6.7	2.60	0.11	2.7	53.8	89.18	27.4	61.74	0.16
5.15	221	5.6	2.53	0.09	2.0	57.6	93.73	29.9	63.84	0.22
5.40	240	5.7	2.62	0.09	2.1	61.9	98.28	32.3	65.94	0.21
5.65	232	4.6	2.07	0.07	1.9	65.5	102.83	34.8	68.04	0.24
5.90	293	9.5	3.17	0.13	2.6	67.2	107.38	37.2	70.14	0.16
6.15	432	16.0	3.70	0.22	4.4	72.0	111.93	39.7	72.24	0.10
6.40	515	21.6	4.24	0.29	5.4	70.2	116.48	42.1	74.34	0.07
6.65	402	16.4	4.12	0.21	3.7	68.4	121.03	44.6	76.44	0.08
6.90	350	14.7	4.26	0.19	2.9	67.6	125.58	47.0	78.54	0.09

7.15	305	8.7	2.86	0.11	2.2	69.0	130.13	49.5	80.64	0.11
7.40	352	9.4	2.70	0.11	2.6	71.8	134.68	51.9	82.74	0.09
7.65	240	5.4	2.33	0.06	1.2	73.5	139.23	54.4	84.84	0.19
7.90	264	5.0	1.92	0.06	1.4	75.8	143.78	56.8	86.94	0.16
8.15	313	11.9	3.91	0.13	1.8	104.1	148.33	59.3	89.04	0.27
8.40	383	16.6	4.38	0.18	2.5	160.4	152.88	61.7	91.14	0.43
8.65	413	14.2	3.41	0.15	2.7	143.1	157.43	64.2	93.24	0.31
8.90	310	7.7	2.55	0.08	1.6	147.1	161.98	66.6	95.34	0.54
9.15	358	11.9	3.33	0.12	2.0	156.2	166.53	69.1	97.44	0.46
9.40	340	9.0	2.66	0.09	1.7	174.7	171.08	71.5	99.54	0.61
9.65	506	16.2	3.20	0.16	3.3	199.1	175.63	74.0	101.64	0.38
9.90	516	14.0	2.73	0.13	3.2	193.2	180.18	76.4	103.74	0.35
10.15	401	9.4	2.40	0.09	2.0	194.7	184.73	78.9	105.84	0.54
10.40	376	10.8	2.93	0.10	1.7	212.0	189.28	81.3	107.94	0.70
10.65	383	8.7	2.28	0.08	1.7	226.6	193.83	83.8	110.04	0.75
10.90	357	8.0	2.27	0.07	1.4	225.3	198.38	86.2	112.14	0.88
11.15	460	9.8	2.19	0.09	2.2	219.5	202.93	88.7	114.24	0.51
11.40	438	10.4	2.43	0.09	2.0	163.4	207.48	91.1	116.34	0.31
11.65	456	8.0	1.81	0.07	2.1	134.3	212.03	93.6	118.44	0.17
11.90	446	9.5	2.14	0.08	1.9	161.8	216.58	96.0	120.54	0.29
12.15	416	8.2	2.02	0.07	1.6	175.3	221.13	98.5	122.64	0.39
12.40	974	21.7	2.74	0.17	6.0	156.0	225.68	100.9	124.74	0.07
12.65	648	23.5	3.61	0.18	3.3	206.0	230.23	103.4	126.84	0.25
12.90	802	32.0	4.01	0.25	4.4	127.6	234.78	105.8	128.94	0.04
13.15	1087	50.1	4.64	0.38	6.5	121.5	239.33	108.3	131.04	0.02
13.40	2673	114.0	4.51	0.85	18.2	54.3	243.88	110.7	133.14	-0.02
13.65	2619	120.1	4.68	0.89	17.5	55.4	248.43	113.2	135.24	-0.02
13.90	2781	113.1	4.19	0.82	18.4	54.5	252.98	115.6	137.34	-0.02
14.15	4034	122.2	3.10	0.88	27.1	90.6	257.53	118.1	139.44	-0.01
14.40	3632	144.5	4.00	1.02	23.8	75.3	262.08	120.5	141.54	-0.01
14.65	3611	141.1	3.93	0.98	23.3	87.7	266.63	123.0	143.64	-0.01
14.90	5381	151.2	2.84	1.04	35.1	152.4	271.18	125.4	145.74	0.01
15.15	6271	253.3	4.10	1.71	40.5	281.5	275.73	127.9	147.84	0.03
15.40	5799	208.4	3.71	1.39	36.8	571.9	280.28	130.3	149.94	0.08

Table D3. Piezocone Penetration Data for CPTU-3

Depth (m)	q_T (kPa)	f_s (kPa)	R_f (%)	f_s/σ'_{vo}	Q	μ (kPa)	σ_{vo} (kPa)	μ_0 (kPa)	σ'_{vo} (kPa)	B_q
0.15	549	20.5	3.87	9.85	301.6	-5.7	2.73	0.0	2.73	-0.01
0.40	1847	39.5	2.42	5.54	246.0	3.6	7.28	0.0	7.28	0.00
0.65	1101	21.6	2.01	1.92	96.2	9.7	11.83	0.0	11.83	0.01
0.90	1202	21.8	1.81	1.34	73.1	9.1	16.38	0.0	16.38	0.01
1.15	810	9.5	1.17	0.46	38.0	2.2	20.93	0.0	20.93	0.00
1.40	468	20.5	4.82	0.80	17.6	4.7	25.48	0.0	25.48	0.01
1.65	434	21.8	5.04	0.73	13.5	-1.1	30.03	0.0	30.03	0.00
1.90	362	21.5	5.98	0.62	9.5	-0.6	34.58	0.0	34.58	0.00
2.15	212	12.2	5.83	0.31	4.4	-2.1	39.13	0.0	39.13	-0.01
2.40	267	13.9	5.30	0.32	5.2	11.0	43.68	0.0	43.68	0.05
2.65	253	11.7	4.65	0.24	4.3	16.0	48.23	0.0	48.23	0.08

2.90	258	10.6	4.19	0.20	3.9	17.0	52.78	0.0	52.78	0.08
3.15	135	6.0	4.99	0.11	1.4	21.5	57.33	0.1	57.23	0.27
3.40	131	5.5	4.30	0.09	1.2	28.4	61.88	2.0	59.92	0.38
3.65	117	5.2	4.39	0.08	0.8	31.4	66.43	4.4	62.02	0.53
3.90	137	6.0	4.40	0.09	1.0	34.8	70.98	6.9	64.12	0.42
4.15	105	4.8	4.59	0.07	0.4	36.5	75.53	9.3	66.22	0.92
4.40	158	4.1	2.61	0.06	1.1	53.0	80.08	11.8	68.32	0.53
4.65	200	5.1	2.54	0.07	1.6	62.2	84.63	14.2	70.42	0.42
4.90	214	5.1	2.38	0.07	1.7	69.0	89.18	16.7	72.52	0.42
5.15	184	4.0	2.20	0.05	1.2	75.7	93.73	19.1	74.62	0.63
5.40	205	4.9	2.40	0.06	1.4	93.2	98.28	21.6	76.72	0.67
5.65	209	4.1	2.15	0.05	1.3	105.5	102.83	24.0	78.82	0.77
5.90	206	4.3	2.09	0.05	1.2	112.5	107.38	26.5	80.92	0.87
6.15	220	6.3	2.85	0.08	1.3	120.5	111.93	28.9	83.02	0.84
6.40	265	8.0	3.13	0.09	1.7	94.2	116.48	31.4	85.12	0.42
6.65	231	3.4	1.46	0.04	1.3	94.0	121.03	33.8	87.22	0.55
6.90	302	7.5	2.45	0.08	2.0	103.0	125.58	36.3	89.32	0.38
7.15	330	11.7	3.58	0.13	2.2	111.4	130.13	38.7	91.42	0.36
7.40	347	11.2	3.25	0.12	2.3	128.5	134.68	41.2	93.52	0.41
7.65	310	11.3	3.65	0.12	1.8	138.6	139.23	43.6	95.62	0.56
7.90	377	16.5	4.39	0.17	2.4	151.1	143.78	46.1	97.72	0.45
8.15	483	19.9	4.16	0.20	3.3	163.8	148.33	48.5	99.82	0.34
8.40	466	19.2	4.12	0.19	3.1	170.2	152.88	51.0	101.92	0.38
8.65	433	18.7	4.31	0.18	2.6	180.4	157.43	53.4	104.02	0.46
8.90	445	18.1	4.04	0.17	2.7	185.8	161.98	55.9	106.12	0.46
9.15	726	30.7	4.26	0.28	5.2	201.3	166.53	58.3	108.22	0.26
9.40	777	36.9	4.76	0.33	5.5	183.7	171.08	60.8	110.32	0.20
9.65	435	14.8	3.34	0.13	2.3	163.1	175.63	63.2	112.42	0.39
9.90	397	7.5	1.88	0.07	1.9	166.0	180.18	65.7	114.52	0.46
10.15	447	16.7	3.71	0.14	2.2	178.9	184.73	68.1	116.62	0.42
10.40	398	13.3	3.34	0.11	1.8	194.7	189.28	70.6	118.72	0.59
10.65	424	14.7	3.46	0.12	1.9	206.3	193.83	73.0	120.82	0.58
10.90	483	17.4	3.60	0.14	2.3	205.6	198.38	75.5	122.92	0.46
11.15	383	10.6	2.77	0.09	1.4	200.1	202.93	77.9	125.02	0.68
11.40	343	8.8	2.56	0.07	1.1	209.7	207.48	80.4	127.12	0.96
11.65	307	5.2	1.67	0.04	0.7	220.4	212.03	82.8	129.22	1.44
11.90	361	6.9	1.92	0.05	1.1	231.7	216.58	85.3	131.32	1.01
12.15	393	6.5	1.67	0.05	1.3	241.0	221.13	87.7	133.42	0.89
12.40	371	5.2	1.39	0.04	1.1	262.4	225.68	90.2	135.52	1.18
12.65	409	5.8	1.44	0.04	1.3	267.5	230.23	92.6	137.62	0.98
12.90	492	6.2	1.35	0.04	1.8	264.5	234.78	95.1	139.72	0.66
13.15	405	7.3	1.82	0.05	1.2	270.3	239.33	97.5	141.82	1.05
13.40	437	7.9	1.81	0.05	1.3	253.9	243.88	100.0	143.92	0.80
13.65	521	8.2	1.59	0.06	1.9	262.6	248.43	102.4	146.02	0.59
13.90	623	9.0	1.51	0.06	2.5	181.9	252.98	104.9	148.12	0.21
14.15	610	11.6	2.04	0.08	2.3	173.9	257.53	107.3	150.22	0.19
14.40	1158	12.7	1.09	0.08	5.9	74.1	262.08	109.8	152.32	-0.04

APPENDIX E: PROJECT NO. 2 DMT RESULTS

Table E1. DMT1 Data Readings

m	ft	bar	var	bar	bar	delta p	bar	bar
Depth	Depth	A	B	po	p1		Vert Eff. Stress	uo
0.30	1	2.45	7.6	1.40	5.97	4.57	0.05	0.00
0.61	2	1	3.6	0.08	1.97	1.89	0.10	0.00
0.91	3	1	2.5	0.14	0.87	0.74	0.15	0.00
1.22	4	1	2.5	0.14	0.87	0.74	0.20	0.00
1.52	5	1.25	3.1	0.37	1.47	1.10	0.25	0.00
1.83	6	0.8	2	-0.05	0.37	0.42	0.30	0.00
2.13	7	1	2.6	0.13	0.97	0.84	0.32	0.03
2.44	8	1.6	3.8	0.70	2.17	1.47	0.34	0.06
2.74	9	2.5	5.2	1.58	3.57	2.00	0.36	0.09
3.05	10	1.6	3.4	0.72	1.77	1.05	0.38	0.12
3.35	11	1.7	3.2	0.84	1.57	0.74	0.40	0.15
3.66	12	1.8	3.2	0.94	1.57	0.63	0.42	0.18
3.96	13	1.8	3.2	0.94	1.57	0.63	0.44	0.21
4.27	14	1.7	2.85	0.85	1.22	0.37	0.46	0.24
4.57	15	2	3.2	1.15	1.57	0.42	0.49	0.27
4.88	16	1.8	2.8	0.96	1.17	0.21	0.51	0.30
5.18	17	1.7	2.6	0.87	0.97	0.11	0.53	0.33
5.49	18	2.3	3.7	1.44	2.07	0.63	0.55	0.36
5.79	19	1.8	2.9	0.96	1.27	0.32	0.57	0.39
6.10	20	1.9	2.8	1.07	1.17	0.11	0.59	0.42
6.40	21	1.7	2.8	0.86	1.17	0.32	0.61	0.45
6.71	22	1.8	3.2	0.94	1.57	0.63	0.63	0.48
7.01	23	1.7	2.8	0.86	1.17	0.32	0.65	0.51
7.32	24	2.3	3.2	1.47	1.57	0.11	0.67	0.54
7.62	25	2.3	3.3	1.46	1.67	0.21	0.69	0.57
7.92	26	2.2	3.3	1.36	1.67	0.32	0.71	0.60
8.23	27	2.3	3.4	1.46	1.77	0.32	0.73	0.63
8.53	28	2.5	3.8	1.65	2.17	0.53	0.75	0.66
8.84	29	2.6	4.2	1.73	2.57	0.84	0.77	0.69
9.14	30	2.4	3.8	1.54	2.17	0.63	0.79	0.72
9.45	31	2.8	4.4	1.93	2.77	0.84	0.81	0.75
9.75	32	2.9	4.1	2.05	2.47	0.42	0.83	0.78
10.06	33	3.4	5.55	2.50	3.92	1.42	0.85	0.81
10.36	34	3.1	4.4	2.25	2.77	0.53	0.87	0.84
10.67	35	2.9	3.9	2.06	2.27	0.21	0.89	0.87
10.97	36	3.1	4.3	2.25	2.67	0.42	0.91	0.90
11.28	37	3.1	4.2	2.26	2.57	0.32	0.93	0.93
11.58	38	3.3	4.3	2.46	2.67	0.21	0.95	0.96
11.89	39	3.5	4.7	2.65	3.07	0.42	0.97	0.99
12.19	40	3.2	4.2	2.36	2.57	0.21	1.00	1.02
12.50	41	3	4.7	2.13	3.07	0.95	1.02	1.05
12.80	42	3.3	4.4	2.46	2.77	0.32	1.04	1.08
13.11	43	3.5	4.5	2.66	2.87	0.21	1.06	1.11
13.41	44	3.4	4.4	2.56	2.77	0.21	1.08	1.14
13.72	45	5.8	10.4	4.78	8.77	3.99	1.10	1.17
14.02	46	9.6	20.3	8.28	18.67	10.40	1.12	1.20

Table E2. Reduced DMT1 Data

Material Index	Classification	Horiz. Stress Index	Dilat. Modulus	Coeff Earth Press	Undrained Shear
I _d		K _d	E _d	K _o	C _u (bars)
3.26	sand	27.90	158.49	2.05	0.30
23.63	sand	0.80	65.58	0.30	0.01
5.44	sand	0.90	25.50	0.32	0.01
5.44	sand	0.67	25.50	0.27	0.01
3.00	silty sand	1.46	38.26	0.42	0.04
-8.40	n/a	-0.17	14.57	#NUM!	#NUM!
8.39	sand	0.31	29.15	0.18	0.01
2.30	silty sand	1.87	51.01	0.48	0.07
1.34	sandy silt	4.09	69.23	0.73	0.20
1.75	sandy silt	1.57	36.44	0.43	0.06
1.07	silt	1.70	25.50	0.45	0.07
0.83	clayey silt	1.79	21.86	0.47	0.08
0.86	clayey silt	1.64	21.86	0.44	0.08
0.60	silty clay	1.32	12.75	0.39	0.06
0.48	silty clay	1.82	14.57	0.47	0.09
0.32	clayey silt	1.31	7.29	0.39	0.07
0.20	clayey silt	1.02	3.64	0.34	0.05
0.58	silty clay	1.98	21.86	0.49	0.12
0.56	silty clay	1.00	10.93	0.34	0.05
0.16	clayey silt	1.10	3.64	0.36	0.06
0.77	clayey silt	0.67	10.93	0.27	0.03
1.36	sandy silt	0.74	21.86	0.29	0.04
0.91	clayey silt	0.54	10.93	0.24	0.03
0.11	clay	1.39	3.64	0.41	0.09
0.24	clay	1.29	7.29	0.39	0.09
0.42	silty clay	1.07	10.93	0.35	0.07
0.38	silty clay	1.13	10.93	0.36	0.08
0.53	silty clay	1.32	18.22	0.39	0.10
0.81	clayey silt	1.35	29.15	0.40	0.10
0.77	clayey silt	1.04	21.86	0.35	0.08
0.71	clayey silt	1.46	29.15	0.42	0.12
0.33	clay	1.53	14.57	0.43	0.13
0.84	clayey silt	1.99	49.19	0.49	0.19
0.37	silty clay	1.61	18.22	0.44	0.15
0.18	clay	1.34	7.29	0.40	0.12
0.31	clay	1.48	14.57	0.42	0.14
0.24	clay	1.42	10.93	0.41	0.13
0.14	clay	1.58	7.29	0.43	0.16
0.25	clay	1.71	14.57	0.45	0.18
0.16	clay	1.35	7.29	0.40	0.13
0.88	clayey silt	1.06	32.79	0.35	0.10
0.23	clay	1.33	10.93	0.40	0.14
0.14	clay	1.47	7.29	0.42	0.16
0.15	clay	1.32	7.29	0.40	0.14
1.10	silt	3.29	138.45	0.65	0.45
1.47	sandy silt	6.34	360.71	0.92	1.04

Table E3. DMT2 Data Readings

m	ft	bar	var	bar	bar	delta p	bar	bar
Depth	Depth	A	B	po	p1		Vert Eff. Stress	uo
0.30	1.00	2.10	6.00	1.12	4.37	3.26	0.05	0.00
0.61	2.00	1.60	4.15	0.68	2.52	1.84	0.10	0.00
0.91	3.00	1.00	2.10	0.16	0.47	0.32	0.15	0.00
1.22	4.00	1.10	2.30	0.25	0.67	0.42	0.20	0.00
1.52	5.00	0.80	2.10	-0.06	0.47	0.53	0.25	0.00
1.83	6.00	0.80	1.80	-0.04	0.17	0.21	0.30	0.00
2.13	7.00	1.30	2.90	0.43	1.27	0.84	0.32	0.03
2.44	8.00	1.70	3.10	0.84	1.47	0.63	0.34	0.06
2.74	9.00	1.15	2.20	0.31	0.57	0.26	0.36	0.09
3.05	10.00	1.40	2.35	0.56	0.72	0.16	0.38	0.12
3.35	11.00	1.50	2.40	0.67	0.77	0.11	0.40	0.15
3.66	12.00	1.60	2.70	0.76	1.07	0.32	0.42	0.18
3.96	13.00	1.80	2.80	0.96	1.17	0.21	0.44	0.21
4.27	14.00	1.80	2.60	0.97	0.97	0.00	0.46	0.24
4.57	15.00	1.90	3.05	1.05	1.42	0.37	0.49	0.27
4.88	16.00	2.10	3.10	1.26	1.47	0.21	0.51	0.30
5.18	17.00	2.30	3.40	1.46	1.77	0.32	0.53	0.33
5.49	18.00	2.30	3.20	1.47	1.57	0.11	0.55	0.36
5.79	19.00	2.10	3.00	1.27	1.37	0.11	0.57	0.39
6.10	20.00	2.00	3.00	1.16	1.37	0.21	0.59	0.42
6.40	21.00	2.00	2.90	1.17	1.27	0.11	0.61	0.45
6.71	22.00	1.90	2.85	1.06	1.22	0.16	0.63	0.48
7.01	23.00	2.10	3.10	1.26	1.47	0.21	0.65	0.51
7.32	24.00	2.30	3.10	1.47	1.47	0.00	0.67	0.54
7.62	25.00	2.50	3.80	1.65	2.17	0.53	0.69	0.57
7.92	26.00	2.75	3.80	1.91	2.17	0.26	0.71	0.60
8.23	27.00	2.60	3.70	1.76	2.07	0.32	0.73	0.63
8.53	28.00	2.60	3.60	1.76	1.97	0.21	0.75	0.66
8.84	29.00	2.70	3.60	1.87	1.97	0.11	0.77	0.69
9.14	30.00	2.70	3.50	1.87	1.87	0.00	0.79	0.72
9.45	31.00	2.80	3.70	1.97	2.07	0.11	0.81	0.75
9.75	32.00	2.20	3.60	1.34	1.97	0.63	0.83	0.78
10.06	33.00	2.50	3.70	1.65	2.07	0.42	0.85	0.81
10.36	34.00	3.10	4.75	2.23	3.12	0.89	0.87	0.84
10.67	35.00	3.85	5.50	2.98	3.87	0.89	0.89	0.87
10.97	36.00	3.00	4.00	2.16	2.37	0.21	0.91	0.90
11.28	37.00	2.90	3.70	2.07	2.07	0.00	0.93	0.93
11.58	38.00	2.70	3.60	1.87	1.97	0.11	0.95	0.96
11.89	39.00	2.70	4.30	1.83	2.67	0.84	0.97	0.99
12.19	40.00	2.50	3.50	1.66	1.87	0.21	1.00	1.02
12.50	41.00	2.50	4.00	1.64	2.37	0.74	1.02	1.05
12.80	42.00	2.70	6.30	1.73	4.67	2.94	1.04	1.08
13.11	43.00	3.00	4.30	2.15	2.67	0.53	1.06	1.11
13.41	44.00	2.80	3.80	1.96	2.17	0.21	1.08	1.14
13.72	45.00	2.50	3.90	1.64	2.27	0.63	1.10	1.17
14.02	46.00	2.80	6.80	1.81	5.17	3.36	1.12	1.20
14.33	47.00	3.50	7.30	2.52	5.67	3.15	1.14	1.22
14.48	47.50	3.80	13.10	2.55	11.47	8.93	1.15	1.24

Table E4. Reduced DMT2 Data

Material Index	Classification	Horiz. Stress Index	Dilat. Modulus	Coeff Earth Press	Undrained Shear
Id		Kd	Ed	Ko	Cu (bars)
2.92	silty sand	22.18	112.95	1.81	0.22
2.69	silty sand	6.79	63.76	0.96	0.10
2.03	silty sand	1.03	10.93	0.35	0.01
1.68	silty sand	1.24	14.57	0.38	0.02
-9.55	n/a	-0.22	18.22	#NUM!	#NUM!
-5.25	n/a	-0.13	7.29	#NUM!	#NUM!
2.10	silty sand	1.24	29.15	0.38	0.04
0.81	silt	2.28	21.86	0.53	0.09
1.20	sandy silt	0.60	9.11	0.26	0.02
0.36	silty clay	1.16	5.47	0.37	0.04
0.20	silty clay	1.28	3.64	0.39	0.05
0.55	clayey silt	1.36	10.93	0.40	0.06
0.28	silty clay	1.69	7.29	0.45	0.08
0.00	clay	1.57	0.00	0.43	0.08
0.47	clayey silt	1.61	12.75	0.44	0.08
0.22	clay	1.90	7.29	0.48	0.10
0.28	silty clay	2.14	10.93	0.51	0.13
0.09	clay	2.02	3.64	0.50	0.12
0.12	clay	1.55	3.64	0.43	0.09
0.28	silty clay	1.26	7.29	0.39	0.07
0.15	clay	1.18	3.64	0.37	0.07
0.27	silty clay	0.93	5.47	0.33	0.05
0.28	silty clay	1.16	7.29	0.37	0.07
0.00	clay	1.39	0.00	0.41	0.09
0.49	silty clay	1.56	18.22	0.43	0.11
0.20	clay	1.85	9.11	0.47	0.14
0.28	clay	1.54	10.93	0.43	0.12
0.19	clay	1.47	7.29	0.42	0.11
0.09	clay	1.53	3.64	0.43	0.12
0.00	clay	1.46	0.00	0.42	0.12
0.09	clay	1.50	3.64	0.42	0.12
1.12	sandy silt	0.68	21.86	0.28	0.05
0.50	clayey silt	0.99	14.57	0.34	0.08
0.64	clayey silt	1.59	30.97	0.44	0.14
0.42	silty clay	2.36	30.97	0.54	0.24
0.17	clay	1.38	7.29	0.41	0.13
0.00	clay	1.22	0.00	0.38	0.11
0.12	clay	0.95	3.64	0.33	0.08
1.00	silt	0.87	29.15	0.31	0.08
0.33	silty clay	0.65	7.29	0.27	0.05
1.25	sandy silt	0.58	25.50	0.25	0.05
4.49	sand	0.63	102.02	0.27	0.05
0.51	clayey silt	0.98	18.22	0.34	0.10
0.25	silty clay	0.77	7.29	0.29	0.07
1.33	sandy silt	0.43	21.86	0.22	0.04
5.46	sand	0.55	116.59	0.25	0.05
2.43	silty sand	1.14	109.31	0.36	0.12
6.84	sand	1.14	309.70	0.36	0.12

APPENDIX F: PROJECT NO. 2 PMT RESULTS

Table F1. PMT1 Data at 4.57 m

Depth (m)	V30	V60	Volume (cm3)	Creep	Creep V (cm3)	P (psi)	P (kPa)
4.57	16.50	16.70	1338.84	0.00	0.00	5.00	34.47
4.57	17.70	17.90	1435.04	0.20	16.03	10.00	68.95
4.57	19.10	19.30	1547.28	0.20	16.03	15.00	103.42
4.57	20.30	20.40	1635.47	0.10	8.02	20.00	137.89
4.57	21.40	21.60	1731.67	0.20	16.03	25.00	172.37
4.57	22.80	23.00	1843.91	0.20	16.03	30.00	206.84
4.57	23.90	25.00	2004.25	1.10	88.19	35.00	241.31
4.57	27.20	28.00	2244.76	0.80	64.14	39.00	268.89

Membrane Resistance (kPa)	Head (kPa)	Final Corr P (kPa)	Compressibility (cm3)	Initial (cm3)	Final Corr. V (cm3)
19.09	44.52	59.91	0.00	1258.67	80.17
26.55	44.52	86.92	0.00	1258.67	176.37
34.46	44.52	113.48	0.00	1258.67	288.61
40.08	44.52	142.33	0.00	1258.67	376.80
45.62	44.52	171.27	0.00	1258.67	473.00
51.30	44.52	200.07	2.87	1258.67	582.37
57.94	44.52	227.90	6.38	1258.67	739.20
64.67	44.52	248.75	8.85	1258.67	977.24

PMT1 4.57m

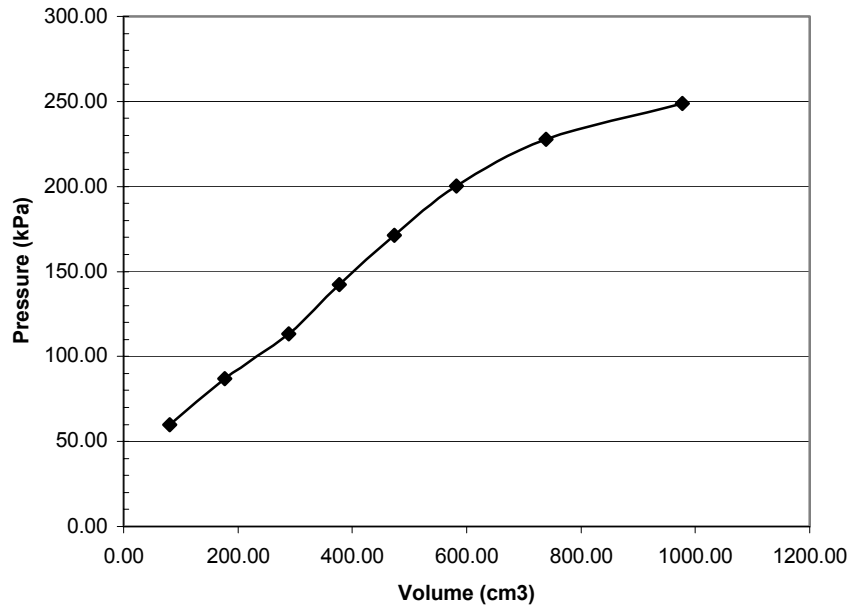


Figure F1. PMT1 Curve at 4.57 m

Table F2. PMT1 Data at 6.10 m

Depth (m)	V30	V60	Volume (cm3)	Creep	Creep V (cm3)	P (psi)	P (kPa)
6.10	17.1	17.7	1419.01	0.00	0.00	5.00	34.47
6.10	19.2	19.6	1571.33	0.40	32.07	10.00	68.95
6.10	20.8	21.2	1699.60	0.40	32.07	15.00	103.42
6.10	22.3	22.6	1811.84	0.30	24.05	20.00	137.89
6.10	23.7	24.1	1932.10	0.40	32.07	25.00	172.37
6.10	25.6	25.9	2076.40	0.30	24.05	30.00	206.84
6.10	27.5	28.1	2252.78	0.60	48.10	34.00	234.42
6.10	29.8	30.3	2429.15	0.50	40.09	37.00	255.10

Membrane Resistance (kPa)	Head (kPa)	Final Corr P (kPa)	Compressibility (cm3)	Initial (cm3)	Final Corr. V (cm3)
25.35	59.36	68.49	0.00	1202.55	216.46
36.04	59.36	92.27	0.00	1202.55	368.78
43.84	59.36	118.94	0.00	1202.55	497.05
49.76	59.36	147.50	0.00	1202.55	609.29
55.17	59.36	176.57	0.00	1202.55	729.55
60.37	59.36	205.84	2.87	1202.55	870.98
64.83	59.36	228.96	5.72	1202.55	1044.51
67.20	59.36	247.27	7.65	1202.55	1218.95

PMT 6.10 m

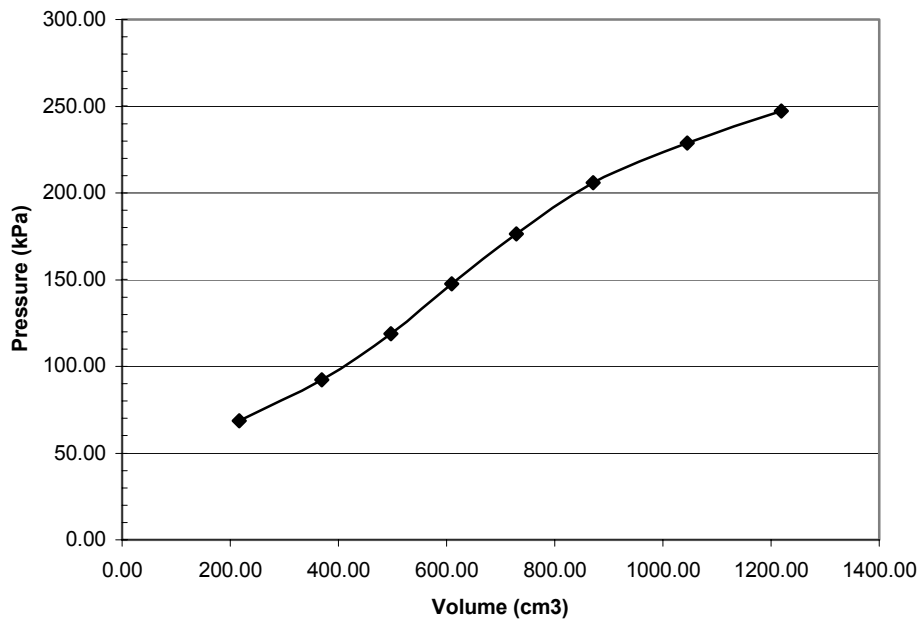


Figure F2. PMT1 Curve at 6.10 m

Table F3. PMT Data at 7.62 m

Depth (m)	V30	V60	Volume (cm3)	Creep	Creep V (cm3)	P (psi)	P (kPa)
7.62	16.2	16.3	1306.771	0	0	5	34.4735
7.62	17.8	18.2	1459.094	0.4	32.068	10	68.947
7.62	19.2	19.3	1547.281	0.1	8.017	15	103.421
7.62	20.3	20.5	1643.485	0.2	16.034	20	137.894
7.62	21.6	21.7	1739.689	0.1	8.017	25	172.368
7.62	23	23.3	1867.961	0.3	24.051	30	206.841
7.62	25.1	25.6	2052.352	0.5	40.085	35	241.315
7.62	27.6	27.9	2236.743	0.3	24.051	39	268.893
7.62	29.8	30.5	2445.185	0.7	56.119	44	303.367

Membrane Resistance (kPa)	Head (kPa)	Final Corr P (kPa)	Compressibility (cm3)	Initial (cm3)	Final Corr. V (cm3)
16.46842552	74.205701	92.21077531	0	1202.55	104.221
28.31360755	74.205701	114.8390933	0	1202.55	256.544
34.45931228	74.205701	143.1668886	0	1202.55	344.731
40.56819956	74.205701	171.5315013	0	1202.55	440.935
46.05567689	74.205701	200.5175239	0	1202.55	537.139
52.40567562	74.205701	228.6410252	2.868535548	1202.55	662.5424645
59.59836571	74.205701	255.9218351	6.381668813	1202.55	843.4203312
64.50823727	74.205701	278.5907636	8.852519495	1202.55	1025.340481
67.30965089	74.205701	310.2628499	11.6113447	1202.55	1231.023655

PMT 7.62 m

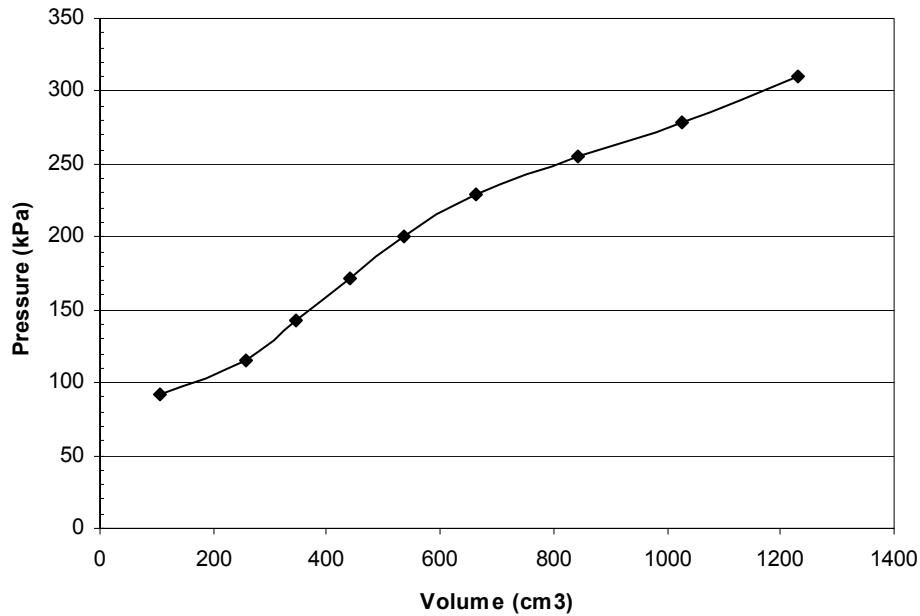


Figure F3. PMT1 Curve at 7.62 m

Table F4. PMT Data at 9.14 m

Depth (m)	V30	V60	Volume (cm3)	Creep	Creep V (cm3)	P (psi)	P (kPa)
9.14	16.2	16.3	1306.771	0	0	5	34.4735
9.14	17.6	17.7	1419.009	0.1	8.017	10	68.947
9.14	18.5	18.6	1491.162	0.1	8.017	15	103.421
9.14	19.2	19.3	1547.281	0.1	8.017	20	137.894
9.14	19.9	20	1603.4	0.1	8.017	25	172.368
9.14	20.7	20.9	1675.553	0.2	16.034	30	206.841
9.14	21.7	21.9	1755.723	0.2	16.034	35	241.315
9.14	23.1	23.2	1859.944	0.1	8.017	40	275.788
9.14	24.9	25.1	2012.267	0.2	16.034	45	310.262
9.14	27.1	27.6	2212.692	0.5	40.085	50	344.735
9.14	29.6	30	2405.1	0.4	32.068	54	372.314
9.14	31.5	32.1	2573.457	0.6	48.102	57	392.998

Membrane Resistance (kPa)	Head (kPa)	Final Corr P (kPa)	Compressibility (cm3)	Initial (cm3)	Final Corr. V (cm3)
16.46842552	89.046841	107.0519155	0	1202.55	104.221
25.34749153	89.046841	132.6463495	0	1202.55	216.459
30.60882413	89.046841	161.8585169	0	1202.55	288.612
34.45931228	89.046841	192.4815287	0	1202.55	344.731
38.09834843	89.046841	223.3159926	0	1202.55	400.85
42.46640422	89.046841	253.4214368	2.868535548	1202.55	470.1344645
46.90984159	89.046841	283.4514994	6.381668813	1202.55	546.7913312
52.0411658	89.046841	312.7936752	9.431156057	1202.55	647.9628439
58.22892804	89.046841	341.079413	12.12583733	1202.55	797.5911627
63.99727965	89.046841	369.7845613	14.54016493	1202.55	995.6018351
66.99747322	89.046841	394.3631678	16.30602379	1202.55	1186.243976
67.58364117	89.046841	414.4610998	17.5477516	1202.55	1353.359248

PMT 9.14 m

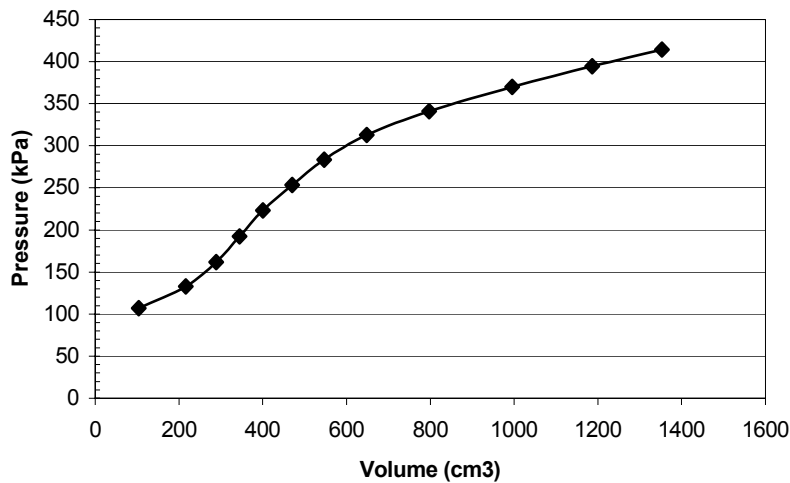


Figure F4. PMT1 Curve at 9.14 m

Table F5. PMT Data at 10.67 m

Depth (m)	V30	V60	Volume (cm3)	Creep	Creep V (cm3)	P (psi)	P (kPa)
10.67	16	16.1	1290.737	0	0	5	34.4735
10.67	17.4	17.7	1419.009	0.3	24.051	10	68.947
10.67	19.2	19.3	1547.281	0.1	8.017	15	103.421
10.67	20.6	20.8	1667.536	0.2	16.034	20	137.894
10.67	21.9	22.2	1779.774	0.3	24.051	25	172.368
10.67	23.7	23.9	1916.063	0.2	16.034	30	206.841
10.67	25.7	26.1	2092.437	0.4	32.068	35	241.315
10.67	28	28.4	2276.828	0.4	32.068	40	275.788
10.67	30.2	31	2485.27	0.8	64.136	45	310.262

Membrane Resistance (kPa)	Head (kPa)	Final Corr P (kPa)	Compressibility (cm3)	Initial (cm3)	Final Corr. V (cm3)
15.13094197	103.88798	123.2305392	0	1202.55	88.187
25.34749153	103.88798	147.4874896	0	1202.55	216.459
34.45931228	103.88798	172.8491689	0	1202.55	344.731
41.99832608	103.88798	199.7836551	0	1202.55	464.986
48.15872354	103.88798	228.0967576	0	1202.55	577.224
54.50211225	103.88798	256.2268689	2.868535548	1202.55	710.6444645
60.8599197	103.88798	284.3425615	6.381668813	1202.55	883.5053312
65.27352638	103.88798	314.4024548	9.431156057	1202.55	1064.846844
67.51394489	103.88798	346.6355363	12.12583733	1202.55	1270.594163

PMT 10.67 m

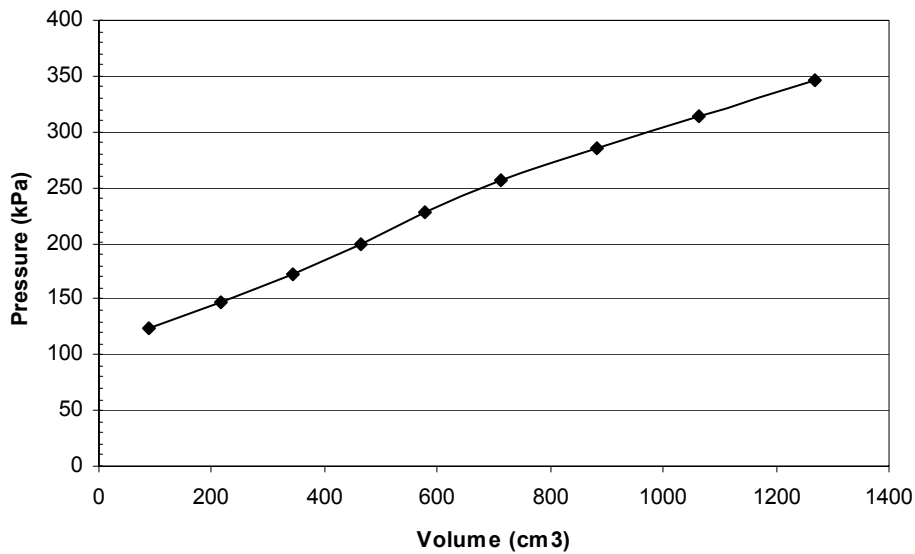


Figure F5. PMT1 Curve at 10.67 m

Table F6. PMT2 Data at 4.0 m

Depth (m)	V30	V60	Volume (cm3)	Creep	Creep V (cm3)	P (psi)	P (kPa)
4.00	1.38	1.38	110.63	0.00	0.00	4.00	27.58
4.00	2.48	2.60	208.44	0.12	9.62	10.00	68.95
4.00	3.70	3.80	304.65	0.10	8.02	15.00	103.42
4.00	4.90	5.05	404.86	0.15	12.03	20.00	137.89
4.00	6.40	6.65	533.13	0.25	20.04	25.00	172.37
4.00	8.25	8.70	697.48	0.45	36.08	30.00	206.84
4.00	10.75	11.70	937.99	0.95	76.16	35.00	241.31
4.00	14.20	15.70	1258.67	1.50	120.26	40.00	275.79

Membrane Resistance (kPa)	Head (kPa)	Final Corr P (kPa)	Compress (cm3)	Initial (cm3)	Final Corr. V (cm3)
18.87	39.33	48.04	0.00	80.17	30.46
27.30	39.33	80.98	0.00	80.17	128.27
34.95	39.33	107.80	0.00	80.17	224.48
42.25	39.33	134.97	0.00	80.17	324.69
50.60	39.33	161.09	0.00	80.17	452.96
59.66	39.33	186.51	3.33	80.17	613.98
69.59	39.33	211.05	6.58	80.17	851.24
76.69	39.33	238.42	9.43	80.17	1169.07

PMT2 4.0 m

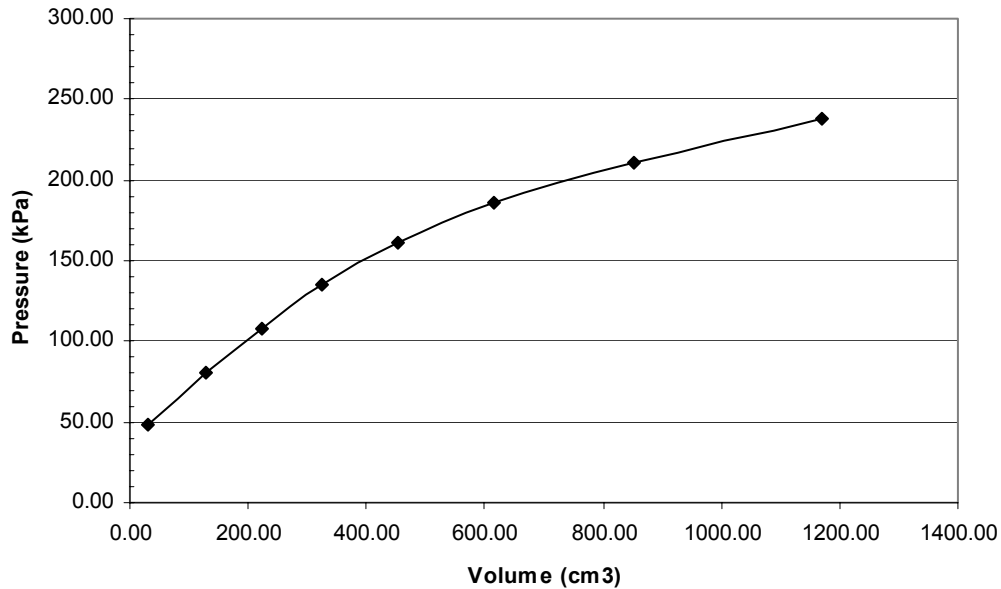


Figure F6. PMT2 Curve at 4.0 m

Table F7. PMT2 Data at 5.50 m

Depth (m)	V30	V60	Volume (cm3)	Creep	Creep V (cm3)	P (psi)	P (kPa)
5.50	0.6	0.6	48.102	0	0	3	20.6841
5.50	1.15	1.15	92.1955	0	0	6	41.3682
5.50	1.55	1.6	128.272	0.05	4.0085	9	62.0523
5.50	2.05	2.1	168.357	0.05	4.0085	12	82.7364
5.50	2.5	2.65	212.4505	0.15	12.0255	15	103.421
5.50	3.12	3.25	260.5525	0.13	10.4221	18	124.105
5.50	3.7	3.9	312.663	0.2	16.034	21	144.789
5.50	4.3	4.4	352.748	0.1	8.017	24	165.473
5.50	5	5.15	412.8755	0.15	12.0255	27	186.157
5.50	5.85	6.13	491.4421	0.28	22.4476	30	206.841
5.50	6.9	7.3	585.241	0.4	32.068	33	227.525
5.50	8.2	8.7	697.479	0.5	40.085	36	248.209
5.50	9.7	10.4	833.768	0.7	56.119	39	268.893
5.50	11.6	12.35	990.0995	0.75	60.1275	42	289.577
5.50	13.2	14.2	1138.414	1	80.17	45	310.262

Membrane Resistance (kPa)	Head (kPa)	Final Corr P (kPa)	Compressibility (cm3)	Initial (cm3)	Final Corr. V (cm3)
13.13536801	54.170162	61.71889359	0	80.17	0
17.20450041	54.170162	78.3338612	0	80.17	12.0255
20.43515405	54.170162	95.78730756	0	80.17	48.102
23.9206529	54.170162	112.9859087	0	80.17	88.187
27.62811812	54.170162	129.9625435	0	80.17	132.2805
31.52138301	54.170162	146.7533786	0	80.17	180.3825
35.56099295	54.170162	163.3978687	0	80.17	232.493
38.54234968	54.170162	181.1006119	0	80.17	272.578
42.80889207	54.170162	197.5181695	1.122401813	80.17	331.5830982
48.0122223	54.170162	212.9989393	3.326498197	80.17	407.9456018
53.67298341	54.170162	228.0222782	5.334029704	80.17	499.7369703
59.65789009	54.170162	242.7214715	7.178186854	80.17	610.1308131
65.77013376	54.170162	257.2933279	8.884333998	80.17	744.713666
71.22113613	54.170162	272.5264255	10.47230102	80.17	899.457199
74.85167858	54.170162	289.579983	11.9578913	80.17	1046.286109

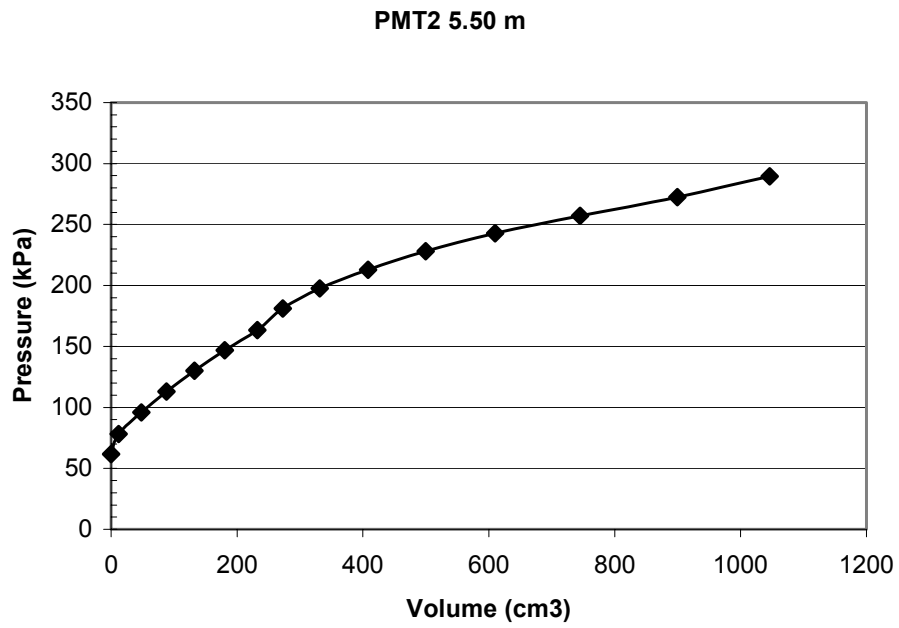


Figure F7. PMT2 curve at 5.50 m

APPENDIX G: PROJECT NO. 2 BST RESULTS

Table G1. Borehole Shear Test Data at 4.19 m

Depth (m)	Normal Stress (kPa)	Shear Stress (kPa)
4.19	12	5
4.19	20	8
4.19	32	13
4.19	38	16
4.19	50	19
4.19	60	25
	phi (deg)	22
	c (kPa)	0.05

Table G2. Borehole Shear Test Data at 2.29 m

Depth (m)	Normal Stress (kPa)	Shear Stress (kPa)
2.29	10	11
2.29	14	15
2.29	19	18
2.29	24	20
2.29	30	26
2.29	38	28
2.29	50	31
2.29	60	36
	phi (deg)	25.4
	c (kPa)	8.6

APPENDIX H: PROJECT NO. 2 DESIGN CALCULATIONS

Design Zone A

UPPER ZONE				
Parameter		Value	Units	Notes
Allowable bearing pressure	q_a	2000	psf	
Calculated bearing pressure	q	3412	psf	130 pcf fill material
Geopier element modulus	k_{gp}	125.0	pci	from Table 4.2
Matrix soil modulus	k_m	13.9	pci	$q_a/144\text{in}^2/\text{ft}^2/1\text{ in}$
Area ratio	R_a	0.25		assumed trial no. 1
Modulus ratio of a Geopier element to matrix soil	R_s	9.0	pci	k_{gp}/k_m
Bearing stress on Geopier element	q_{gp}	71.08	psi	$qR_s/(R_aR_s-R_a+1)$
Bearing stress on matrix soil	q_m	7.90	psi	q_{gp}/R_s
Settlement Upper Zone	S_{UZ}	0.57	inches	q_{gp}/k_{gp} 14 mm
Spacing				
Geopier element diameter	D_{gp}	30	in	
Area of a Geopier element	A_{gp}	4.91	ft ²	
Number of Rows	n	6		
Center-to-Center Spacing	s	6.16	ft	R_a 0.164
LOWER ZONE				
Analysis Approach: Heavily Loaded Continuous Footing				
Foundation Width	B	51	ft	
Influence Depth	4	204	ft	
Geopier Shaft Length	L	22.0	ft	6.71 m
Depth of compressible layer	z	31.7	ft	
Upper Zone Thickness	z_u	24.5	ft	
Lower Zone Thickness	z_l	7.2	ft	
<i>Ooulos and David (1974)</i>				
Center of Lower Zone	z_{lc}	28.08	ft	
Using Figure 4.2.3	h/a	0.96	psf	
	E_1/E_2	2.0		
Modulus of Lower Zone	E_2	41770	psf	
Influence Factor for Lower Zone	$\sigma z/q$	0.63		
Stress on Lower Zone		2149.6	psf	
Lower Zone Settlement	S_{LZ}	4.42	inches	112 mm
TOTAL SETTLEMENT		12.7	cm	

Figure H1. Zone A Design Calculations

Design Zone B

UPPER ZONE				
Parameter		Value	Units	Notes
Allowable bearing pressure	q_a	2000	psf	
Calculated bearing pressure	q	2560	psf	130 pcf fill material
Geopier element modulus	k_{gp}	125.0	pci	from Table 4.2
Matrix soil modulus	k_m	13.9	pci	$q_a/144\text{in}^2/\text{ft}^2/1\text{ in}$
Area ratio	R_a	0.25		assumed trial no. 1
Modulus ratio of a Geopier element to matrix soil	R_s	9.0	pci	k_{gp}/k_m
Bearing stress on Geopier element	q_{gp}	53.33	psi	$qR_s/(R_aR_s-R_a+1)$
Bearing stress on matrix soil	q_m	5.93	psi	q_{gp}/R_s
Settlement Upper Zone	S_{UZ}	0.43	inches	q_{gp}/k_{gp} 11 mm
Spacing				
Geopier element diameter	D_{gp}	30	in	
Area of a Geopier element	A_{gp}	4.91	ft ²	
Number of Rows	n	6		
Center-to-Center Spacing	s	4.92	ft	R_a 0.251
LOWER ZONE				
Analysis Approach: Heavily Loaded Continuous Footing				
Foundation Width	B	51	ft	
Influence Depth	4	204	ft	
Geopier Shaft Length	L	19.0	ft	5.79 m
Depth of compressible layer	z	31.7	ft	
Upper Zone Thickness	z_u	21.5	ft	
Lower Zone Thickness	z_l	10.2	ft	
<i>Ooulos and David (1974)</i>				
Center of Lower Zone	z_{lc}	26.58	ft	
Using Figure 4.2.3	h/a	0.84	psf	
	E_1/E_2	2.0		
Modulus of Lower Zone	E_2	41770	psf	
Influence Factor for Lower Zone	$\sigma z/q$	0.63		
Stress on Lower Zone		1612.8	psf	
Lower Zone Settlement	S_{LZ}	4.71	inches	120 mm
TOTAL SETTLEMENT		13.0	cm	

Figure H2. Zone B Design Calculations

Design Zone C

UPPER ZONE				
Parameter		Value	Units	Notes
Allowable bearing pressure	q_a	2000	psf	
Calculated bearing pressure	q	1706	psf	130 pcf fill material
Geopier element modulus	k_{gp}	125.0	pci	from Table 4.2
Matrix soil modulus	k_m	13.9	pci	$q_a/144\text{in}^2/\text{ft}^2/1\text{ in}$
Area ratio	R_a	0.25		assumed trial no. 1
Modulus ratio of a Geopier element to matrix soil	R_s	9.0	pci	k_{gp}/k_m
Bearing stress on Geopier element	q_{gp}	35.54	psi	$qR_s/(R_aR_s-R_a+1)$
Bearing stress on matrix soil	q_m	3.95	psi	q_{gp}/R_s
Settlement Upper Zone	S_{UZ}	0.28	inches	q_{gp}/k_{gp} 7 mm
Spacing				
Geopier element diameter	D_{gp}	30	in	
Area of a Geopier element	A_{gp}	4.91	ft ²	
Number of Rows	n	6		
Center-to-Center Spacing	s	4.92	ft	R_a 0.251
LOWER ZONE				
Analysis Approach: Heavily Loaded Continuous Footing				
Foundation Width	B	51	ft	
Influence Depth	4	204	ft	
Geopier Shaft Length	L	14.0	ft	4.27 m
Depth of compressible layer	z	31.7	ft	
Upper Zone Thickness	z_u	16.5	ft	
Lower Zone Thickness	z_l	15.2	ft	
<i>Ooulos and David (1974)</i>				
Center of Lower Zone	z_{lc}	24.08	ft	
Using Figure 4.2.3	h/a	0.65	psf	
	E_1/E_2	2.0		
Modulus of Lower Zone	E_2	41770	psf	
Influence Factor for Lower Zone	$\sigma z/q$	0.63		
Stress on Lower Zone		1074.8	psf	
Lower Zone Settlement	S_{LZ}	4.68	inches	119 mm
TOTAL SETTLEMENT		12.6	cm	

Figure H3. Zone C Design Calculations

Design Zone D

UPPER ZONE				
Parameter		Value	Units	Notes
Allowable bearing pressure	q_a	2000	psf	
Calculated bearing pressure	q	853	psf	130 pcf fill material
Geopier element modulus	k_{gp}	125.0	pci	from Table 4.2
Matrix soil modulus	k_m	13.9	pci	$q_a/144\text{in}^2/\text{ft}^2/1\text{ in}$
Area ratio	R_a	0.25		assumed trial no. 1
Modulus ratio of a Geopier element to matrix soil	R_s	9.0	pci	k_{gp}/k_m
Bearing stress on Geopier element	q_{gp}	17.77	psi	$qR_s/(R_aR_s-R_a+1)$
Bearing stress on matrix soil	q_m	1.97	psi	q_{gp}/R_s
Settlement Upper Zone	S_{UZ}	0.14	inches	q_{gp}/k_{gp} 4 mm
Spacing				
Geopier element diameter	D_{gp}	30	in	
Area of a Geopier element	A_{gp}	4.91	ft ²	
Number of Rows	n	6		
Center-to-Center Spacing	s	4.92	ft	R_a 0.251
LOWER ZONE				
Analysis Approach: Heavily Loaded Continuous Footing				
Foundation Width	B	51	ft	
Influence Depth	4	204	ft	
Geopier Shaft Length	L	3.0	ft	0.91 m
Depth of compressible layer	z	31.7	ft	
Upper Zone Thickness	z_u	5.5	ft	
Lower Zone Thickness	z_l	26.2	ft	
<i>Ooulos and David (1974)</i>				
Center of Lower Zone	z_{lc}	18.58	ft	
Using Figure 4.2.3	h/a	0.22	psf	
	E_1/E_2	2.0		
Modulus of Lower Zone	E_2	41770	psf	
Influence Factor for Lower Zone	$\sigma z/q$	0.63		
Stress on Lower Zone		537.4	psf	
Lower Zone Settlement	S_{LZ}	4.04	inches	103 mm
TOTAL SETTLEMENT		10.6	cm	

Figure H4. Zone D Design Calculations